

# Development of a beam-based phase feed-forward demonstration at the CLIC Test Facility (CTF3).

Jack Roberts  
New College, Oxford

Thesis submitted in fulfilment of the requirements for the degree of Doctor of Philosophy at the University of Oxford

Trinity Term, 2016

## **Abstract**

This is the abstract TeX for the thesis and the stand-alone abstract.

Dedication.

# Acknowledgements

Acknowledgements.

# Contents

<b>1</b>	<b>Introduction</b>	<b>1</b>
1.1	Particle Physics . . . . .	1
1.2	Particle Colliders . . . . .	1
1.3	Motivation for Future Linear Colliders . . . . .	1
1.4	CLIC . . . . .	1
1.5	FONT . . . . .	1
1.6	Phase Feedforward for CLIC . . . . .	1
1.7	Thesis Overview . . . . .	1
<b>2</b>	<b>Design of the PFF Prototype at CTF3</b>	<b>2</b>
2.1	CTF3 . . . . .	2
2.1.1	Goals of CTF3 . . . . .	2
2.1.2	Layout of CTF3 . . . . .	2
2.2	Design of the PFF Prototype at CTF3 . . . . .	2
2.2.1	Schematic Overview of PFF System . . . . .	2
2.2.2	Latency . . . . .	3
2.3	PFF Hardware . . . . .	3
2.3.1	FONT5 Board . . . . .	3
2.3.2	Amplifier . . . . .	3
2.3.3	Phase Monitors . . . . .	3
2.3.4	Kickers . . . . .	3
2.4	Differences Between PFF at CTF and CLIC . . . . .	3
2.4.1	Phase Sag . . . . .	3
2.4.2	Pulse Length . . . . .	3
2.5	Feedforward Algorithm . . . . .	3
2.5.1	Theoretical Corrected Jitter . . . . .	3
2.5.2	Theoretical Optimal Gain . . . . .	3
<b>3</b>	<b>Optics for the PFF Prototype</b>	<b>4</b>
3.1	Introduction to Optics . . . . .	4
3.1.1	MADX . . . . .	5
3.2	TL2 . . . . .	5
3.2.1	Lattice . . . . .	5
3.2.2	Integration of PFF Hardware . . . . .	5
3.2.3	Optics Constraints . . . . .	5
3.3	TL2 Optics Measurements . . . . .	5

3.3.1	Method . . . . .	5
3.3.2	Results . . . . .	5
3.3.3	Sources of Errors in MADX Model . . . . .	5
3.3.4	Corrections to MADX Model . . . . .	5
3.4	Matched TL2 Optics . . . . .	5
3.4.1	MADX Optics Matching . . . . .	5
3.4.2	Nominal Optics . . . . .	5
3.4.3	PFF Optics . . . . .	5
<b>4</b>	<b>Phase Monitor Performance</b>	<b>6</b>
4.1	Phase Monitor Electronics . . . . .	7
4.2	Signal Response Measurements . . . . .	7
4.2.1	Experimental Setup . . . . .	7
4.2.2	Saturation . . . . .	7
4.2.3	Cross-Talk . . . . .	7
4.3	Calibrations . . . . .	7
4.3.1	Procedure . . . . .	7
4.3.2	Single Sample Results . . . . .	7
4.3.3	Multi-Sample Results . . . . .	7
4.4	Digitiser Noise . . . . .	7
4.4.1	On FONT5 Board . . . . .	7
4.4.2	On SiS Digitiser . . . . .	7
4.5	Phase Shifter Noise . . . . .	7
4.5.1	Digital Phase Shifters . . . . .	7
4.5.2	Mechanical Phase Shifters . . . . .	7
4.6	Resolution . . . . .	7
4.7	Linearity . . . . .	10
4.8	Bandwidth . . . . .	10
4.9	Dependence on Position . . . . .	10
<b>5</b>	<b>Phase Propagation</b>	<b>11</b>
5.1	Definitions of Different Phase Statistics . . . . .	11
5.2	Characteristics of Uncorrected Phase Jitter . . . . .	11
5.3	First Order Energy Dependencies . . . . .	11
5.3.1	Correlation between Phase and Energy . . . . .	11
5.3.2	Beam Energy Variations . . . . .	11
5.3.3	R56 . . . . .	12
5.3.4	Effect of R56 in TL2 . . . . .	14
5.4	Mitigation of First Order Energy Dependence . . . . .	17
5.4.1	Matched Optics for TL1 . . . . .	21
5.4.2	Scans of R56 in TL1 . . . . .	23
5.5	Higher Order Energy Dependencies . . . . .	30
5.5.1	Expected Dependence due to Optics . . . . .	32
5.5.2	R56 Scans whilst Varying Beam Energy . . . . .	32
5.5.3	Mitigation of Higher Order Dependencies . . . . .	41

5.5.4	Effect on PFF Operation . . . . .	41
5.6	Other Sources of Phase Jitter . . . . .	41
5.6.1	Combiner Ring Septum . . . . .	41
5.6.2	TL1 & Combiner Ring Bends . . . . .	41
5.7	Best Phase Propagation . . . . .	42
<b>6</b>	<b>Setup and Commissioning of the PFF System</b>	<b>43</b>
6.1	Feedforward Controller (FONT5a Board) . . . . .	43
6.1.1	Installation . . . . .	43
6.1.2	Setup Parameters and DAQ . . . . .	43
6.1.3	ADC Droop Correction . . . . .	48
6.1.4	Implementation of PFF Algorithm in Firmware . . . . .	53
6.2	Amplifier . . . . .	56
6.2.1	Installation . . . . .	57
6.2.2	Linearity . . . . .	59
6.2.3	Shape . . . . .	62
6.2.4	Bandwidth . . . . .	64
6.3	Data Acquisition and Signal Processing . . . . .	65
6.3.1	SiS Digitiser Setup . . . . .	65
6.3.2	Acquisition Tools . . . . .	65
6.3.3	Monitoring Tools . . . . .	65
6.3.4	Time Alignment of Signals . . . . .	66
6.3.5	Definition of Zero Phase . . . . .	66
6.4	Kicker and Optics Performance Verification . . . . .	66
6.4.1	Correction Range . . . . .	66
6.4.2	Variations Along Pulse . . . . .	70
6.4.3	Shape . . . . .	70
6.4.4	Orbit Closure . . . . .	71
6.5	Correction Output Timing . . . . .	74
6.5.1	Kicker Cable Lengths . . . . .	76
6.5.2	Absolute Timing . . . . .	78
6.5.3	Relative Kicker Timing . . . . .	83
<b>7</b>	<b>Early Phase Feedforward Attempts and Simulations</b>	<b>90</b>
7.1	Gain Scans . . . . .	90
7.2	Simulation Method . . . . .	90
7.3	Effect of Limited Correction Range . . . . .	90
7.4	Effect of Timing Offsets . . . . .	90
7.5	Effect of Limited Bandwidth . . . . .	90
7.6	Effect of Variations Along the Pulse . . . . .	90
7.7	Effect of Amplifier Non-linearities . . . . .	90
<b>8</b>	<b>Best Achieved Phase Stabilisation</b>	<b>91</b>
8.1	Lowest Achieved Phase Jitter . . . . .	91
8.1.1	Mean Phase Jitter . . . . .	92

8.1.2	Correction of Pulse Shape . . . . .	94
8.1.3	Phase Jitter Along the Pulse . . . . .	95
8.2	Correction on Longer Time Scales . . . . .	96
8.2.1	Upstream Phase Drifts . . . . .	100
8.2.2	Gain Stability . . . . .	102
8.2.3	Results . . . . .	105
8.3	Possible Areas for Future Improvement . . . . .	110
<b>9</b>	<b>Alternative Phase Feedforward Setups and Complementary Systems</b>	<b>114</b>
9.1	Correction with Additional Jitter Source . . . . .	114
9.2	Slow Correction . . . . .	114
9.2.1	Implementation . . . . .	115
9.2.2	Results . . . . .	115
<b>10</b>	<b>Conclusions</b>	<b>116</b>
10.1	Summary . . . . .	116
10.2	Future Work . . . . .	116
	<b>Bibliography</b>	<b>117</b>

# List of Figures

2.1	CTF3 schematic.	2
3.1	New TL2 lattice for PFF. Changes highlighted yellow.	4
3.2	Mean phase along.	5
4.1	Dig shifter 1.	8
4.2	Dig shifter 2.	8
4.3	Dig shifter 3.	8
4.4	Mech shifter.	9
4.5	Resolution.	9
5.1	Downstream phase jitter vs. residual $R_{56}$ between monitors.	15
5.2	Phase correlation vs. residual $R_{56}$ between monitors.	16
5.3	Phase correlation vs. residual $R_{56}$ between monitors.	17
5.4	Phase correlation vs. residual $R_{56}$ between monitors.	18
5.5	TL1 [REF].	20
5.6	Matched $R_{56}$ values for TL1.	22
5.7	Current vs. $R_{56}$ for the CT.QFG0750 quadrupole in TL1.	23
5.8	Horizontal beta in TL1 for all $R_{56}$ optics.	24
5.9	Vertical beta in TL1 for all $R_{56}$ optics.	25
5.10	Dispersion in TL1 for all $R_{56}$ optics.	26
5.11	Phase jitter during scan of $R_{56}$ in TL1.	27
5.12	Correlation during scan of $R_{56}$ in TL1.	28
5.13	Upstream and downstream beam conditions during the $R_{56}$ scan.	29
5.14	Mean phase jitter during $R_{56}$ scan 2.	30
5.15	Mean phase jitter during $R_{56}$ scan 3.	31
5.16	$T_{566}$ coefficient for all sets of TL1 optics.	32
5.17	Phase shift between the upstream and downstream phase monitors for all sets of TL1 optics when only $R_{56}$ is considered.	33
5.18	Phase shift between the upstream and downstream phase monitors for all sets of TL1 optics when both $R_{56}$ and $T_{566}$ are considered.	34
5.19	Downstream phase jitter vs. residual $R_{56}$ in TL1 including the effects of $T_{566}$ with $\sigma_u = 0.8^\circ$ , $\rho_{up} = 0.2$ and $\sigma_p = 1 \times 10^{-3}$ .	35
5.20	Upstream-downstream phase correlation vs. residual $R_{56}$ in TL1 including the effects of $T_{566}$ with $\sigma_u = 0.8^\circ$ , $\rho_{up} = 0.2$ and $\sigma_p = 1 \times 10^{-3}$ .	36
5.21	Best possible upstream-downstream phase correlation vs. beam energy jitter both with and without including the effects of $T_{566}$ .	37

5.22	Phase jitter for different R56 whilst wiggling gun current. . . . .	38
5.23	Mean downstream phase along the pulse for different R56 values. . . . .	39
5.24	Mean downstream phase along the pulse for different R56 values. . . . .	40
5.25	Phase vs. energy for different R56 in TL1. . . . .	41
6.1	Front panel of the FONT5a board. . . . .	44
6.2	Diode output along the pulse with the IIR filter off and on. . . . .	45
6.3	Diode output along the pulse with the IIR filter off and on. . . . .	48
6.4	Exponential fit to diode droop. . . . .	49
6.5	Residuals between diode exponential fit and actual diode output. . . . .	50
6.6	Diode output along the pulse with the IIR filter off and on. Zoomed in. . . . .	52
6.7	Phase along the pulse with the IIR filter off and on. . . . .	52
6.8	Difference between the phase reconstruction method used in the PFF algorithm on the FONT5a board (with the small angle approximation) and the full reconstruction used with data acquired from the SiS digitisers. . . . .	55
6.9	Achievable PFF jitter versus phase offset for full phase reconstruction and with the small angle approximation. . . . .	56
6.10	Front panel of the amplifier. . . . .	57
6.11	Cabling setup for cables between the amplifier and kickers. . . . .	58
6.12	Amplifier output vs. input. . . . .	60
6.13	Residual between amplifier output and linear fit. . . . .	61
6.14	Amp L along pulse at 1 V input . . . . .	62
6.15	Amp R along pulse at 1 V input . . . . .	63
6.16	Flatness of potential difference sent to kickers. . . . .	64
6.17	Residual kick along pulse. . . . .	65
6.18	Residual kick along pulse: deviation from flat. . . . .	66
6.19	Phase shift versus amplifier input voltage. . . . .	67
6.20	Phase shift versus amplifier input voltage. . . . .	68
6.21	Traces relative timing scan. . . . .	70
6.22	Traces relative timing scan. . . . .	71
6.23	Horizontal orbit offset in and around the TL2 chicane at different input voltages sent to the amplifier. . . . .	72
6.24	Orbit in the TL2 chicane at 1 V amplifier input for the BPM data, nominal model and model taking in to account the difference in amplifier output voltage to each kicker. . . . .	73
6.25	Orbit in the TL2 chicane at 1 V amplifier input for the BPM data, nominal model and model taking in to account the quadrupole currents in the real machine setup. . . . .	75
6.26	Beam pickup on kicker strips as seen on amplifier monitoring signals. . . . .	79
6.27	Output delay of 0 clock cycles. Full pulse. . . . .	80
6.28	Output delay scan, end of pulse. . . . .	81
6.29	Output delay of 7 clock cycles. Full pulse. . . . .	82
6.30	Output delay of 7 clock cycles. End of pulse. . . . .	82
6.31	Kick output with no delay as seen on BPM and phase signals. . . . .	84
6.32	Fit time offset between kick and beam at different output delays. . . . .	85

6.33	Alignment between BPMs and phase signals with optimal delay applied in analysis.	86
6.34	Simulated response to offset kicks.	87
6.35	Measured BPM offset for different relative kick delays.	88
6.36	Fitted peak BPM offset vs. relative kick delay.	89
8.1	Mean phase.	92
8.2	Simulated PFF.	94
8.3	Mean phase along.	95
8.4	Flatness.	96
8.5	Std phase along.	97
8.6	Std phase along.	97
8.7	History of mean phase across datasets.	99
8.8	History of mean phase across datasets, with mean subtraction.	99
8.9	Fraction of pulses outside the correction range along the pulse. [TODO: Add line using real dataset offsets]	101
8.10	Offset between downstream phase with FF off and FF on.	102
8.11	Upstream and downstream phase jitter in each data set.	104
8.12	Upstream-downstream mean phase correlation in each dataset with PFF off.	104
8.13	Correlation vs. phase jitter ratio.	105
8.14	Gain used in each dataset compared to the optimal gain.	106
8.15	Theoretical corrected downstream jitter with optimal and used gain.	108
8.16	Corrected downstream jitter with the actual PFF system.	108
8.17	Histogram showing overall distribution of downstream phase with FF off and on.	110
8.18	Downstream phase vs. upstream phase with FF off.	111
8.19	Downstream phase vs. upstream phase with FF on.	111
8.20	Downstream phase vs. upstream phase with FF simulated at optimal gain.	112
8.21	Downstream phase vs. upstream phase with FF simulated with actual gain used.	112

# List of Tables

5.1	Typical upstream phase and energy conditions at CTF3. . . . .	14
5.2	Initial and final conditions for optics matching in TL1. . . . .	21
6.1	IIR filter weights for the FONT5a board ADCs. . . . .	51
6.2	Feedforward results using combined data from 20th November 2015. . . . .	61
6.3	Phase shift at +1 volt input to the amplifier. . . . .	67
6.4	Lengths of cables between the amplifier and the patch panel. . . . .	77
6.5	Lengths of cables between the patch panel and the kickers. . . . .	78
8.1	Best PFF results. . . . .	93
8.2	Simulated feedforward results from 20th November 2015. . . . .	109
8.3	Feedforward results from 20th November 2015. . . . .	109
8.4	Feedforward results using combined data from 20th November 2015. [TODO: this table shows results from old simulations!] . . . . .	113

# Glossary

**Item1** Description.

**Item2** Description.

**Item3** Description.

# Chapter 1

## Introduction

This is the introductory text.

### 1.1 Particle Physics

### 1.2 Particle Colliders

### 1.3 Motivation for Future Linear Colliders

### 1.4 CLIC

### 1.5 FONT

### 1.6 Phase Feedforward for CLIC

### 1.7 Thesis Overview

# Chapter 2

## Design of the PFF Prototype at CTF3

This is the introductory text.

### 2.1 CTF3

#### 2.1.1 Goals of CTF3

CLIC and PFF

#### 2.1.2 Layout of CTF3

### 2.2 Design of the PFF Prototype at CTF3

#### 2.2.1 Schematic Overview of PFF System

;

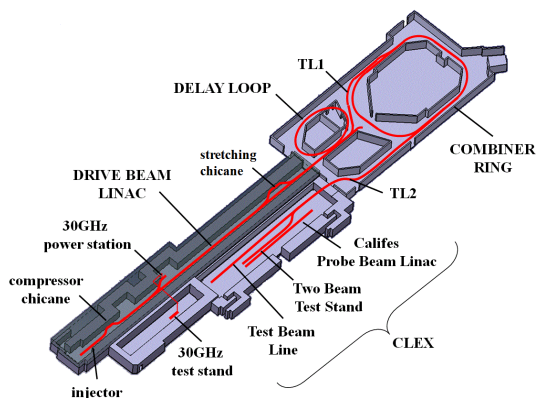


Figure 2.1: CTF3 schematic.

### 2.2.2 Latency

;

## 2.3 PFF Hardware

### 2.3.1 FONT5 Board

### 2.3.2 Amplifier

### 2.3.3 Phase Monitors

### 2.3.4 Kickers

Kicker why drive downstream end theory

## 2.4 Differences Between PFF at CTF and CLIC

### 2.4.1 Phase Sag

### 2.4.2 Pulse Length

## 2.5 Feedforward Algorithm

### 2.5.1 Theoretical Corrected Jitter

$$\sigma_{PFF}^2 = (1 - \rho^2)\sigma_d^2 \quad (2.1)$$

### 2.5.2 Theoretical Optimal Gain

$$g = \rho \cdot \frac{\sigma_d}{\sigma_u} \quad (2.2)$$

# Chapter 3

## Optics for the PFF Prototype

This is the introductory text.

### 3.1 Introduction to Optics

transverse focusing, dispersion, twiss etc.

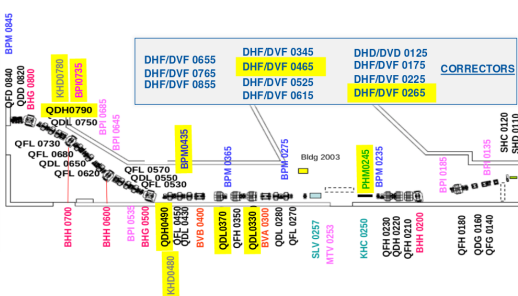


Figure 3.1: New TL2 lattice for PFF. Changes highlighted yellow.

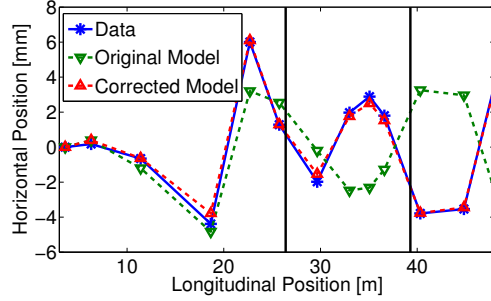


Figure 3.2: Mean phase along.

### 3.1.1 MADX

## 3.2 TL2

### 3.2.1 Lattice

### 3.2.2 Integration of PFF Hardware

### 3.2.3 Optics Constraints

Nominal Optics

PFF Optics

## 3.3 TL2 Optics Measurements

### 3.3.1 Method

### 3.3.2 Results

### 3.3.3 Sources of Errors in MADX Model

Dipole Edge Focusing

Quadrupole Strengths

### 3.3.4 Corrections to MADX Model

## 3.4 Matched TL2 Optics

### 3.4.1 MADX Optics Matching

### 3.4.2 Nominal Optics

### 3.4.3 PFF Optics

# Chapter 4

## Phase Monitor Performance

This is the introductory text.

## 4.1 Phase Monitor Electronics

### 4.2 Signal Response Measurements

#### 4.2.1 Experimental Setup

#### 4.2.2 Saturation

#### 4.2.3 Cross-Talk

### 4.3 Calibrations

#### 4.3.1 Procedure

#### 4.3.2 Single Sample Results

#### 4.3.3 Multi-Sample Results

### 4.4 Digitiser Noise

#### 4.4.1 On FONT5 Board

#### 4.4.2 On SiS Digitiser

### 4.5 Phase Shifter Noise

#### 4.5.1 Digital Phase Shifters

#### 4.5.2 Mechanical Phase Shifters

### 4.6 Resolution

Single sample.

(Multi-sample)

Sample averaging.

Impact for phase correlations.

vs. shifter setting

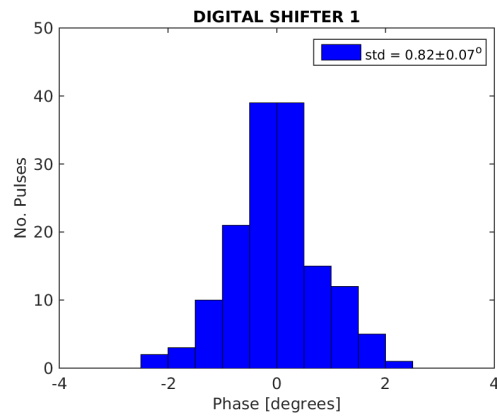


Figure 4.1: Dig shifter 1.

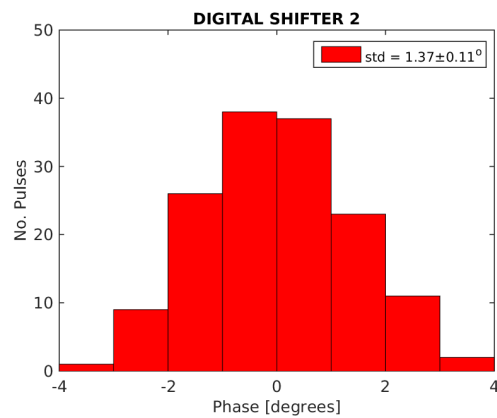


Figure 4.2: Dig shifter 2.

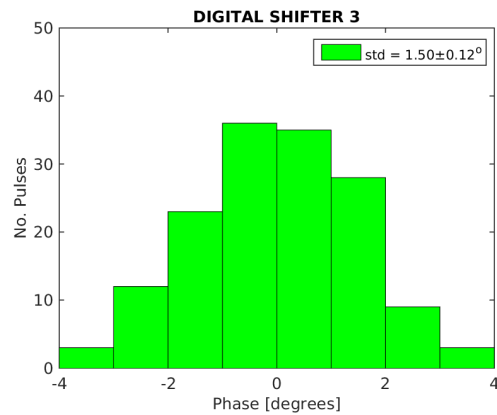


Figure 4.3: Dig shifter 3.

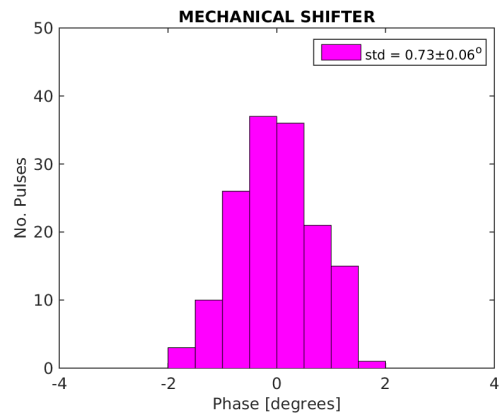


Figure 4.4: Mech shifter.

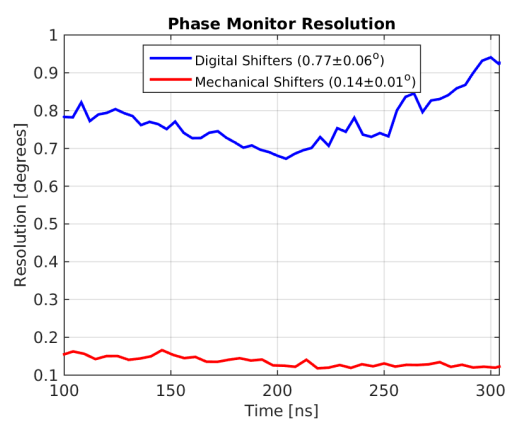


Figure 4.5: Resolution.

## 4.7 Linearity

## 4.8 Bandwidth

## 4.9 Dependence on Position

# Chapter 5

## Phase Propagation

This is the introductory text.

### 5.1 Definitions of Different Phase Statistics

Definitions of different types of phase jitter.

### 5.2 Characteristics of Uncorrected Phase Jitter

Injector feedbacks etc.

### 5.3 First Order Energy Dependencies

#### 5.3.1 Correlation between Phase and Energy

Upstream AND downstream

#### 5.3.2 Beam Energy Variations

Mean Beam Energy

Energy Variations Along the Pulse

and different R56 optimal point along pulse

### 5.3.3 R56

Assuming energy is the only source of differences between the upstream and downstream phase, the downstream phase,  $\phi_d$ , can be expressed in terms of the optics transfer matrix coefficient  $R_{56}$  (Section ??) as follows:

$$\phi_d = \phi_u + R_{56} \frac{\Delta p}{p} \quad (5.1)$$

Where  $\phi_u$  is the upstream phase,  $\Delta p/p$  is the relative energy offset and  $R_{56}$  is the R56 value between the upstream and downstream phase monitors, defined by the machine optics. R56 defines the phase shift between two points in the lattice resulting from a beam energy offset. The units of R56 in the equation above are 12 GHz radians per unit relative energy offset ( $\Delta p/p = 1$ ). MADX uses units of metres and this value is what will be referred to in this chapter. To obtain the R56 value to use in the equation above the MADX value must be multiplied by the conversion factor  $2\pi/0.025$ , where 0.025 m is the 12 GHz wavelength.

In terms of jitters Equation 5.1 becomes:

$$\sigma_d = \sqrt{\sigma_u^2 + R_{56}^2 \sigma_p^2 + 2R_{56} \rho_{up} \sigma_u \sigma_p} \quad (5.2)$$

Where  $\sigma_d$  is the downstream phase jitter,  $\sigma_u$  is the upstream phase jitter,  $\sigma_p$  is the relative energy jitter and  $\rho_{up}$  is the correlation between the upstream phase and the energy. This follows from the result of adding correlated variances. Clearly, any non-zero R56 between the upstream and downstream phase monitors introduces an additional energy component to the downstream phase that increases the downstream phase jitter.

The effect of R56 on the upstream-downstream phase correlation,  $\rho_{ud}$ , can also be defined starting from the definition of the correlation coefficient:

$$\rho_{ud} = \frac{\text{cov} [\phi_u, \phi_d]}{\sigma_u \sigma_d} \quad (5.3)$$

Where  $\text{cov} [\phi_u, \phi_d]$  is the covariance between the upstream and downstream phase, given by:

$$\text{cov} [\phi_u, \phi_d] = \frac{1}{N} \sum_{i=1}^N \phi_{ui} \phi_{di} \quad (5.4)$$

By inserting the definition of the downstream phase from Equation 5.1 and separating the terms in the sum this becomes:

$$\text{cov} [\phi_u, \phi_d] = \frac{1}{N} \sum_{i=1}^N \phi_{ui}^2 + R_{56} \frac{1}{N} \sum_{i=1}^N \phi_{ui} \frac{\Delta p}{p} \quad (5.5)$$

The first term is now the variance of the upstream phase,  $\sigma_u^2$ , and the second term is  $R_{56}$  multiplied by the covariance between the upstream phase and the energy,  $\text{cov} [\phi_u, \frac{\Delta p}{p}]$ , which can be expressed in terms of the correlation between the upstream phase and the energy,  $\rho_{up}$ :

$$\text{cov} \left[ \phi_u, \frac{\Delta p}{p} \right] = \rho_{up} \sigma_u \sigma_p \quad (5.6)$$

Therefore, Equation 5.5 becomes:

$$\text{cov} [\phi_u, \phi_d] = \sigma_u^2 + R_{56}\rho_{up}\sigma_u\sigma_p \quad (5.7)$$

Finally, substituting Equations 5.2 and 5.7 into Equation 5.3 gives:

$$\rho_{ud} = \frac{\sigma_u + R_{56}\rho_{up}\sigma_p}{\sqrt{\sigma_u^2 + R_{56}^2\sigma_p^2 + 2R_{56}\rho_{up}\sigma_u\sigma_p}} \quad (5.8)$$

Considering that in this model the only difference between the upstream and downstream phase results from the R56, it is perhaps obvious that the best conditions for the PFF correction are obtained when the R56 coefficient between the upstream and downstream phase monitors is zero. In these conditions  $\sigma_d = \sigma_u$  and  $\rho_{ud} = 1$ . This can be more formally defined by using the expression for the theoretical corrected downstream phase jitter when using the optimal gain factor as derived in Section 2.5.1:

$$\sigma_{PFF} = \sigma_d \sqrt{1 - \rho_{ud}^2} \quad (5.9)$$

All these quantities have been derived above and inserting them in to this equation gives the following expression for the corrected downstream phase jitter in terms of the R56:

$$\sigma_{PFF} = |R_{56}| \sigma_p \sqrt{1 - \rho_{up}^2} \quad (5.10)$$

As expected the achievable corrected downstream phase jitter is minimised when  $R_{56} = 0$ . Note that this equation does not take in to account the effects of the phase monitor resolution, which in reality limits the minimum achievable downstream phase jitter to  $\sigma_{PFF} = 0.2^\circ$  ([TODO:Section ref]).

In principle the beam conditions for the PFF correction could also be improved by reducing the relative energy jitter ( $\sigma_p$ ) or by increasing the upstream phase-energy correlation ( $\rho_{up}$ ). Reducing the relative energy jitter decreases the additional phase jitter created by non-zero R56. Increasing the upstream phase-energy correlation ( $\rho_{up}$ ) reduces the effect that non-zero R56 has on the upstream-downstream phase correlation ( $\rho_{ud}$ ). For example, if  $\rho_{up} = 1$  the source of all upstream phase jitter is energy jitter. In that case although non-zero R56 would further increase the downstream phase jitter, the additional jitter would be well correlated with the upstream phase and the upstream-downstream phase correlation would not be affected. In practice  $\sigma_p$  and  $\rho_{up}$  are defined by the CTF3 injector and can not be varied with a great degree of flexibility, so having zero R56 is the only way to obtain ideal conditions for the PFF correction. High upstream phase-energy correlations can be created at CTF3 but not without greatly amplifying the upstream phase jitter, which causes issues for the PFF system due to its limited correction range (Section 9.1).

An interesting side note of Equations 5.2 and 5.10 is that the best beam conditions for the PFF correction are not given by minimising the initial downstream phase jitter in the case where the upstream phase-energy correlation,  $\rho_{up}$ , is non-zero. As seen in the previous section in normal conditions there is a small correlation between the upstream phase and the energy at CTF3, typically around  $\rho_{up} = 0.2$ . In these conditions the downstream phase jitter can in

Parameter	Value
$R_{56}$	-0.2 m
$\sigma_u$	0.8°
$\rho_{up}$	0.2
$\sigma_p$	0.001

Table 5.1: Typical upstream phase and energy conditions at CTF3.

theory be reduced to below the level of the upstream phase jitter by using a negative  $R_{56}$  to remove the energy component in the downstream phase. Differentiating Equation 5.2 gives the minimum downstream phase jitter to be obtained when  $R_{56} = -\rho_{up}\sigma_u/\sigma_p$ . However, using this  $R_{56}$  value would degrade the upstream-downstream phase correlation and increase the achievable corrected downstream jitter, which is always minimised when  $R_{56} = 0$  as in Equation 5.10. This is significant for the  $R_{56}$  optimisation attempts presented later in this chapter, as it must always be kept in mind that the goal is to maximise the upstream-downstream phase correlation rather than to create the most stable downstream phase (with the PFF system off).

### 5.3.4 Effect of $R_{56}$ in TL2

Unfortunately, it was not possible to find optics for the TL2 chicane that met all the PFF requirements and thus an  $R_{56}$  in the chicane of close to -0.2 m had to be accepted (Section 3.4.3). All other lines at CTF3 nominally have zero  $R_{56}$  [REF], and therefore don't introduce additional phase jitter via energy, at least to first order and to within the accuracy of the CTF3 MADX model. The overall  $R_{56}$  between the upstream phase monitors (in the CT line) and the downstream phase monitors (in the TBL line, labelled CB, after the TL2 chicane) is therefore -0.2 m also. Whether this can explain the low upstream-downstream phase correlation and high downstream phase jitter seen in Section 5.2, as well as what residual  $R_{56}$  between the two monitors can be tolerated to be able to achieve CLIC-level phase stability at CTF3, is discussed in this section.

Equations 5.2 and 5.8 can be used to estimate the downstream phase jitter and upstream-downstream phase correlation in the conditions at CTF3. Typical values for the various parameters in the equations have already been presented in previous sections, and these values are summarised in Table 5.1. The value  $R_{56} \simeq -0.2$  was obtained in Section 3.4.3 as previously mentioned, the value  $\sigma_u \simeq 0.8^\circ$  in Section 5.2 and the values  $\rho_{up} \simeq 0.2$  and  $\sigma_p \simeq 0.001$  in Section 5.3.1.

With these parameter values the residual  $R_{56}$  of -0.2 m reduces the upstream-downstream phase correlation to below 10% [TODO: 45% on the other side of the crest, and there is ambiguity], and amplifies the downstream phase jitter to above 3 degrees.  $R_{56}$  transforming energy jitter in to downstream phase jitter therefore explains the low upstream-downstream phase correlation and high downstream phase jitter seen in Section 5.2. In order to increase the upstream-downstream phase correlation to 97% and reduce the downstream jitter to 0.8 degrees (the conditions needed to achieve 0.2 degrees corrected downstream phase jitter

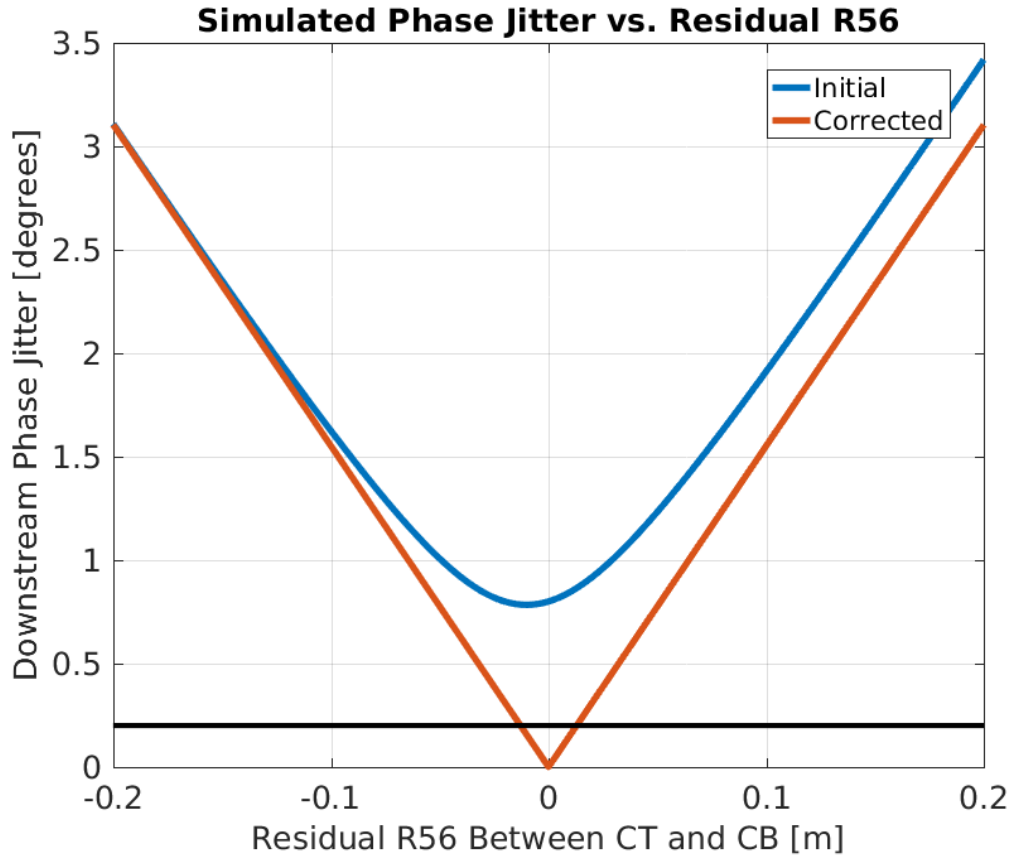


Figure 5.1: Downstream phase jitter vs. residual R56 between monitors.

at CTF3, see Section 2.5) the R56 between the upstream and downstream phase monitors must be removed.

Figure 5.1 and 5.2 show the expected downstream phase jitter and upstream-downstream phase correlation for residual R56 values from  $-0.2$  to  $+0.2$  m between the upstream and downstream phase monitors again using the equations derived in the previous section. The horizontal black line in each figure marks the requirements needed to reduce an initial upstream phase jitter of 0.8 degrees to the CLIC target of 0.2 degrees. The red line, "corrected", in Figure 5.1 shows the theoretical corrected downstream phase jitter using the PFF correction across the range of R56 values. Note the slight asymmetry in the phase jitter and correlation curves, which is caused by the non-zero correlation between the upstream phase and the beam energy. In order to obtain CLIC level phase stability at CTF3 the residual R56 between the upstream and downstream phase monitors must be reduced from the initial  $-0.2\text{m}$  to  $0 \pm 1.3\text{ cm}$ .

To interpret the results of the R56 optimisation attempts presented in the remainder of this chapter it is useful to understand how varying the correlation between the upstream phase and the energy ( $\rho_{up}$ ) changes the dependence of the upstream-downstream phase correlation ( $\rho_{ud}$ ) on the residual R56. In particular, in Section 5.5.2 a machine setup that increases  $\rho_{up}$  to 90% was used. Figure 5.3 shows how  $\rho_{ud}$  varies with  $\rho_{up}$  values between 0% and 40% (typical of normal operation) and with the higher correlation of 90%. With high correlations

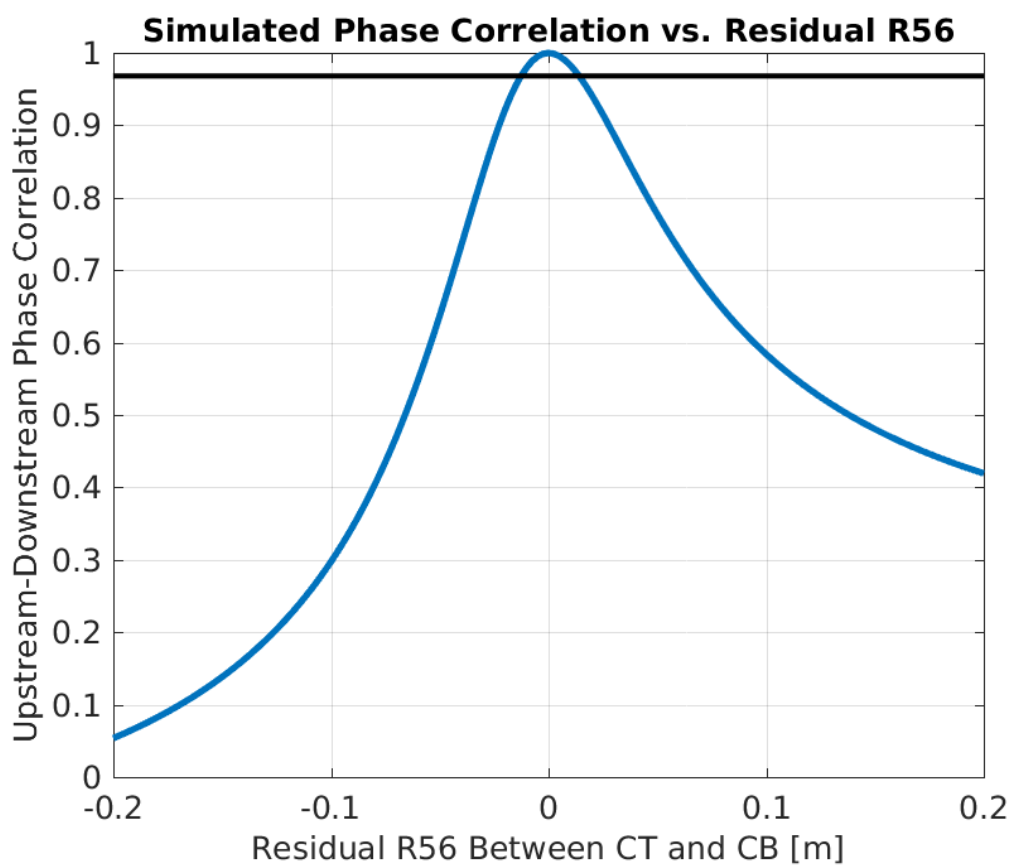


Figure 5.2: Phase correlation vs. residual R56 between monitors.

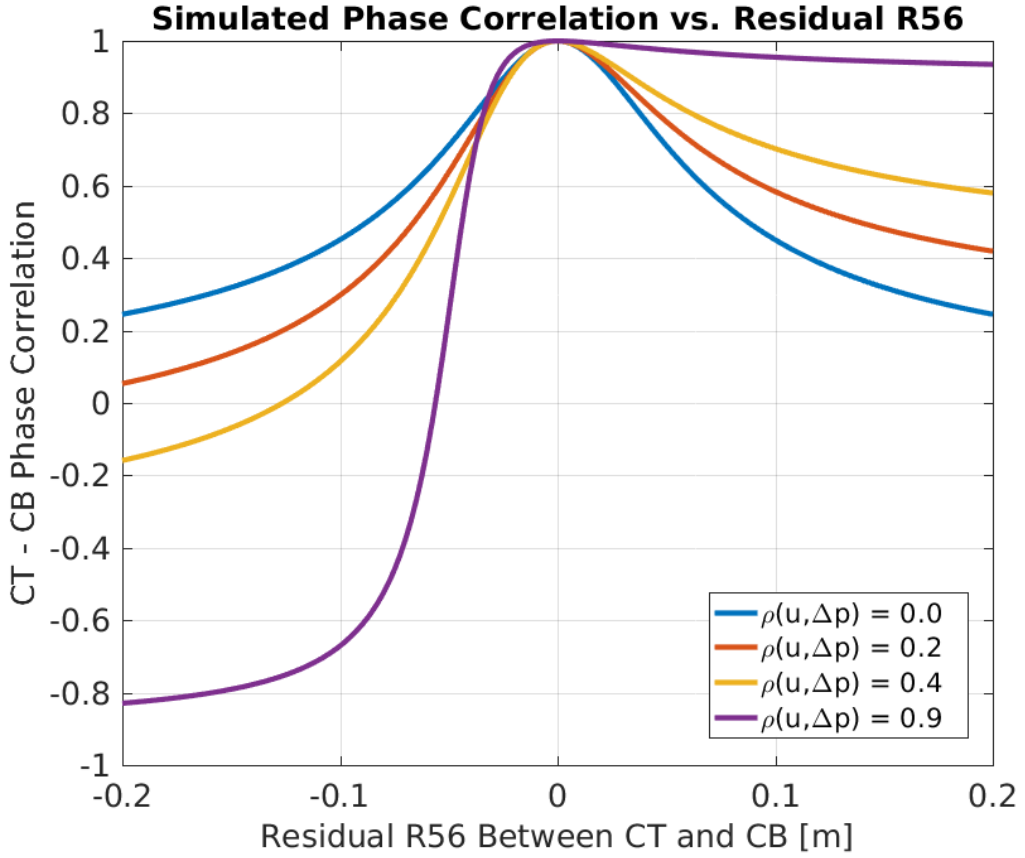


Figure 5.3: Phase correlation vs. residual R56 between monitors.

between the upstream phase and energy there is no longer a well defined peak in  $\rho_{ud}$  versus the residual R56 value. Instead there is an almost constant high upstream-downstream phase correlation with positive R56 values, and a large anti-correlation for negative R56 values (as in this case the residual R56 acts to flip the sign of the phase jitter).

In Figure 5.4 plotting the theoretical downstream jitter with  $\rho_{up} = 0.9$  gives a clear demonstration that the best conditions for the PFF correction are always with  $R_{56} = 0$  rather than with the lowest possible initial downstream jitter, as mentioned in the previous section. In fact, as these conditions relax the requirements on the residual R56 needed to achieve high upstream-downstream phase correlations (as seen in the previous figure) it may be easier to achieve a large factor reduction in the downstream phase jitter with the PFF system with a high  $\rho_{up}$  machine setup. This has been attempted and is presented in Section 9.1.

## 5.4 Mitigation of First Order Energy Dependence

The discussion in the previous section proves that with a residual R56 value of -0.2 m between the upstream and downstream phase monitors it is impossible to achieve the goals of the PFF prototype at CTF3. However, due to the highly constrained optics in TL2 it has already

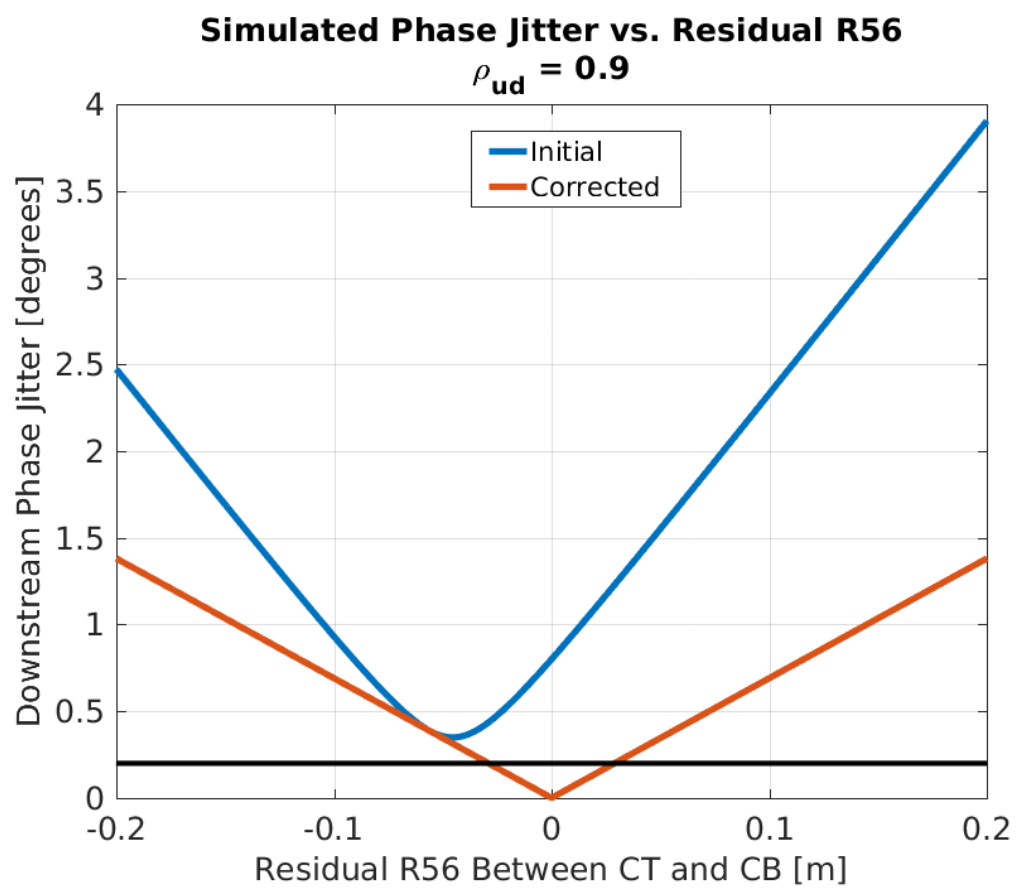


Figure 5.4: Phase correlation vs. residual R56 between monitors.

been seen in Chapter 3 that it was not possible to find optics for the PFF chicane that yield zero R56 whilst also meeting requirements for both the PFF system and transverse matching (dispersion and beta functions). The only way to create a total R56 of zero between the upstream and downstream phase monitors is therefore to add positive R56 to one of the other beam lines at CTF3 in order to compensate for the negative R56 in the TL2 chicane.

The previous transfer line TL1, which transports the beam from the CT line (where the upstream phase monitors are installed) to the combiner ring (see Figure 2.1), has been used to achieve this. The layout of the TL1 transfer line is shown in Figure 5.5. It consists of: 4 dipoles (bending the beam horizontally) of 2 different types, 13 quadrupoles of 5 different types, 7 magnetic correctors, 1 sextupole (usually not used) and 8 BPMs (the dispersive BPM after the first dipole in TL1, labelled CT.BPI0608, is the device that has been used to determine correlations between the phase and energy in this chapter). The total length of TL1 is approximately 30 m. [TODO: more details?]

Preliminary attempts to reduce the residual R56 between the upstream and downstream phase monitors using TL1 yielded correlations up to 60% and reduced the downstream phase jitter to  $2^\circ$ . Conditions similar to these were used for the first PFF tests (Chapter 7) before the energy related effects discussed in this chapter were fully characterised, but in these tests only a modest reduction of 30% in downstream phase jitter was possible due to the limitations of the phase propagation shown here. At this time only a few different optics for TL1 were available in R56 steps of 10 cm. As the total residual R56 must be reduced to the centimetre level to make a correction down to 0.2 degrees jitter theoretically possible with the PFF system, new sets of optics for TL1 were required.

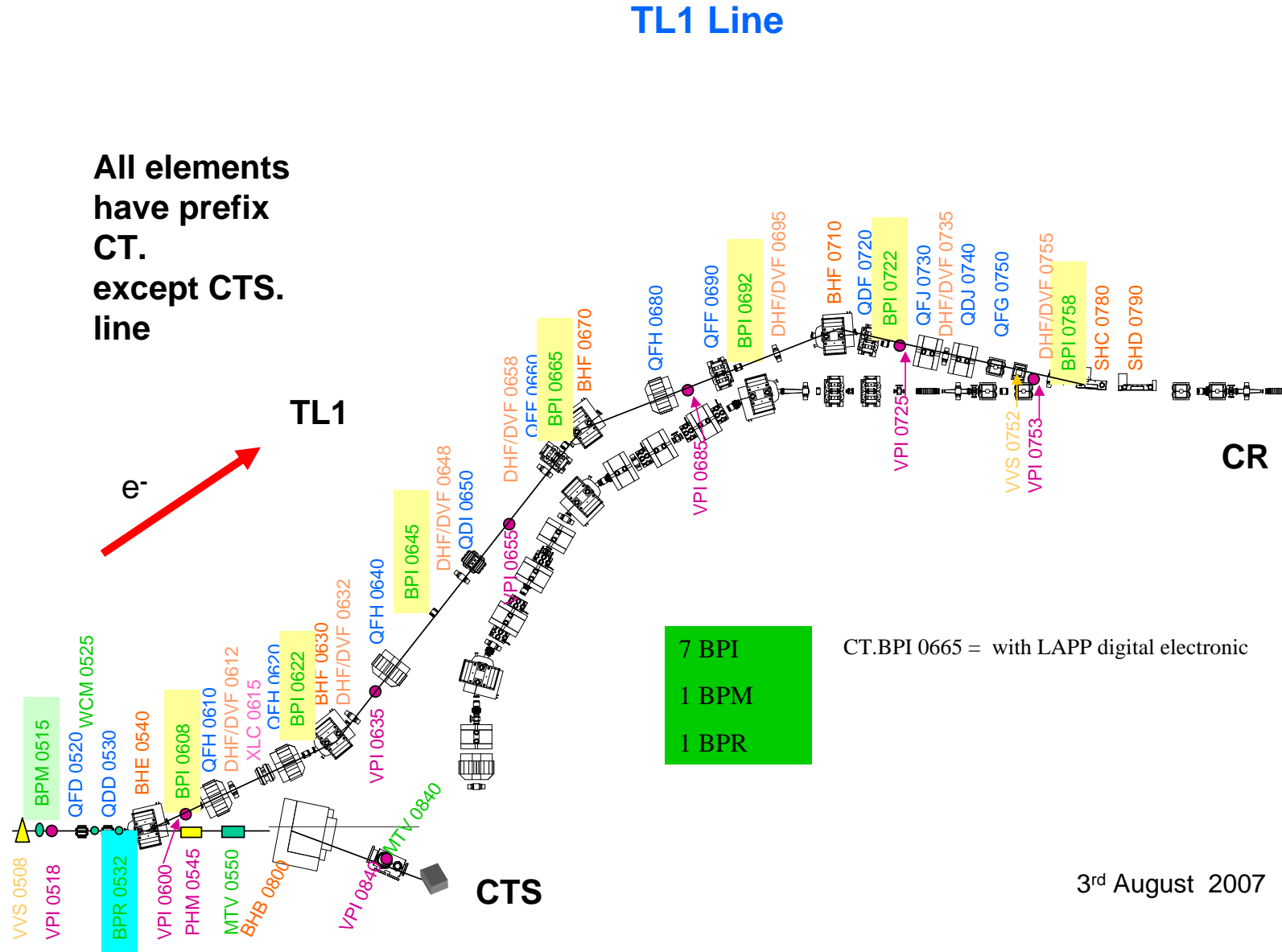


Figure 5.5: TL1 [REF].

Parameter	TL1 Injection	CR Injection
$\beta_x$	8.81 m	4.08 m
$\beta_y$	13.94 m	5.41 m
$\alpha_x$	-0.74	-0.31
$\alpha_y$	-0.45	-0.21
$D_x$	0 m	-0.03 m
$D_{px}$	0	0.02

Table 5.2: Initial and final conditions for optics matching in TL1.

[TODO: Need a better figure]

### 5.4.1 Matched Optics for TL1

Although in theory only one set of optics with  $R_{56} = +0.2$  m in TL1 is required to compensate for the  $R_{56} = -0.2$  m in TL2, in practice errors in the MADX model of CTF3 plus the effect of higher order energy dependencies (see Section 5.5) means it is not possible to know precisely what the optimal R56 to set in TL1 will be, and it is also possible that this value will vary with time. To determine the optimal value of R56 to set it is also useful to scan the R56 value in TL1 across a wide range of values and then fit the maximum resulting upstream-downstream phase correlation.

To allow this, MADX has been used to match optics for TL1 with R56 values ranging from -0.3 m to +0.6 m in steps of 0.5 cm (a total of 181 sets of optics). The optimal R56 value should always be guaranteed to be in this range, and the step size of 0.5 cm allows the residual R56 to be zeroed to within one centimetre as derived to be necessary in Section 5.3.4. As well as the different R56 values, each set of optics must maintain the same initial and final conditions, so that the injection of the beam in to the combiner ring is not affected. Values for the beta functions, alphas and dispersion at the start of TL1 and at the combiner ring injection are summarised in Table 5.2. As well as the initial and final conditions, the maximum beta functions and dispersion in TL1 are constrained to ensure a reasonable beam size throughout the line — the horizontal and vertical beta function is limited to a maximum of 35 m, and the horizontal dispersion to a maximum absolute value of 1.25 m. Around the septum used for injection in to the combiner ring the horizontal beta function is further limited to a maximum of 10 m. The strengths of the 13 quadrupoles in TL1 are varied to meet all these constraints.

Figures 5.6 shows the matched R56 value in TL1 across the range of targeted values. Each matched R56 value is within 10 microns of the desired result. Figure 5.7 then shows an example of how the strength of one of the quadrupoles must be varied in order to achieve each R56 value. If the dependence of each quadrupole strength on the R56 value was continuous the relationship could be fitted to create a set of tuning knobs to allow R56 to be set to any arbitrary value in TL1. However, as seen in the figure there are many discontinuities. The quadrupole strengths for each set of optics are therefore saved to a lookup table, with a MatLab function created to read the table and set the quadrupole currents in the machine

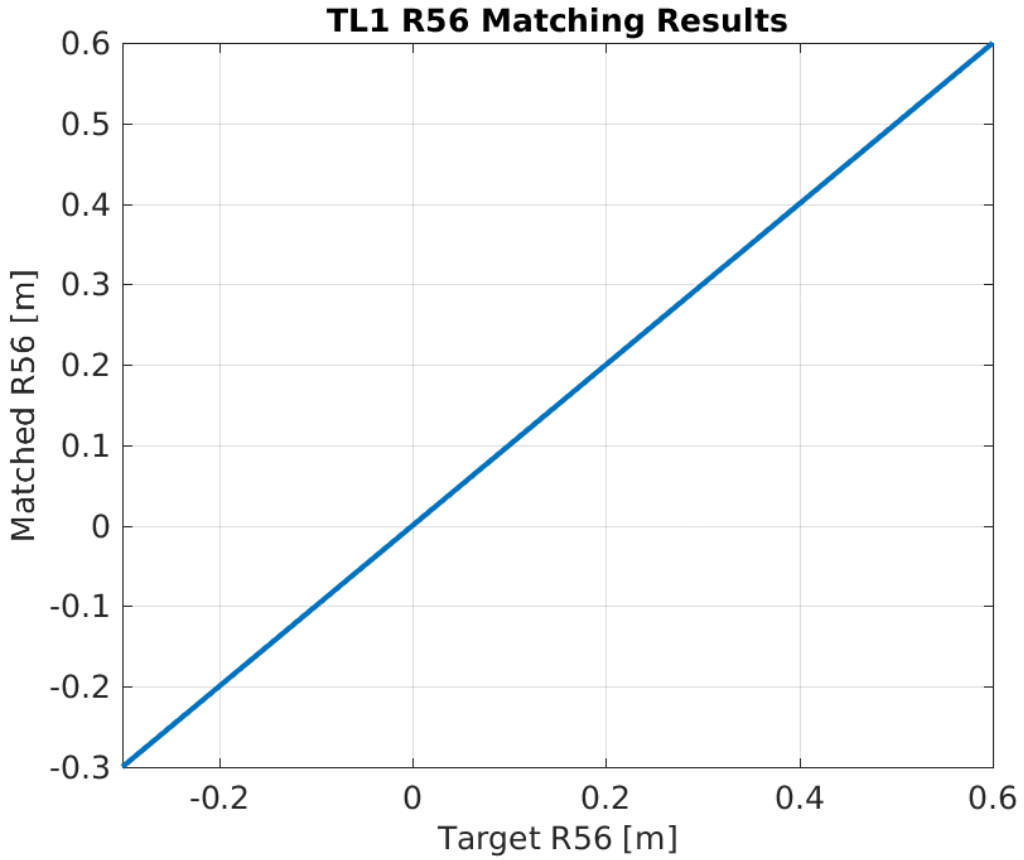


Figure 5.6: Matched R56 values for TL1.

appropriate for the specified R56 value. As already mentioned 0.5 cm precision in R56 should be adequate for the PFF requirements, but the discontinuities mean new optics would have to be matched if optics with an R56 value not included in the discrete set used here were required.

For reference Figures 5.8 5.9 and 5.10 show how the horizontal and vertical beta functions and horizontal dispersion changes in TL1 for each set of optics. For all R56 values each parameter converges to the same value at the start and end of TL1, as needed to ensure that changing the R56 does not impact injection in to the combiner ring. The maximum horizontal and vertical beta functions in TL1 roughly increase with the set R56 value, but in all cases are kept below the set limit of 35 m in the matching procedure. The dispersion pattern in TL1 also changes with the set R56 value, though in most cases the maximum absolute dispersion is around 1 m and only the location of the peak dispersion along the line changes. Again, for each set of optics the maximum absolute dispersion is limited within the set constraint of 1.25 m.

Commissioning of the new TL1 optics in CTF3 was straightforward and in general they can be set with the quadrupole strengths at their nominal matched values without causing issues for the beam quality. At the extremities of the range of optics (close to  $R56 = -0.1$  m and  $R56 = +0.6$  m) some slight beam losses do begin to occur, but this is not a problem for PFF operation where the required R56 is only 0.2 m. However, for each set of optics the

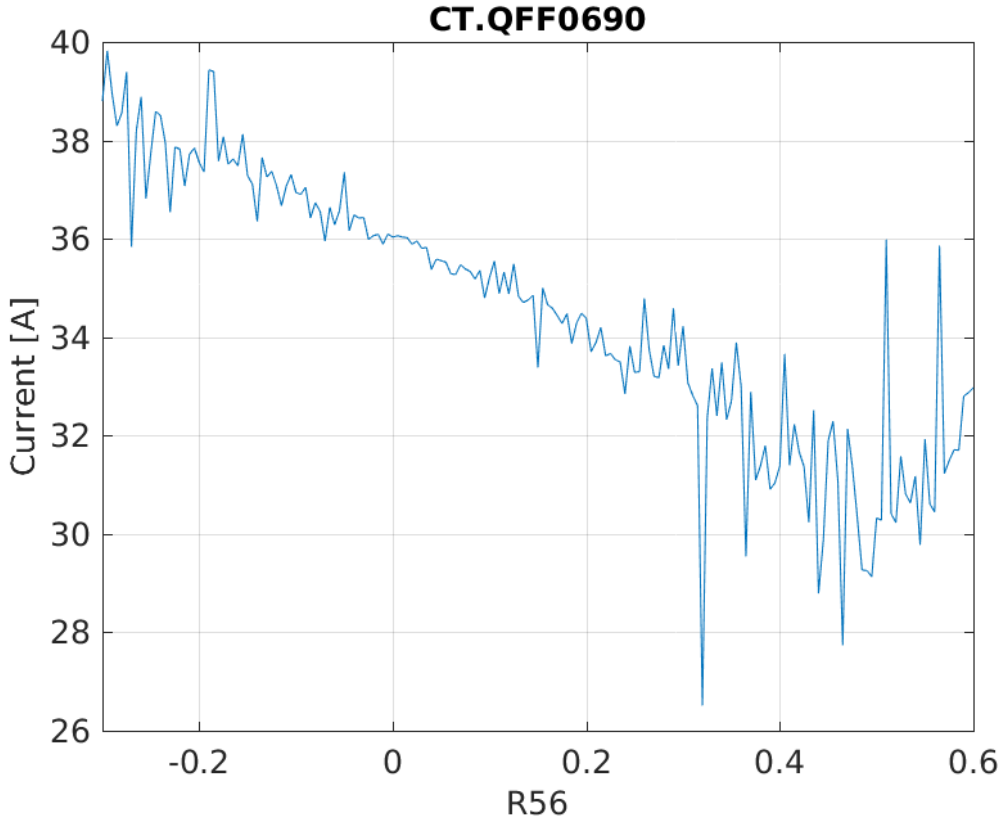


Figure 5.7: Current vs. R56 for the CT.QFG0750 quadrupole in TL1.

magnetic correctors in TL1 may need to be changed to recover the nominal beam orbit, thus taking in to account slight misalignments in elements along the line. [TODO: could expand this]

#### 5.4.2 Scans of R56 in TL1

The sets of matched optics from the previous section can be used to perform scans of the R56 value in TL1 to observe how the downstream phase is affected. Scans of this type must be performed prior to all PFF data taking periods in order to optimise the beam conditions (maximise the upstream-downstream phase correlation) for the correction. More recently scans of R56 in TL1 have been performed whilst varying the beam energy, which produces cleaner results and highlights additional factors that must be taken in to account during the optimisation process, as will be shown in Section 5.5.

As a starting point the simplest case, where only the TL1 optics is changed during the scan and all other parameters in the machine are left unchanged, is presented in this section. This also highlights some of the difficulties in maintaining beam conditions at CTF3, which is discussed further in Section 5.5 and extensively in the context of the PFF correction in Section 8.2. Figures 5.11 and 5.12 show one example of an R56 scan performed across the full range of available optics – from -0.1 m R56 in TL1 to +0.6 m. The R56 is incremented by 2.5 cm between datasets, to give a total of 29 R56 points in the scan, with the whole scan

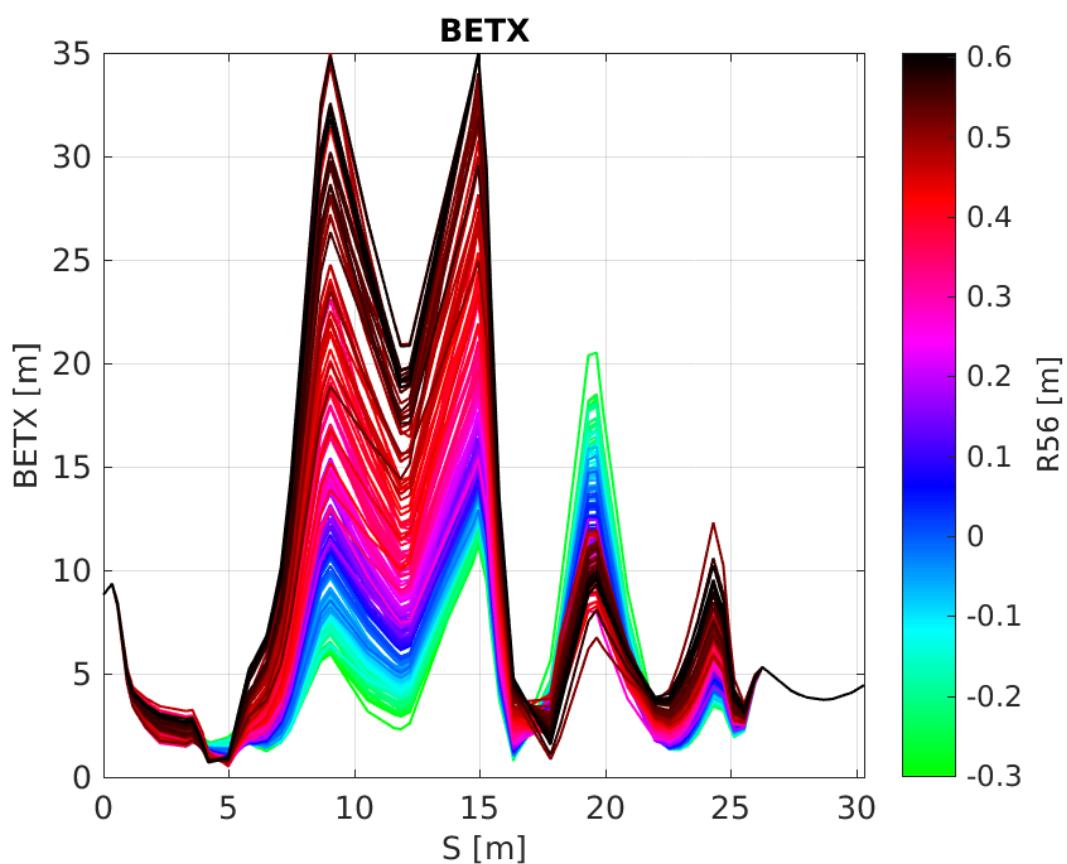


Figure 5.8: Horizontal beta in TL1 for all R56 optics.

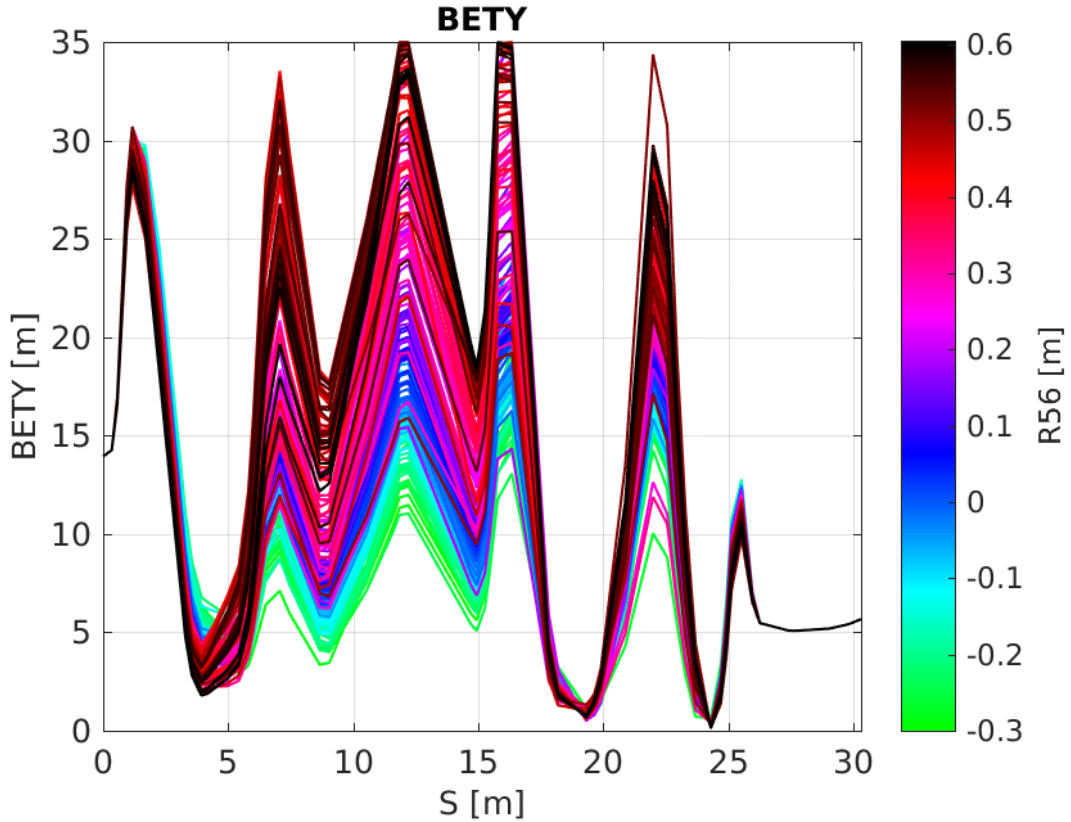


Figure 5.9: Vertical beta in TL1 for all R56 optics.

taking approximately one and a half hours to complete. With the knowledge gained from measurements of this type it is no longer necessary to scan the R56 across the full range to determine the ideal value, thus the optimisation of the phase propagation for PFF attempts can now be achieved on much shorter time scales.

### Mean Phase

Only the mean phase jitters and correlation will be considered here, features along the pulse are discussed in later sections for other scans. Figure 5.11 shows the mean phase jitter during the scan both upstream and downstream. Although the noise in the measurement is quite large, the downstream phase jitter is reduced from above 2.5 degrees with zero R56 in TL1, to below 1 degree and close to the level of the upstream phase jitter by adding positive R56 in TL1. The optimal R56 value is approximately 0.175 m, in close agreement with expectations considering the -0.2 m R56 in TL2. The upstream-downstream phase correlation, in Figure 5.12, is also maximised at this point, from an initial correlation of 20% with zero R56 to up to 80%. In terms of the PFF system, increasing the upstream-downstream phase correlation from 20% to 80% improves the theoretical correction from a 2% reduction in downstream phase jitter to a 40% decrease (Equation 2.1).

As the upstream phase monitors are prior to TL1, changing the TL1 optics has no effect on the upstream phase jitter. All differences in the upstream phase jitter between datasets

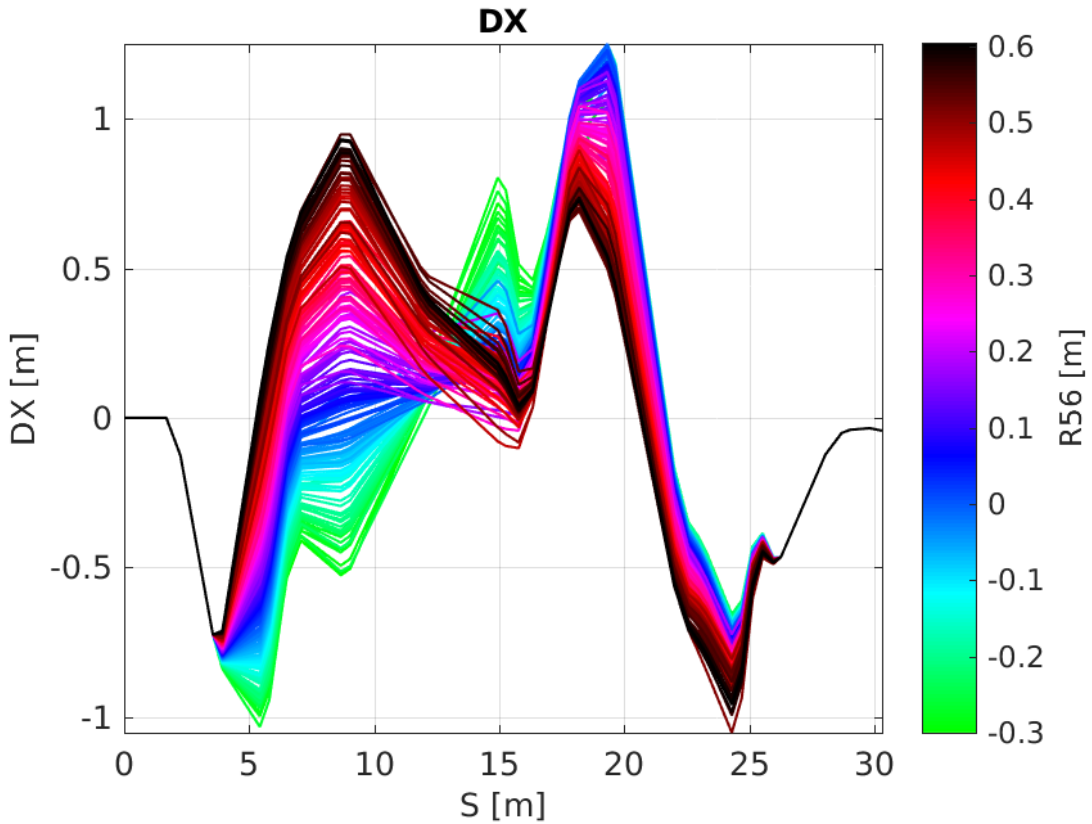


Figure 5.10: Dispersion in TL1 for all R56 optics.

are caused by drifts in the CTF3 injector, typically changes in either klystron phases or beam current. Although the overall stability of the upstream phase jitter during this scan is good, it does vary between 0.5 degrees and 1.2 degrees. In addition to the upstream phase there are also differences in the relative energy jitter and upstream phase-energy correlation during the scan, as seen in Figure 5.13. The relative beam energy jitter varies between  $0.4 \times 10^{-3}$  and  $1.0 \times 10^{-3}$  and the upstream phase-energy correlation between -0.5 and +0.5. All these parameters influence the downstream phase, as per the equations in Section 5.3.3.

The differences in the upstream phase and energy conditions between datasets partially explains the apparent spread of the data points away from the expected clean distribution. The black “simulation” lines in Figures 5.11 and 5.12 represent the expected downstream phase jitter and upstream-downstream phase correlation at each point in the scan given the upstream phase jitter, relative energy jitter and upstream phase-energy correlation at that time (using Equations 5.2 and 5.8). The correlation simulation in Figure 5.12 has been scaled so that the peak value is in agreement with the data, at 0.8. The majority of the data points follow the scaled simulated distribution, with several remaining outliers. For the downstream phase jitter (which uses the simulated result directly with no scaling) the agreement with the simulation is generally good for R56 values below 0.3 m. However, above 0.3 m the actual phase jitter seen in the scan is smaller than the simulation. One possible explanation for this are the changes in downstream beam current between datasets, which varies by a factor 3 during the scan (bottom plot in Figure 5.13). Small beam losses between measurements may change the phase jitter in a way that is not characterised by the R56.

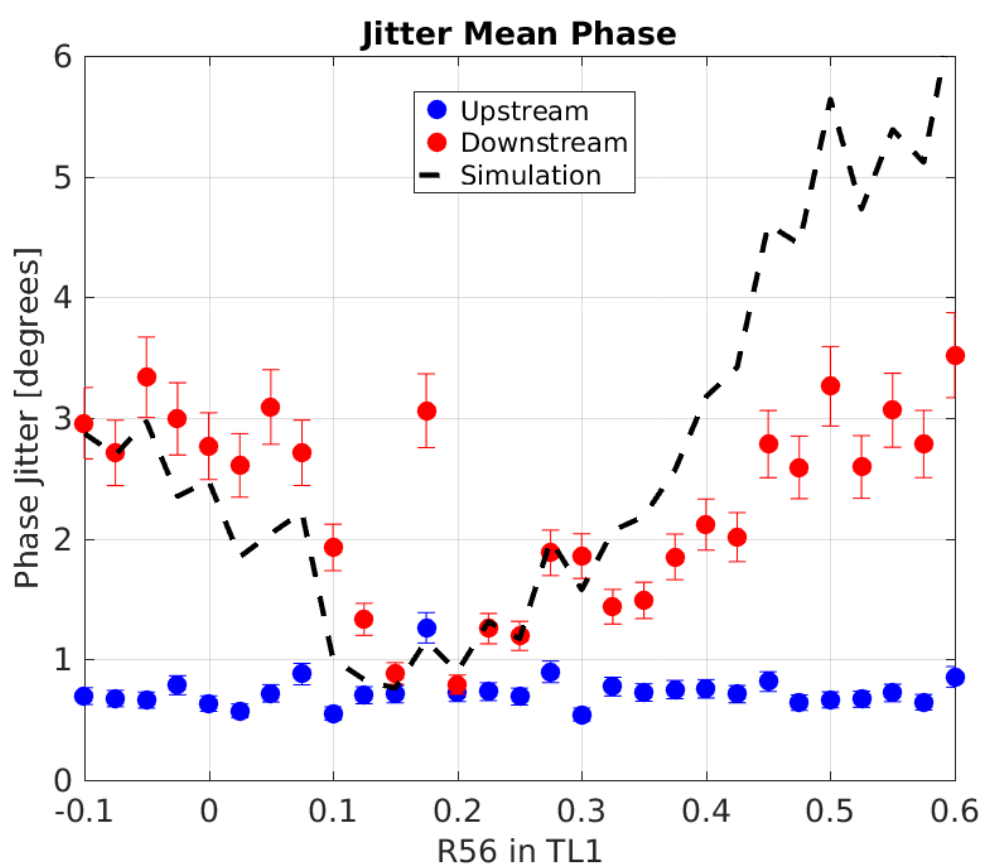


Figure 5.11: Phase jitter during scan of R56 in TL1.

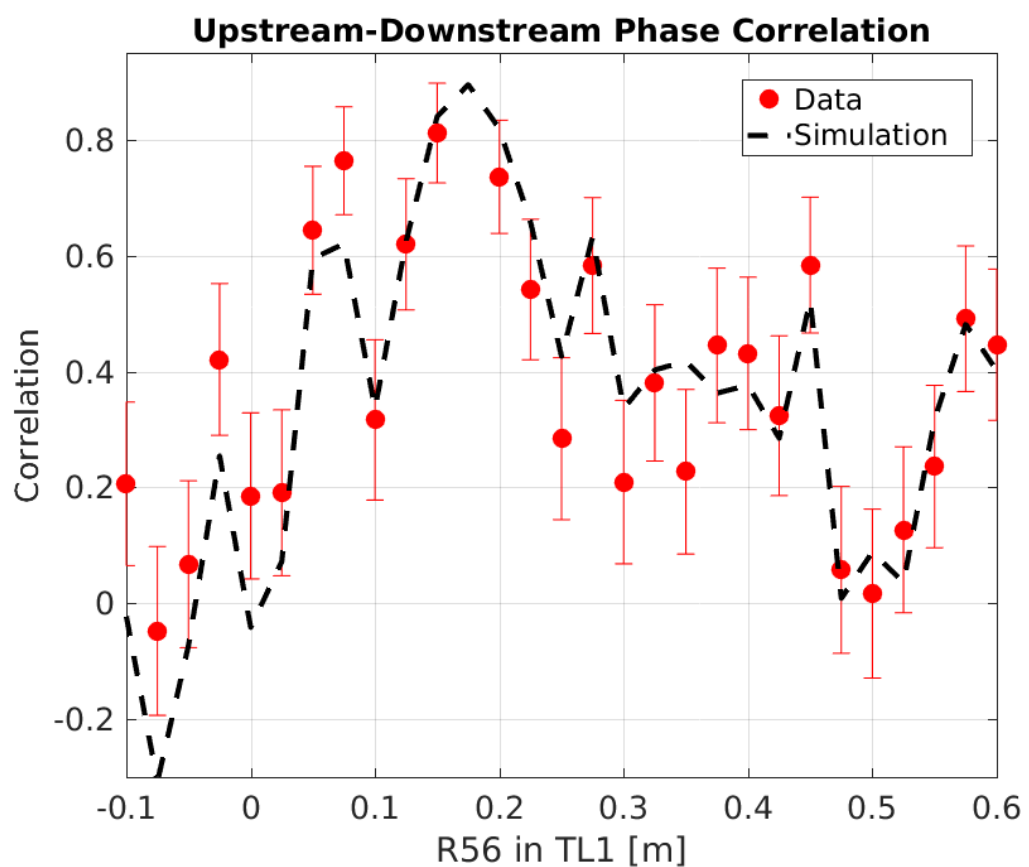


Figure 5.12: Correlation during scan of R56 in TL1.

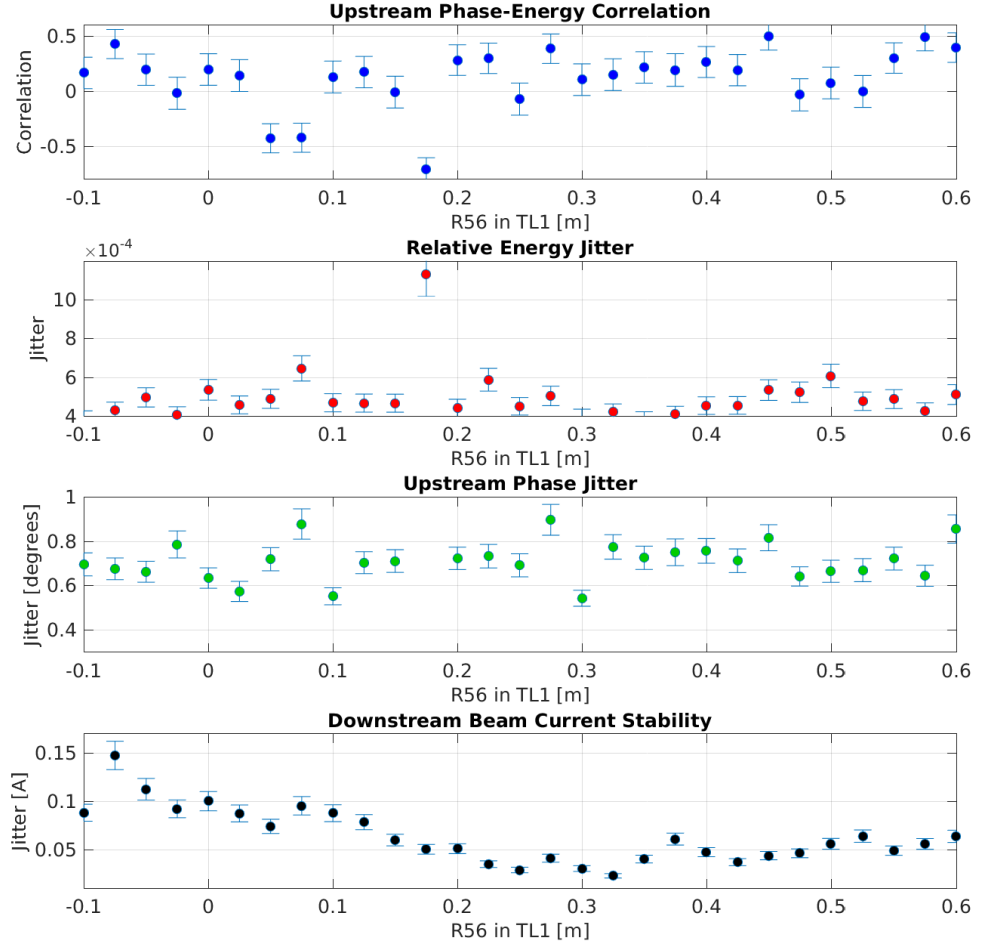


Figure 5.13: Upstream and downstream beam conditions during the R56 scan.

Possible other sources are discussed in Sections 5.5 and 5.6.

### Results from Other Scans

Figures 5.14 and 5.15 show the results of two further scans of R56 in TL1, both taken a few days after the scan previously shown. For both scans the mean downstream phase jitter can again be decreased to the level of the upstream phase jitter by varying the R56 in TL1, and the upstream-downstream correlation increased to 80%. However, the optimal optics to use is different for each scan — the scan in Figure 5.14 has an optimal R56 value of around 0.1 m whereas for the scan in Figure 5.15 the optimal value quite close to zero, around 0.04 m. Both values are also different to the scan previously shown, which had an optimal R56 setting of 0.175 m.

With R56 alone and the model of the phase propagation used to derive the equations in Section 5.3.3 there is no mechanism for the optimal R56 value to vary with time. The best conditions for the phase propagation should always be provided with zero residual R56

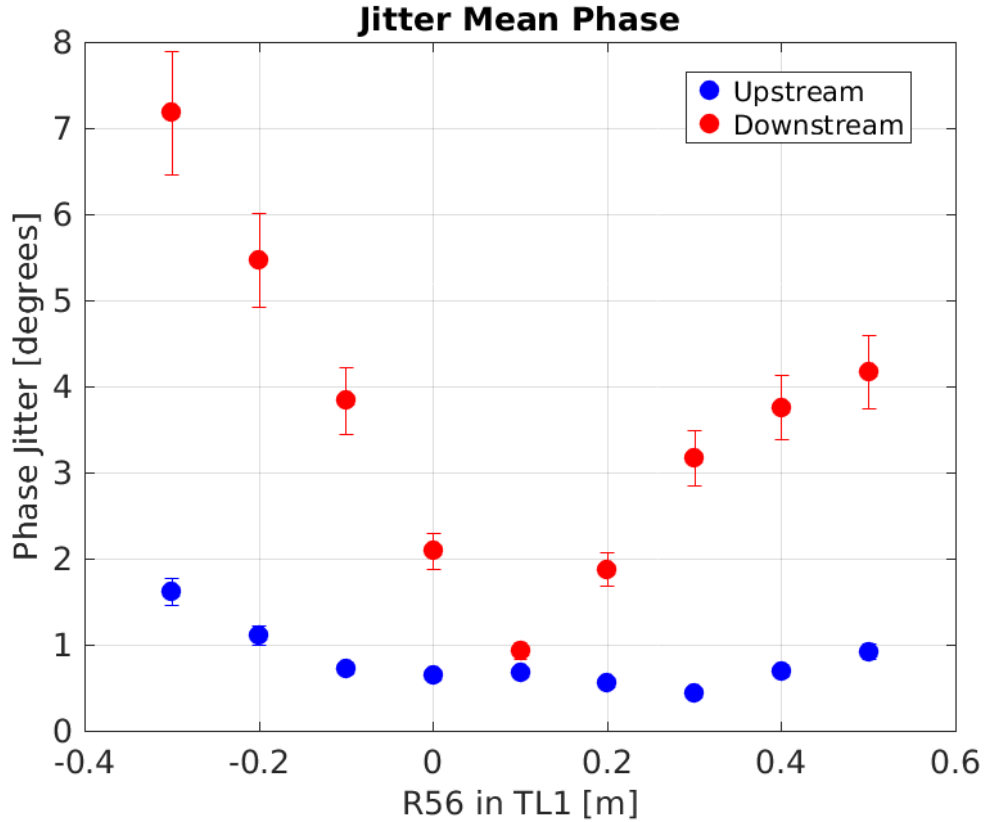


Figure 5.14: Mean phase jitter during R56 scan 2.

between the upstream and downstream phase monitors. As the optics in all beam lines between the upstream and downstream phase monitors (apart from TL1) were unchanged between each scan, the optimal R56 value in TL1 should also be the same for each scan in this model. The most likely explanation is a sensitivity to higher order energy dependencies.

## 5.5 Higher Order Energy Dependencies

In the same way the first order optics dependencies are described by the  $6 \times 6$  R-matrix, the second order effects are described using a three dimensional  $6 \times 6 \times 6$  T-matrix.  $R_{56}$  is the relevant first order transfer matrix coefficient for the energy related effects on the phase propagation, as already discussed, and it then follows that the relevant T-matrix coefficient for second order energy dependencies is  $T_{566}$ . By including the second order term the dependence of the downstream phase on the energy from Equation 5.1 becomes:

$$\phi_d = \phi_u + R_{56} \left( \frac{\Delta p}{p} \right) + T_{566} \left( \frac{\Delta p}{p} \right)^2 \quad (5.11)$$

$T_{566}$  introduces another source of energy dependent phase jitter which is independent from the first order  $R_{56}$  value. The ideal case for the phase propagation would be to have both zero  $R_{56}$  and zero  $T_{566}$  between the upstream and downstream phase monitors. However, constraints are not placed on the  $T_{566}$  in the optics at CTF3 [TODO: elaborate] and it is

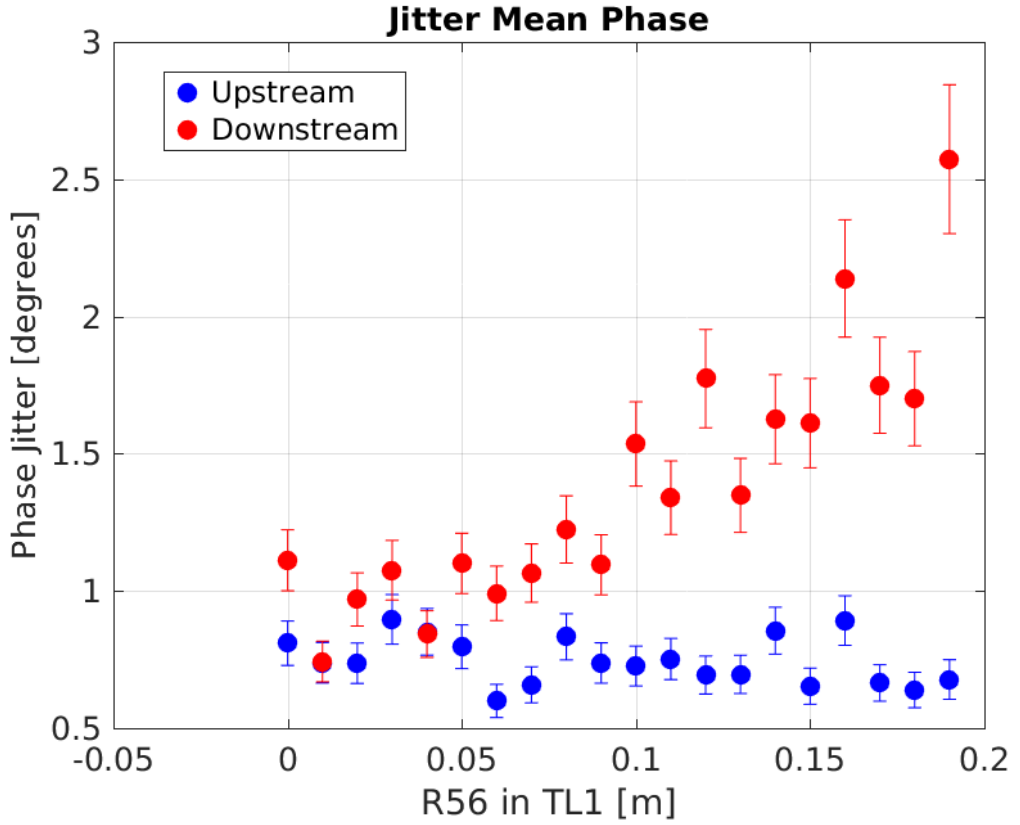


Figure 5.15: Mean phase jitter during R56 scan 3.

therefore typically non-zero. It may be possible to create optics with zero, or at least reduced,  $T_{566}$  for the TL1 and TL2 lines at CTF3 in the future but this has not yet been pursued, thus it will be treated as a fixed property of the optics here. In this case an expression for the optimal  $R_{56}$  value in terms of the  $T_{566}$  can be determined by setting  $\phi_d = \phi_u$  in Equation 5.11:

$$R_{56} = -T_{566} \left( \frac{\Delta p}{p} \right) \quad (5.12)$$

The above dependence of the  $R_{56}$  value on the beam energy offset has many consequences. Firstly, it provides a mechanism by which the apparent optimal  $R_{56}$  value in TL1 can vary with time (and be non-zero), as was seen comparing the results of different  $R_{56}$  scans in the previous section. CTF3 does experience drifts in beam energy (Section 5.3.2), creating small offsets between the actual beam energy and the energy that the optics has been set for (i.e. the strength of bending and focusing elements in the accelerator). In other words, it is possible for the mean of  $\Delta p/p$  to be non-zero. The optimal  $R_{56}$  value to use in TL1 is therefore expected to drift with the beam energy when higher order phase-energy dependencies are included.

Secondly, energy variations along the beam pulse and jitter in the beam energy mean that the phase propagation cannot be perfectly optimised by varying the  $R_{56}$  alone. Due to the energy dependence in Equation 5.12, any energy variations along the pulse cause the optimal  $R_{56}$  value to set in TL1 to also vary along the beam pulse. There are static variations

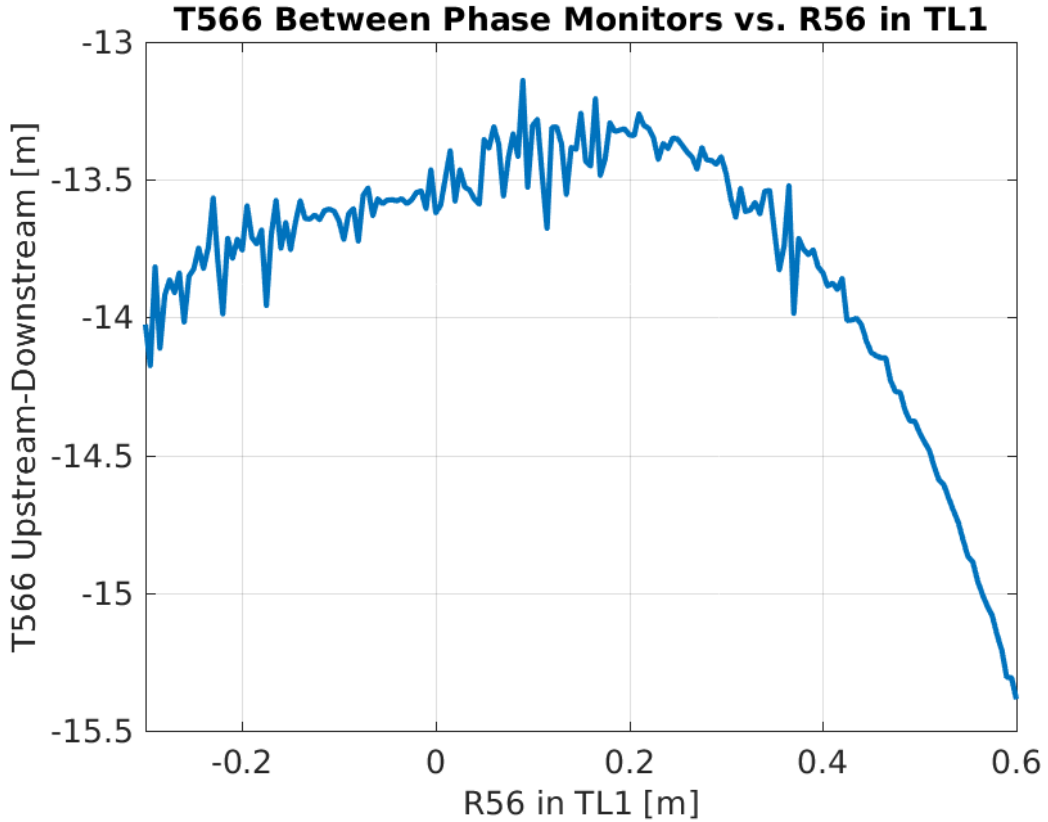


Figure 5.16:  $T_{566}$  coefficient for all sets of TL1 optics.

in the mean phase along the pulse (e.g. as seen in Section 5.3.2) at CTF3, so this means the phase propagation can never be completely optimised along the full pulse length when  $T_{566}$  is non-zero.

### 5.5.1 Expected Dependence due to Optics

### 5.5.2 R56 Scans whilst Varying Beam Energy

By intentionally varying the CTF3 beam energy to artificially increase the energy jitter during an  $R_{56}$  scan the energy dependent effects in both the upstream and the downstream phase are amplified. This has the benefit of increasing the visibility of the higher order effects, but it also improves the results of the scan in general by reducing the sensitivity to other small drifts in beam conditions. In this section the results of an  $R_{56}$  scan in which the  $R_{56}$  value in TL1 was varied between -0.1 m and +0.3 m whilst the beam energy was varied by [TODO: how much?] are discussed. Before considering the effect of the higher order dependencies directly, the overall results of the scan are presented first to expand upon the conclusions from the  $R_{56}$  scans shown in the previous sections.

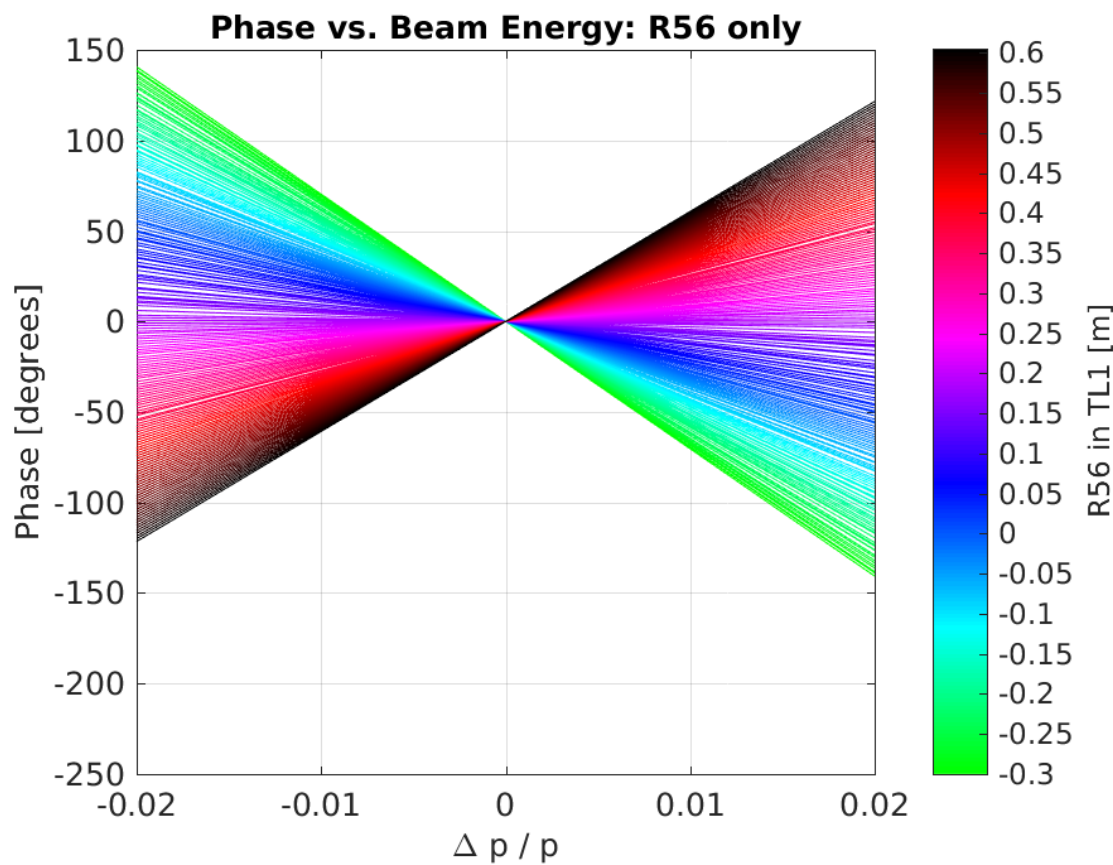


Figure 5.17: Phase shift between the upstream and downstream phase monitors for all sets of TL1 optics when only  $R_{56}$  is considered.

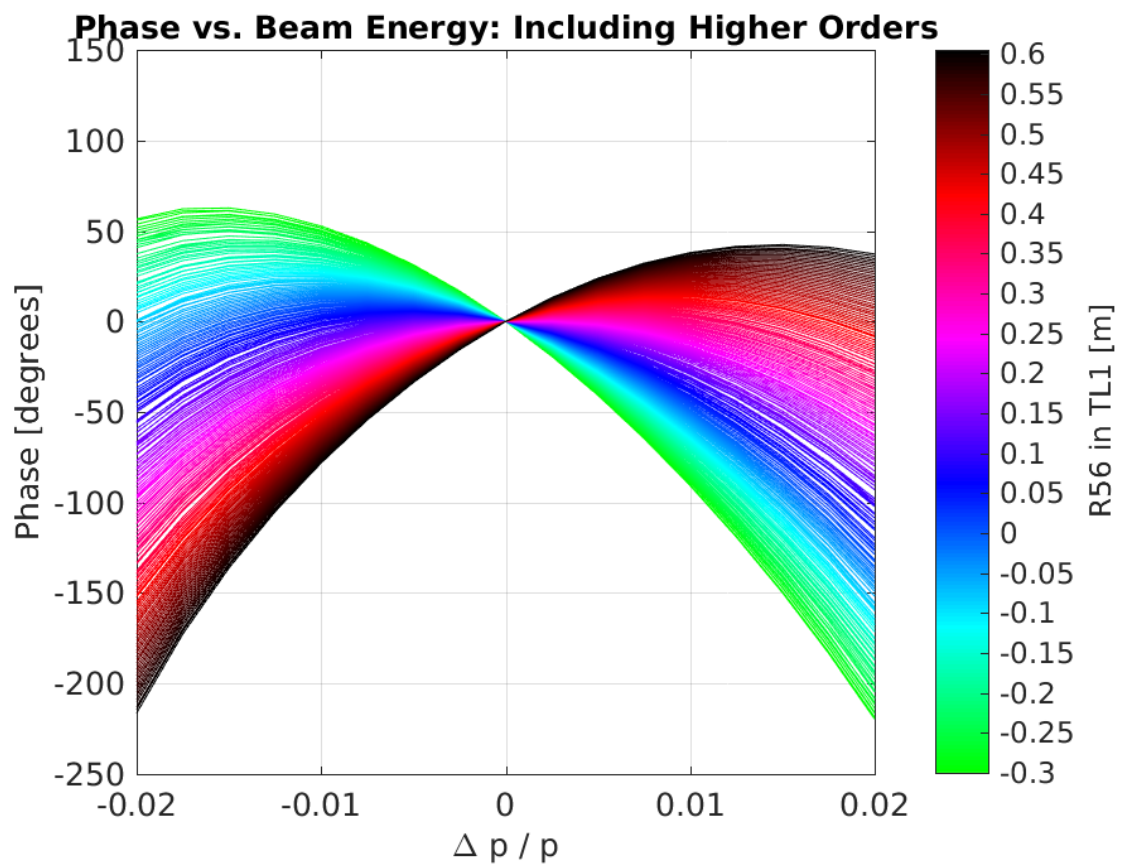


Figure 5.18: Phase shift between the upstream and downstream phase monitors for all sets of TL1 optics when both  $R_{56}$  and  $T_{566}$  are considered.

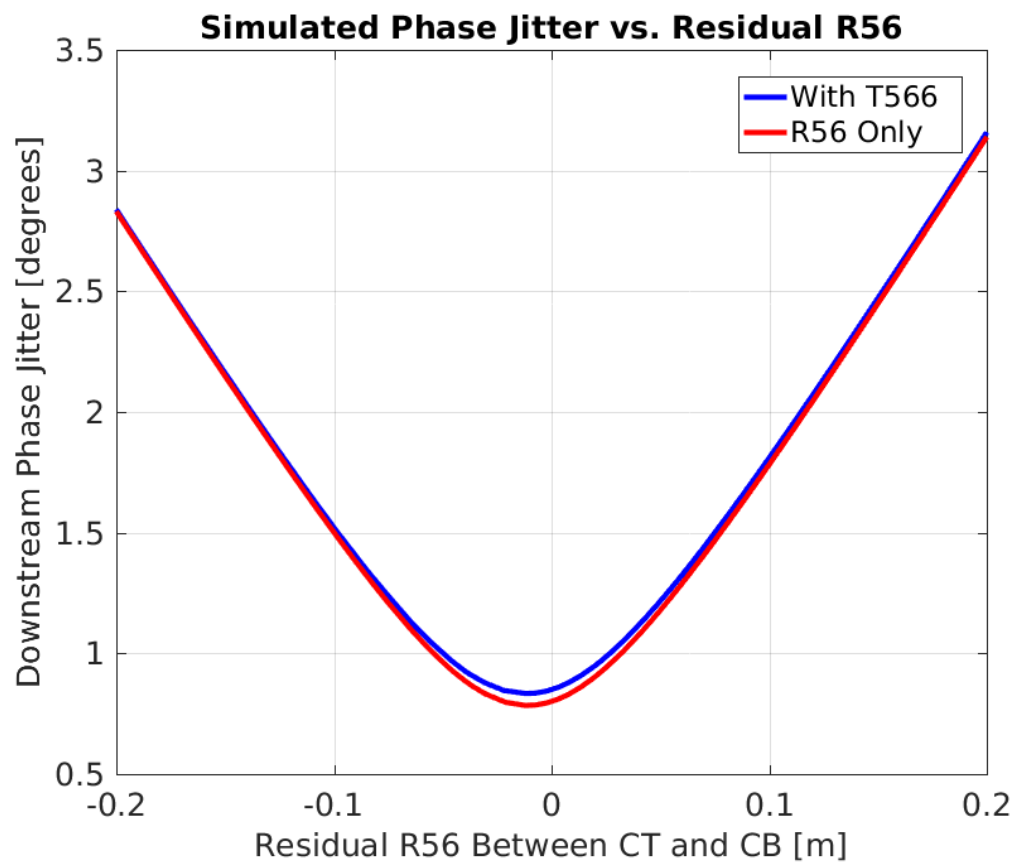


Figure 5.19: Downstream phase jitter vs. residual  $R_{56}$  in TL1 including the effects of  $T_{566}$  with  $\sigma_u = 0.8^\circ$ ,  $\rho_{up} = 0.2$  and  $\sigma_p = 1 \times 10^{-3}$ .

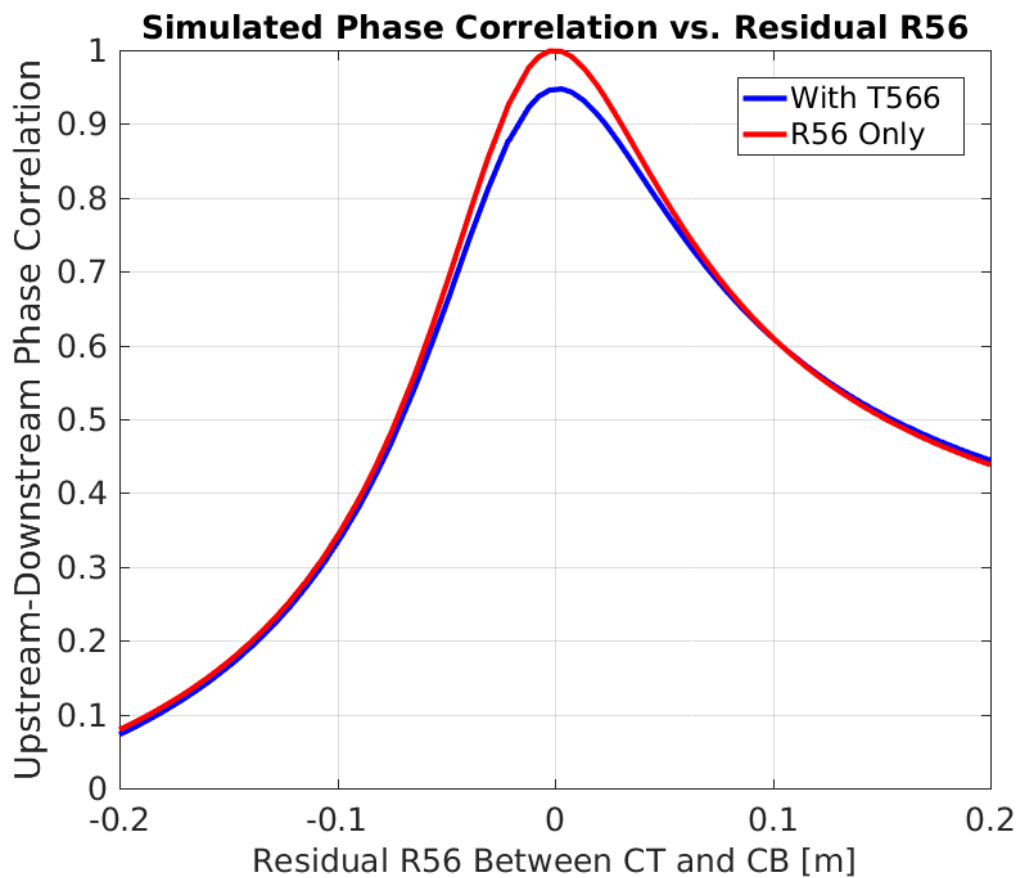


Figure 5.20: Upstream-downstream phase correlation vs. residual  $R_{56}$  in TL1 including the effects of  $T_{566}$  with  $\sigma_u = 0.8^\circ$ ,  $\rho_{up} = 0.2$  and  $\sigma_p = 1 \times 10^{-3}$ .

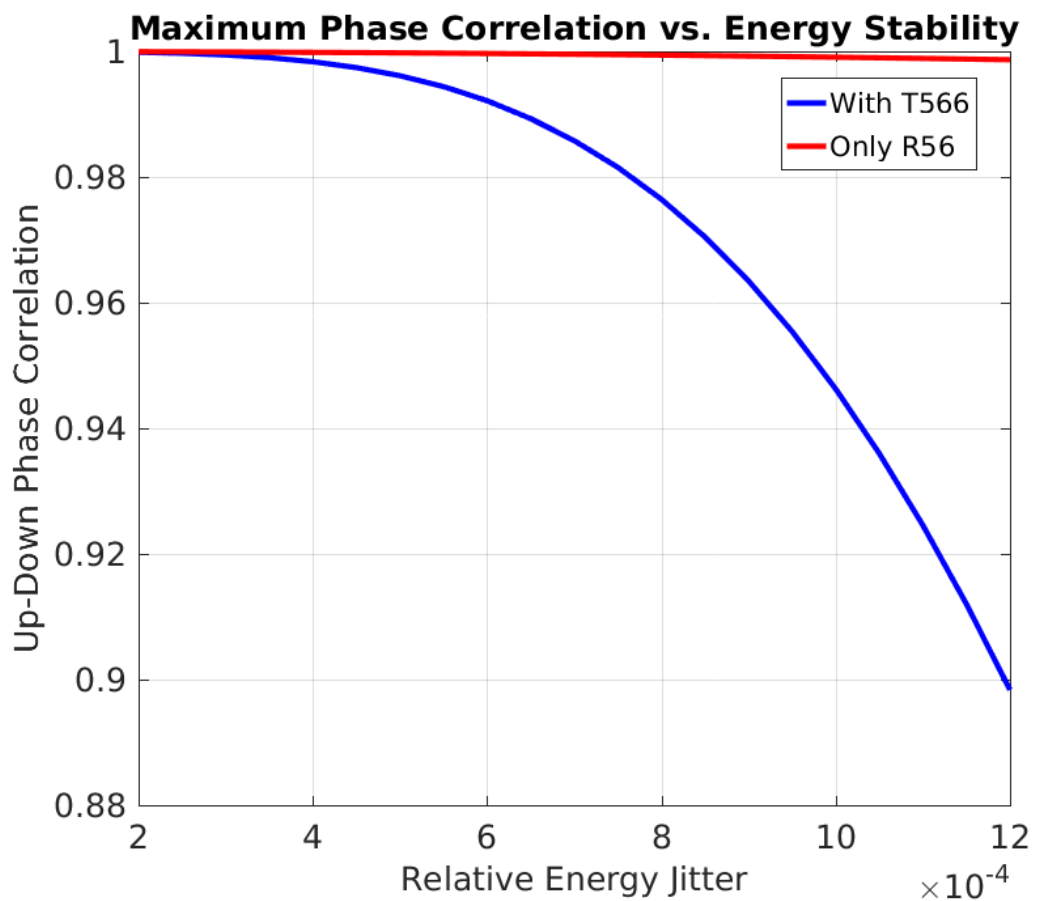


Figure 5.21: Best possible upstream-downstream phase correlation vs. beam energy jitter both with and without including the effects of  $T_{566}$ .

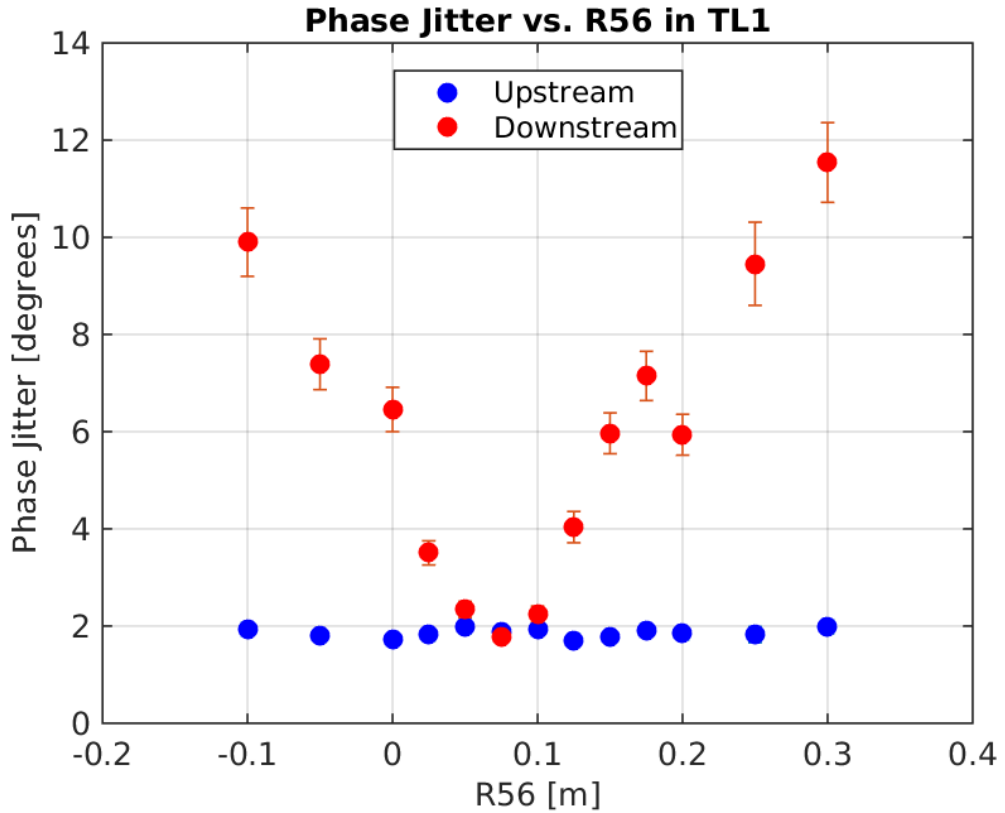


Figure 5.22: Phase jitter for different R56 whilst wiggling gun current.

### Mean Phase

upstream phase-energy plot

### Phase Along the Pulse

As well as the mean phase it is interesting to look at the effect of varying the R56 on the phase along the pulse. Figure 5.23 shows the mean phase along the pulse for each R56 setting in TL1 during the scan. Any difference in the mean (rather than the jitter) along the pulse with the R56 value should originate from static energy variations along the pulse. If the energy along the pulse was constant changing the R56 would only affect the phase jitter and would not change the mean pulse shape. The clear change in certain features along the pulse in the downstream phase is therefore an indication of energy variations in these regions. Perhaps the best example of this is the oscillation around a time of 800 ns, where the phase is flat close to the optimal R56 value of 0.1 m but swings upwards when a negative R56 in TL1 is used or downwards for R56 values above 0.1 m.

The difference between the phase along the pulse for two different settings of R56 in TL1 should be proportional to the beam energy along the pulse. Figure 5.24 plots the difference between the R56 = +0.3 m optics and the roughly optimal R56 = +0.1 m optics, and compares this to the beam energy along the pulse (measured using the horizontal beam position in the dispersive BPM after the first dipole in TL1). Both lines are mean subtracted

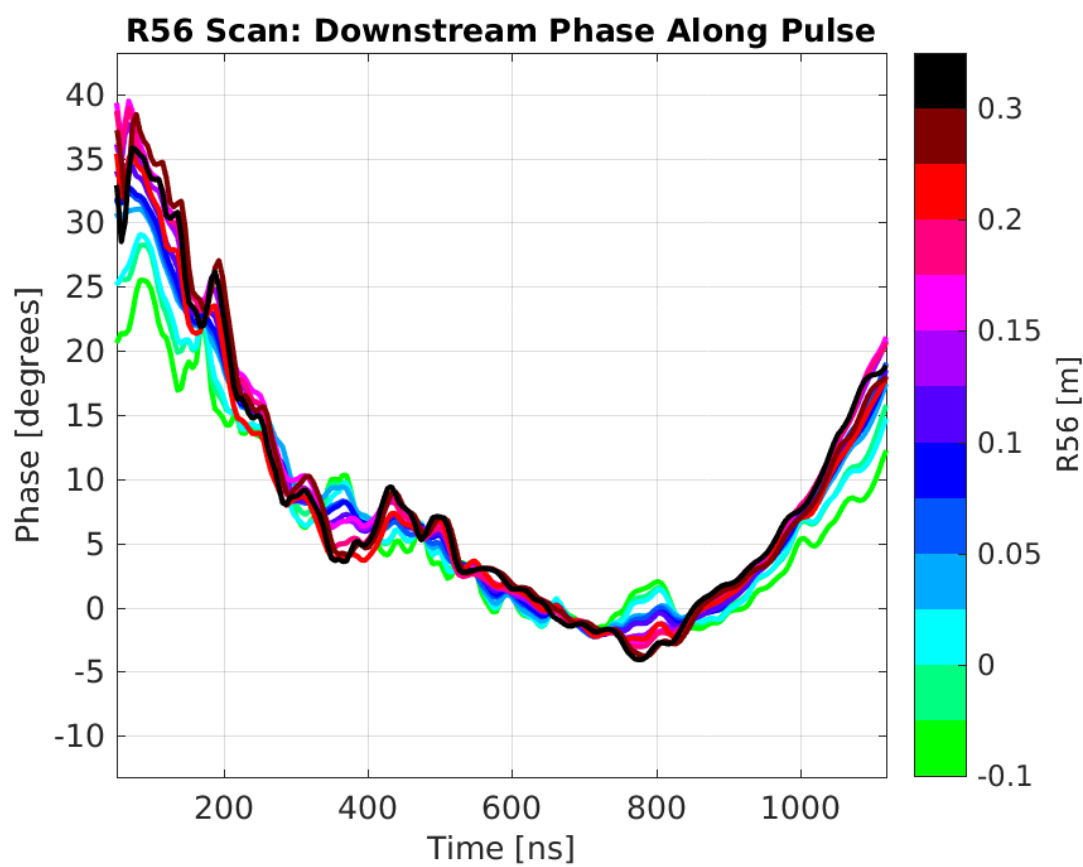


Figure 5.23: Mean downstream phase along the pulse for different R56 values.

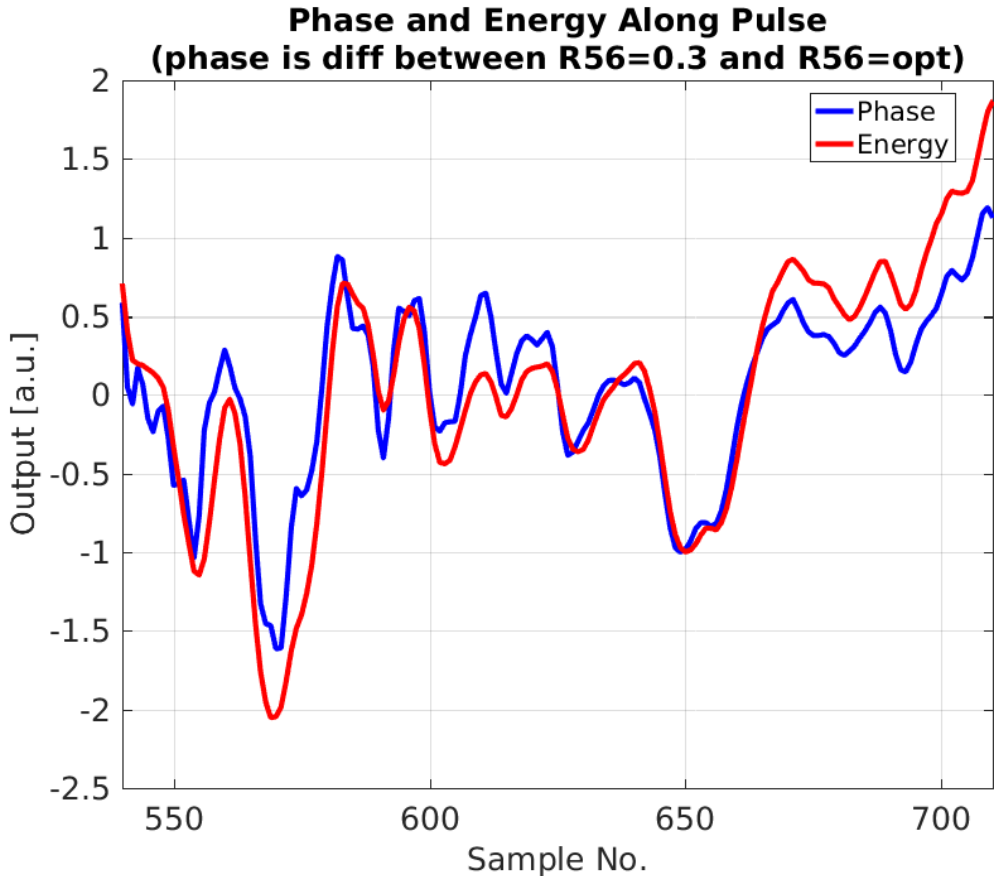


Figure 5.24: Mean downstream phase along the pulse for different R56 values.

and normalised to give equivalent amplitudes in arbitrary units. For reference the peak to peak beam position offset along the pulse is 1.6 mm in this case, corresponding to a relative energy offset along the pulse of  $2.3 \times 10^{-3}$ . Overall, the differences in phase along the pulse resulting from using non-optimal R56 in TL1 are very well matched with the energy variation along the pulse, as expected.

[TODO: comparison of upstream and downstream phase along the pulse]

[TODO: Jitter along the pulse]

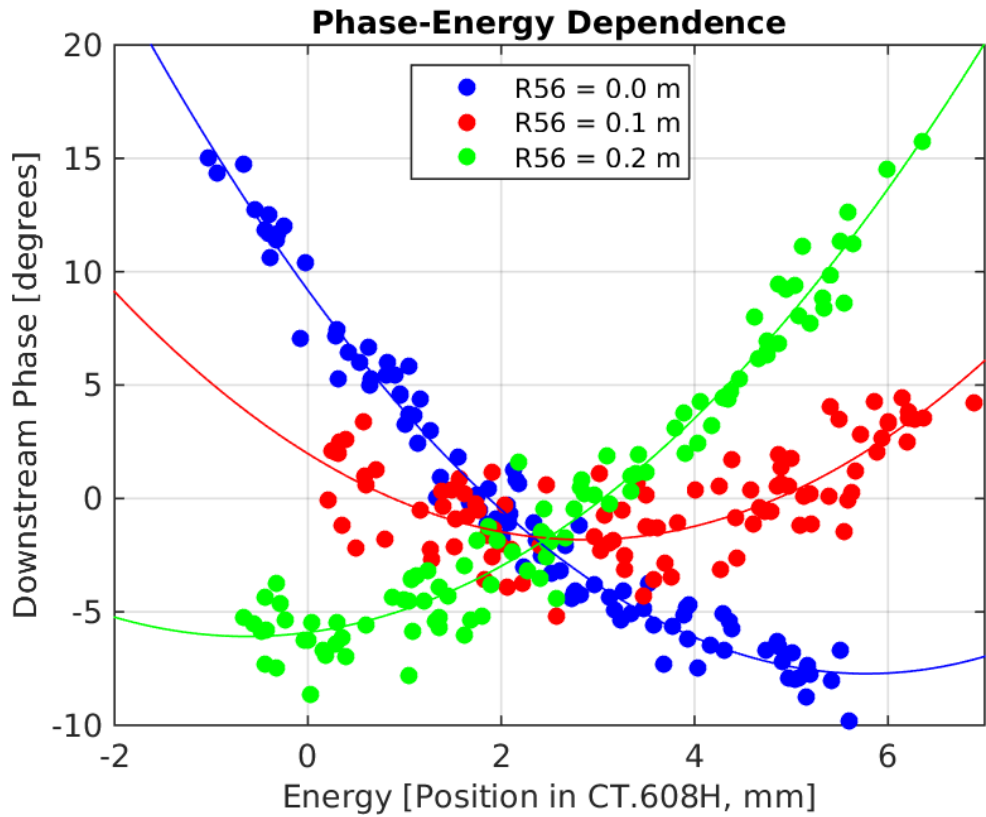


Figure 5.25: Phase vs. energy for different  $R_{56}$  in TL1.

## Higher Order Effects

### 5.5.3 Mitigation of Higher Order Dependencies

### 5.5.4 Effect on PFF Operation

## 5.6 Other Sources of Phase Jitter

### 5.6.1 Combiner Ring Septum

### 5.6.2 TL1 & Combiner Ring Bends

RF Deflector

CR Septum

TL1/CR Bends

## 5.7 Best Phase Propagation

some kind of drift analysis of drift sources to be able to refer back to it in long PFF results section

# Chapter 6

## Setup and Commissioning of the PFF System

This is the introductory text. [1]

### 6.1 Feedforward Controller (FONT5a Board)

#### 6.1.1 Installation

Trigger

ADC1

ADC2

Serial

Amp trigger out

DAC1

DAC2

#### 6.1.2 Setup Parameters and DAQ

The FONT5a board is controlled using a LabVIEW data acquisition system (DAQ) documented in [REF]. An example screenshot from the DAQ is shown in Figure 6.2 [TODO: get a better picture]. It provides functionality to change all the setup parameters in the FONT5a firmware for the PFF system setup, view the current ADC inputs and DAC outputs in real time and to save data directly from the FONT5a board. However, as the FONT5a board and DAQ currently run as a standalone system at CTF3, rather than directly saving data from the FONT5a board PFF data is usually saved via the CERN control system and SiS digitisers where data from other devices, such as BPMs, can be saved in sync with the phase



Figure 6.1: Front panel of the FONT5a board.

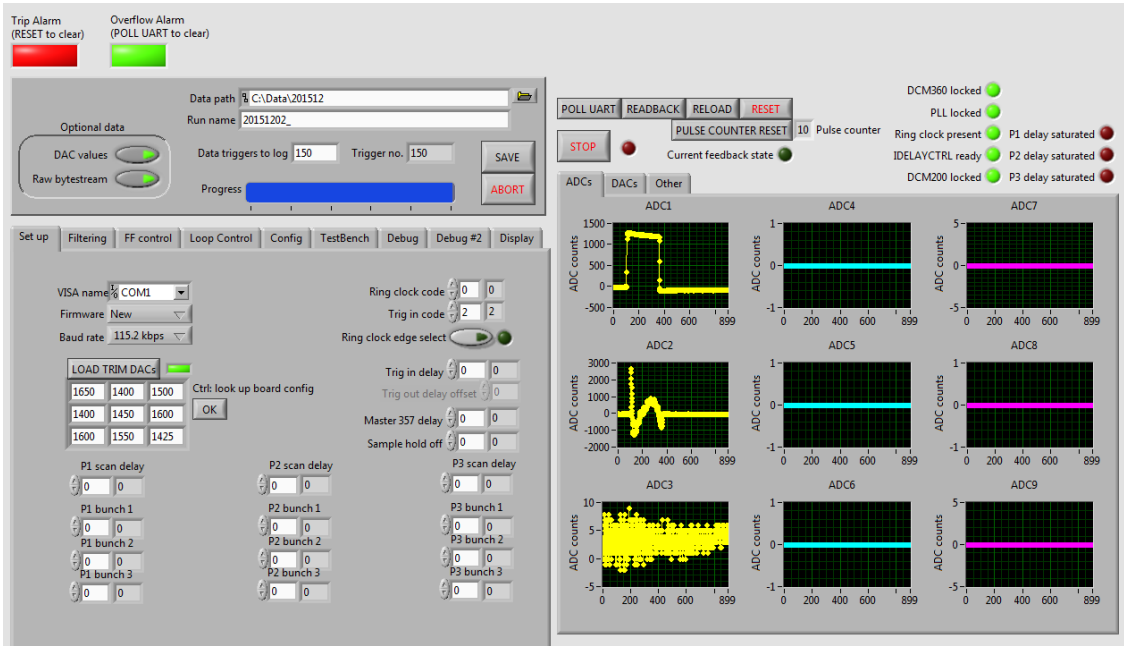


Figure 6.2: Diode output along the pulse with the IIR filter off and on.

monitor signals as discussed in Section 6.3. The DAQ runs on a Windows PC next to the racks used for the phase monitor electronics, FONT5a board and amplifier. The PC can be connected to via remote desktop to allow the FONT5a board to be controlled in the CTF3 control room.

All the parameters and controls that must be adjusted during the PFF system setup, and their respective values where relevant, are listed below for reference. These are only introduced in brief here, but parameters that are either non-trivial to derive or are critical for the PFF performance are described in more detail in later sections and chapters as indicated. The values given are in FONT units as they are set in the DAQ with each parameter expressed by up to a 14 bit number, and the size of each control chosen to give a reasonable degree of flexibility around the expected set point.

[TODO: Order a bit strange. Maybe some not needed. Table of values? Units for some of them - like trig in delay?]

**Trig in delay:** The Trig in delay allows the start of the ADC sampling window to be delayed with respect to the arrival of the external trigger. Timing of the trigger and correction outputs to the amplifier (Trig out delay and K1/K2 delay) are relative to this delay, therefore changing the Trig in delay value does not effect the synchronisation of the correction output with the beam. The only requirement is to ensure that the full acquired upstream phase monitor signals arrive within the sampling window. A value of 2500 is typically used to achieve this. [TODO: Check value is correct.]

**Trim DACs:** The FONT5a board contains DACs, referred to as Trim DACs, prior to each ADC [REF]. By varying the input sent to the Trim DACs the baseline of each ADC channel can be adjusted in order to remove any intrinsic voltage offset in their output. For ADC1 (Diode) and ADC2 (Mixer) the Trim DAC values are 1650 and 1400 counts,

respectively.

**Filter Weights:** IIR filters are implemented in the FONT5a firmware in order to remove droop in the ADC response, see Section 6.1.3. The filter weights for each ADC can be adjusted in the DAQ. The correct values are 50 for ADC1 (Diode) and 56 for ADC2 (Mixer).

**Trig out enable:** The trigger sent to the amplifier can be enabled or disabled as required. Clearly the trigger must be enabled for any correction output to have an effect on the beam (the PFF correction output can be turned on with the amplifier trigger disabled for testing purposes).

**Trig out delay:** The timing of the trigger sent to the amplifier can be delayed with respect to the start of the ADC sampling window. This must be adjusted so that the arrival of the  $1.1 \mu\text{s}$  beam pulse at the kickers is aligned with the  $1.4 \mu\text{s}$  time during which the amplifier is powered and the correction output can be applied. [TODO: Section/plot showing how?]. A value of 110 is typically used. The precise correction timing is set by the K1 and K2 delays below.

**Gate enable:** The correction output can be restricted to a certain sample range by applying a “gate”. The gate can be defined either as a custom sample range picked by the user or the diode signal (ADC1) can be used. Diode gating is typically used so that no output is sent to the amplifier outside the time of the beam pulse. Using a custom sample range has been useful for early PFF tests and to apply a constant kick along only part of the beam pulse (this is used in Section 6.5.3, for example).

**Feedforward enable:** The DAC output can be enabled or disabled, as required.

**Interleaved mode:** With interleaved mode enabled the DAC outputs from the FONT5a board are only sent for half of the triggers, for example being applied to all the odd pulses but not sent for all the even pulses. This is incredibly useful for interpreting the PFF results, as well as being used for many of the other tests presented in this thesis, as it allows a comparison between beam conditions with and without an applied kick at the same time. In this case the effects of any slow drifts should be equivalent in both the kicked and non-kicked data, thus any differences between the two should be a real effect of the PFF system. Data with the DAC output disabled can also be used to simulate the expected effect of the PFF system in those conditions. All the PFF results in Chapters 7 and 8 use interleaved data.

**K1, K2 delay:** The K1 and K2 delay are used to fine tune the timing of the two correction outputs (DAC1/K1 for the first kicker and DAC2/K2 for the second kicker), and can be varied by up to 32 ADC clock cycles (2.8 ns per clock cycle at 357 MHz). The optimal delays are 7 clock cycles for K1 and 7–8 clock cycles for K2. The importance of the correction timing and derivation of these values is presented in Section 6.5.

**DAC Output Mode:** The DAC output to the amplifier can be sent in two modes — Sample-by-sample or Constant DAC. In Sample-by-sample mode the DAC output is as needed for the PFF system, being shaped along the pulse by the reconstructed phase (the mixer on ADC2 and, if used, the diode on ADC1) multiplied by the set gain. More details are given in Section 6.1.4. In Constant DAC output mode a constant output voltage can be sent to the amplifier across the full length of the ADC sampling window (or for a shorter

time with an applied gate). The majority of the results presented in the remainder of this chapter use constant DAC outputs for verification of the amplifier, optics, correction range and correction timing.

**K1, K2 const DAC:** Constant DAC values can range between  $\pm 4096$  counts, or  $\pm 2$  V sent to the amplifier, and can be varied independently for each output.

**Gain:** The PFF gain can also be set independently for each correction output, with each being a 14-bit value ( $\pm 8192$  units). The conversion between the gain in FONT units and the real applied gain is derived in Section 6.1.4. An applied gain of 624 units corresponds to a real gain of approximately 1 (with a gain of 624 an upstream phase offset of 1 degree corresponds to a downstream phase correction of approximately -1 degrees).

**Channel Offset:** To maximise the effect of the PFF system it is necessary to zero the mean upstream mixer (ADC2) output in the central region of the pulse where the correction is being attempted (the start and end of the pulse can not be fully corrected due to the large phase sag, so the central portion is usually used). Ideally this should be adjusted by varying the Mon1 phase shifter, but this can not be done remotely so the channel offset on the FONT5a board can be used instead to make small adjustments from the control room. For large phase offsets giving close to maximum mixer output the phase monitor resolution is degraded (Section 4.6) and the small angle approximation used in the FONT5a phase reconstruction (Section 6.1.4) becomes invalid, in which case the phase shifter should still be used to zero the phase. The channel offset adds a static offset in counts to the ADC2 output, allowing the mixer output to be zeroed at any point along the pulse. The consequences of using a non-optimal Channel Offset are discussed in Section 8.2.1.

**Diode Mode:** The FONT5a firmware provides three modes for the treatment of the diode signal on ADC1 — normalisation, gating and unused. With diode normalisation enabled the PFF system reconstructs the phase as originally envisaged using Mixer/sqrt(Diode). Due to the issues with the phase monitor diodes as discussed in Chapter 4 the option to not include the diode in the PFF calculation and only include the mixer was later added. Rather than leaving the diode completely unused, it is usually used to gate the correction output as mentioned above.

**Overflow Mode:** The PFF correction output can behave in three ways in the case where the calculated output is outside the maximum range of  $\pm 4096$  DAC counts. In the first iteration of the PFF firmware the calculated correction output would overflow, causing sign flips in the output in the regions where the correction range was exceeded. This behaviour can still be applied in the current firmware if desired. However, in normal operation the output is set to Saturate, so that any calculated values outside  $\pm 4096$  DAC counts are sent as the maximum  $\pm 4096$  DAC counts or  $\pm 2V$  to the amplifier. A final option to provide no output at samples where the calculated output is outside  $\pm 4096$  DAC counts, is also provided.

**Enabled channels:** The FONT5a board has 9 ADCs but only two are usually needed for the PFF system (for the mixer and diode of Mon1 connected to ADC1 and ADC2, with the other two monitors normally connected to the SiS digitisers). To avoid hitting the limits of the baud rate [TODO: value?] of the RS232 port on the PC the remaining ADC channels

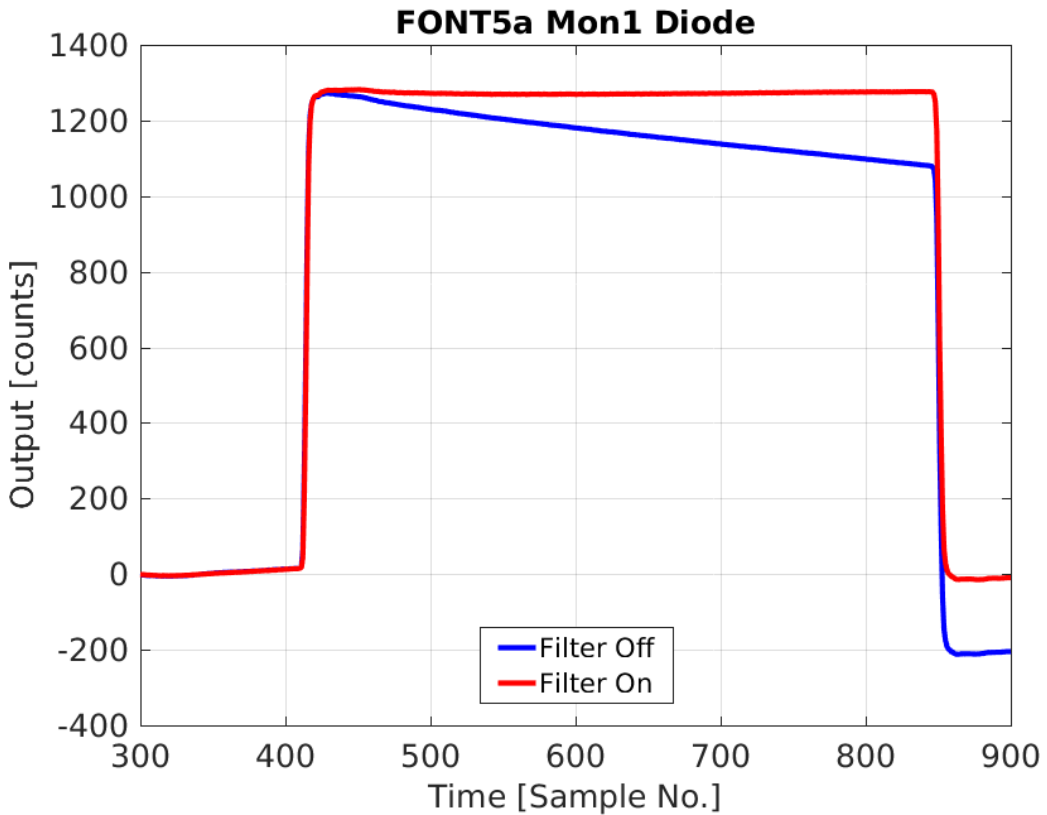


Figure 6.3: Diode output along the pulse with the IIR filter off and on.

can be disabled so their data is not transmitted.

**No. samples:** The length of the ADC sampling window, in number of samples, can also be varied. Typically 900 samples are used, covering a time window of  $2.5 \mu\text{s}$  with the 357 MHz clock. If the signal from more than two ADCs is needed the number of samples can be reduced to avoid hitting the baud rate limit of the RS232 port on the PC, the only requirement is that the time window is long enough to encompass the full  $1.1 \mu\text{s}$  beam pulse length.

### 6.1.3 ADC Droop Correction

Although the FONT5a (and previous FONT5) boards have been (and still are) used extensively at ATF2, KEK for IP feedback tests by the FONT group [REF] prior to its application for the PFF system, it had not been routinely used to process long, microsecond like, pulse lengths such as the CTF3 beam signals. During the first tests of the FONT5 board at CTF3 (prior to the FONT5a board being available) it was immediately apparent that there was a large droop in the measured phase monitor diode outputs using the FONT ADCs. An example of this, taken from the FONT5a board, is shown in Figure 6.3, remembering that as the diodes are highly saturated the response should be close to a perfect square wave. The measured diode output droops by 200 counts (approximately 15%) across the pulse length, with this difference also visible as an offset in the baseline after the pulse.

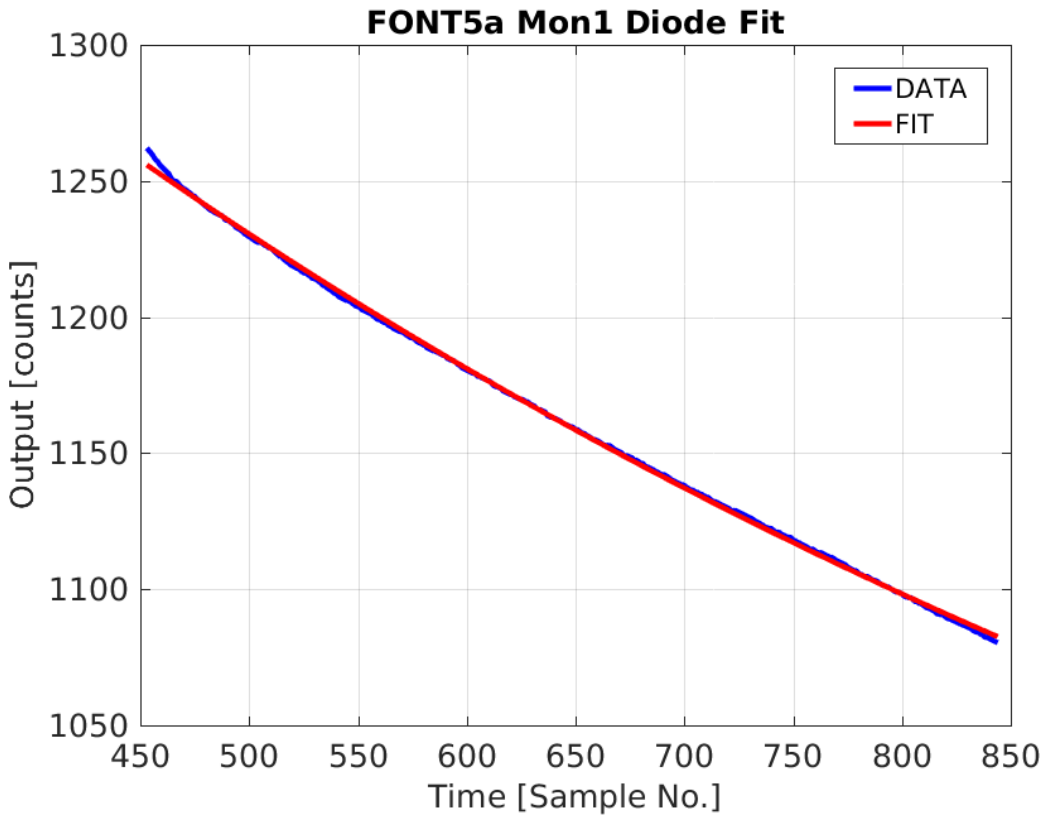


Figure 6.4: Exponential fit to diode droop.

The droop emerges as a result of the use of AC coupling on the ADC input transformers for electrical isolation. This involves using a capacitor, the current across which is dependent on  $dV/dt$  ( $V$  being voltage and  $t$  time), to remove the DC component (or mean offset) from a signal [REF]. In particular for the diode channel the output is increasingly well described by a DC signal on the flat top as you move away from the leading edge of the pulse, with the capacitor causing droop in the response as a result. There is also a small effect on the mixer output, as will be seen later. [TODO: Is the effect on the diode and mixer really different? Is this correctly taken in to account by the IIR filter?]

In the simplest case the droop should be well described by an exponential decay of the form  $A \exp(-t/\tau)$ , where  $t$  is the time or sample number along the pulse and  $\tau$  is the decay time constant. For the FONT5 board this only gave a rough approximation of the true droop characteristics due to non-linear properties of the input transformers. On the updated FONT5a board the transformers were changed to both reduce the magnitude of the droop and give closer to the expected exponential decay [REF]. Figure 6.4 shows an exponential fit to the Mon1 diode output as seen on the FONT5a board (ADC1). Apart from a small deviation at the beginning of the pulse the agreement is excellent, with residuals to the fit of only up to 2 counts compared to a signal magnitude of 1250 counts. For ADC1 the fitted decay time constant is  $\tau = 838 \pm 16$  samples, or  $2.35 \pm 0.05 \mu\text{s}$  (with one ADC sample every 2.8 ns at 357 MHz). Each ADC on the FONT5a board has slightly different droop characteristics, with the decay time constant for ADC2 being  $938 \pm 18$  samples, for example (calculated with the diode moved on to ADC2).

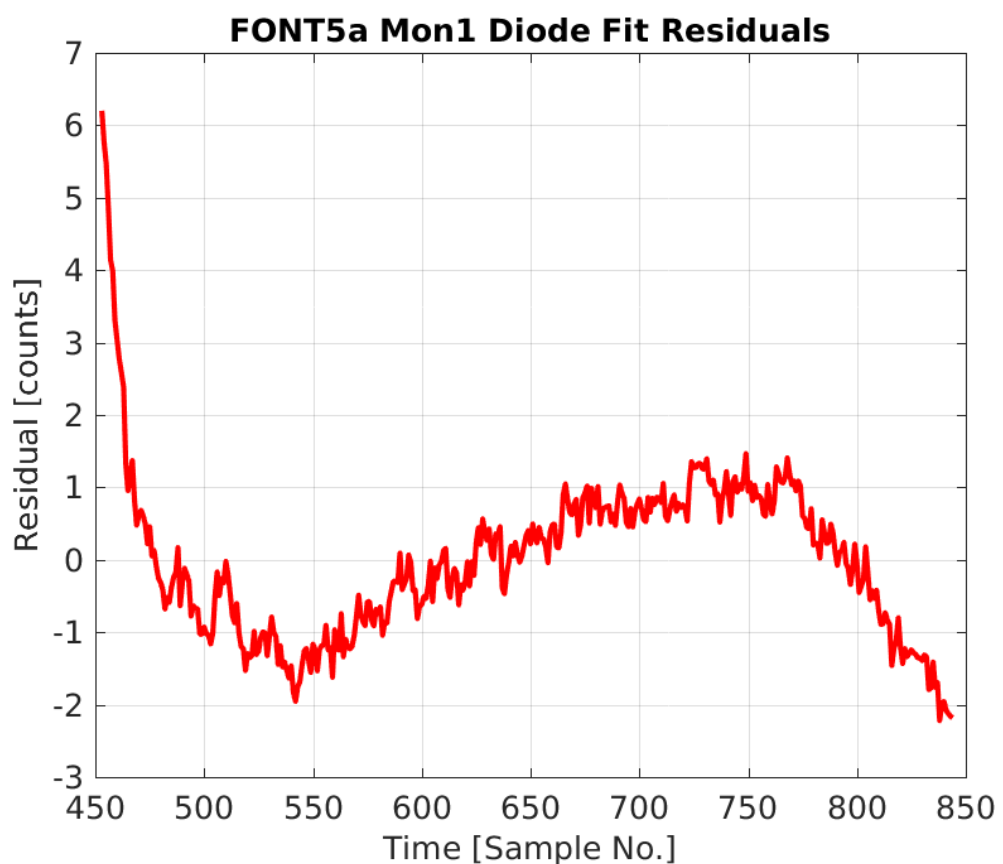


Figure 6.5: Residuals between diode exponential fit and actual diode output.

ADC	Filter Weight
1 (Mon1 Diode)	50
2 (Mon1 Mixer)	56
3	50
4	53
5	45
6	51
7	48
8	55
9	49

Table 6.1: IIR filter weights for the FONT5a board ADCs.

In the case where the diode is used in the phase reconstruction as originally envisaged the ADC droop would propagate in to the applied correction and create an output to the amplifier that increases with time with respect to the ideal value (as the Mixer is divided by  $\text{sqrt}(\text{Diode})$ ). The effect on the correction is much smaller without diode normalisation but it still slightly distorts the measured Mixer input to ADC2. Therefore, a digital IIR filter has been implemented in the FONT5a board firmware to remove the exponential droop in the ADC outputs [REF]. This works by recursively adding the expected droop to the ADC output based on the known decay constants, so that:

$$y(t) = x(t) + \frac{1}{\tau} \sum_{i=1}^t x(i-1) \quad (6.1)$$

Where  $y(t)$  is the filtered ADC output at sample  $t$ ,  $x(t)$  is the original unfiltered output at sample  $t$ , and  $\tau$  is the decay time constant. Rather than being hard-coded in the firmware the applied decay constant in the filter for each ADC is calculated using an 8-bit  $\pm 64$  filter weight, which can be changed in the DAQ, which is then divided by a common division factor to get the real applied value of  $1/\tau$  [REF]. The optimal filter weights for each ADC in the FONT5a board currently used for PFF operation are shown in Table 6.1, these can be converted in to the true decay constant values using the fitted values for ADC1 and ADC2 quoted above.

With the IIR filters enabled on the FONT5a board the droop on the diode (ADC1) is almost perfectly removed as shown in Figures 6.3 and 6.6, although in the zoomed in figure some slight deviation from flat is visible due to the residuals around the exponential fit seen previously. The effect on the reconstructed phase using only the mixer (ADC2) is shown in Figure 6.7, with a modest adjustment to the overall shape that is most visible at the start and end of the pulse.

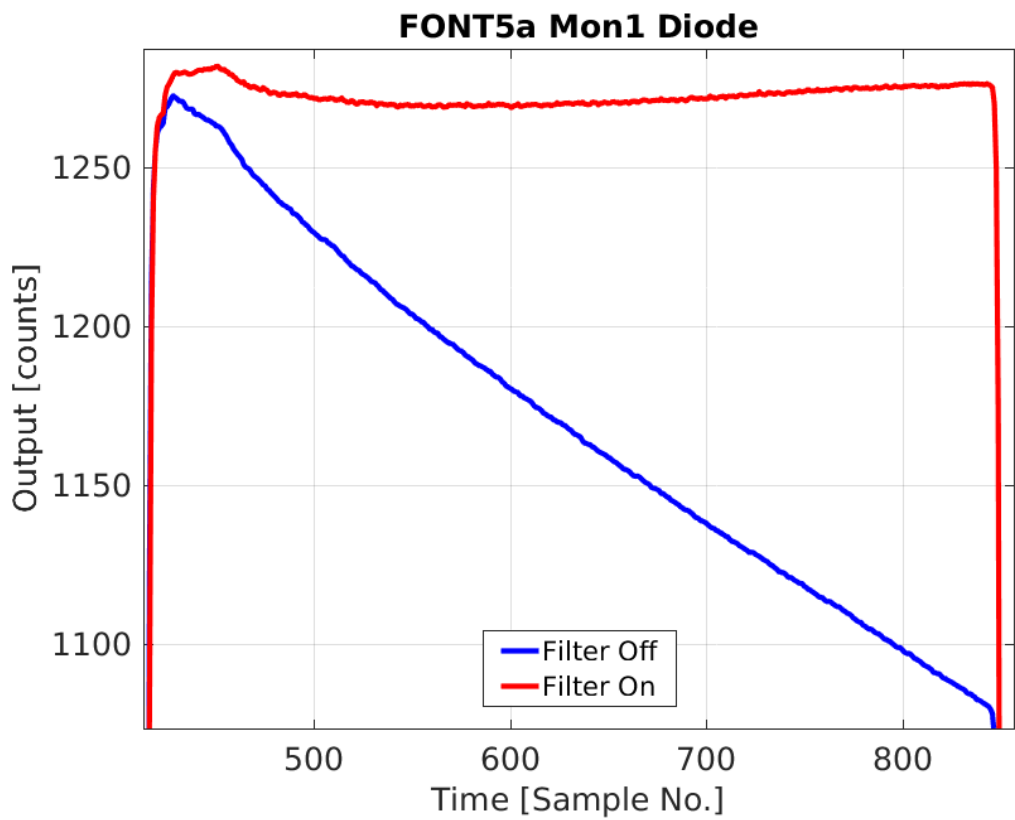


Figure 6.6: Diode output along the pulse with the IIR filter off and on. Zoomed in.

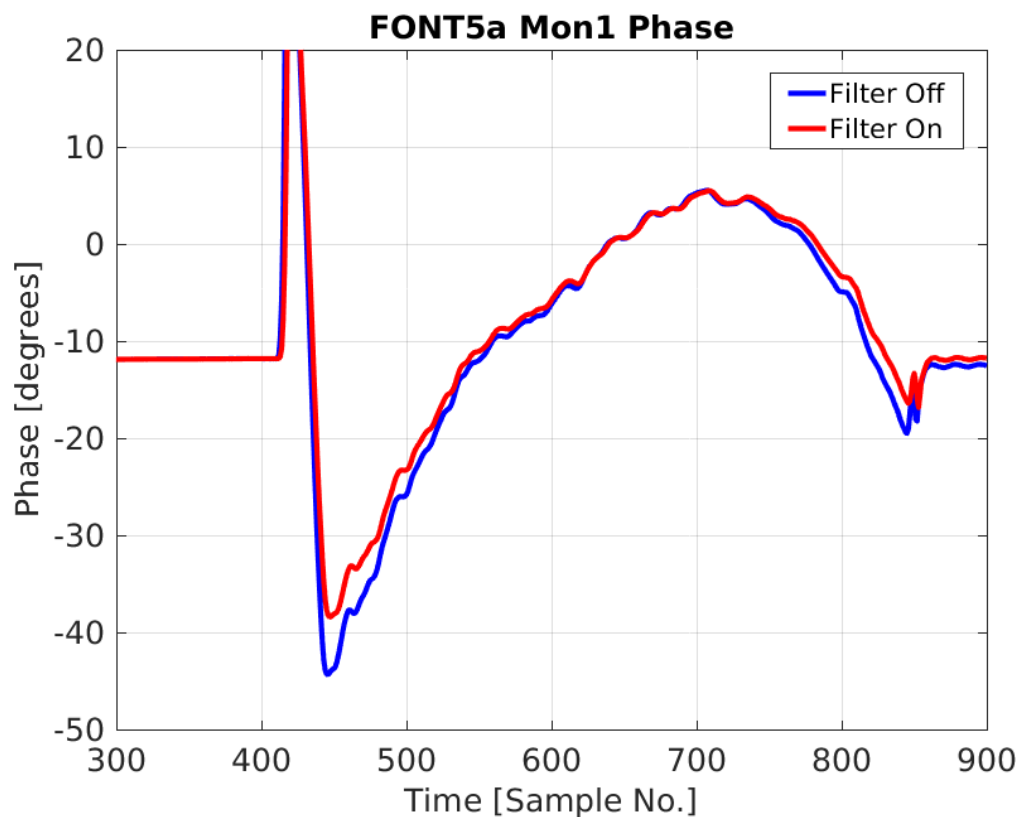


Figure 6.7: Phase along the pulse with the IIR filter off and on.

### 6.1.4 Implementation of PFF Algorithm in Firmware

As shown in Section 2.5 the effect of the PFF system can be modelled by simply subtracting the measured upstream phase,  $\phi_u$ , from the downstream phase,  $\phi_d$  with a gain factor,  $g$ :

$$\phi_{PFF} = \phi_d - g\phi_u \quad (6.2)$$

Where  $\phi_{PFF}$  is the corrected downstream phase. The way this algorithm is implemented in the FONT5a board firmware is discussed in this section, highlighting some important aspects of the gain calculation and the phase reconstruction using the input phase monitor signals.

In the case where diode normalisation is not used, which is the nominal setup, the FONT5a DAC outputs when the PFF system is enabled are given by:

$$\begin{aligned} \text{DAC1} &= \frac{F1}{64} \text{ADC2} \\ \text{DAC2} &= \frac{F2}{64} \text{ADC2} \end{aligned} \quad (6.3)$$

Where DAC1 and DAC2 are the two DAC outputs, in DAC counts, F1 and F2 are the respective gains for each DAC output set in the DAQ, and ADC2 is the Mon1 mixer signal level in ADC counts, which is connected to ADC2 for normal PFF operation. The whole calculation uses 16-bit architecture, with the 3 sub-integer bits discarded when sent to the 13-bit DACs. The FONT gains F1 and F2 are 14-bit ( $\pm 8192$ ) and the common division factor of 1/64 is set by several parameters fixed in the FONT5a firmware in order to give a sensible range of gain values based on the approximate signal levels [REF]. Typically  $F2 = -F1$ , so that the beam is deflected in opposite directions in each kicker to achieve orbit closure in the chicane. With a maximum FONT gain of 8192 an ADC2 input of 1 ADC count gives an output of 128 DAC counts. If diode normalisation is enabled the expressions above are multiplied by  $1/\sqrt{\text{ADC1}}$  (with the Mon1 diode signal connected to ADC1 in normal operation). Values for the square root are taken from a lookup table, rather than being calculated directly, in order to save latency [REF].

To determine the optimal values for  $F1$  and  $F2$  given the current beam conditions it is important to know how they translate in to the real applied gain  $g$  from Equation 6.2. The real gain  $g$  is related to the DAC outputs derived above by:

$$g\phi_u = k\text{DAC} \quad (6.4)$$

Where  $k$  is the phase shift, in radians, in the chicane resulting from a DAC output of 1 count. The indices 1 and 2 are dropped from DAC1, DAC2, F1 and F2 from this point for simplicity. The upstream phase, also in radians, can then be related to the ADC2 input by:

$$\phi_u \simeq \frac{\text{ADC2}}{A} \quad (6.5)$$

Where  $A$  is the calibrated maximum Mon1 mixer amplitude, in ADC counts, determined in the same way as Section 4.3. Note that both this and the direct proportionality with ADC2 in Equations 6.3 assume the small angle approximation  $\text{ADC2} = A \sin \phi_u \simeq A\phi_u$  for small

$\phi_u$ . This is done for latency reasons and its effect on the accuracy of the applied correction is discussed later in this section.

Combining Equations 6.3, 6.4 and 6.5 gives:

$$\begin{aligned} \frac{g}{A} \text{ADC2} &= \frac{kF}{64} \text{ADC2} \\ g &= \frac{kA}{64} F \end{aligned} \quad (6.6)$$

In Section 6.4.1 a phase shift of  $3.5^\circ$  per volt sent to the amplifier is determined. Knowing that 4096 DAC counts corresponds to 2 V sent to the amplifier this value can be converted into  $k = 29.8 \mu\text{radians}/\text{DAC count}$ . Typical calibrations for Mon1 on the FONT5a board give  $A = 3440$  ADC counts. Overall, the real applied gain therefore relates to the set FONT gain in the DAQ via:

$$g \simeq \frac{F}{624} \quad (6.7)$$

The optimal real gain to apply (Section 2.5.2) is given by the upstream-downstream phase correlation,  $\rho$ , multiplied by downstream-upstream jitter ratio,  $\sigma_d/\sigma_u$ :

$$g_{\text{opt}} = \frac{\sigma_d}{\sigma_u} \rho \quad (6.8)$$

Therefore the optimal FONT gain to set in the DAQ dependent on the current beam conditions is:

$$F_{\text{opt}} \simeq 624 \frac{\sigma_d}{\sigma_u} \rho \quad (6.9)$$

In good conditions the correlation and jitter ratio are close to one, although the downstream phase jitter can be up to a factor two larger than the upstream jitter at CTF3 thus the applied FONT gains are typically in the range between 625 and 1250.

As mentioned previously the phase calculation in the PFF algorithm in the FONT5a firmware uses the small-angle approximation, thus differs from the correct full phase reconstruction method used in Chapter 4 as follows:

$$\phi_{\text{FONT}} = \frac{\text{Mixer}}{A} \quad (6.10)$$

$$\phi_{\text{FULL}} = \arcsin \left( \frac{\text{Mixer} - d}{A} \right) \quad (6.11)$$

Where  $\phi_{\text{FONT}}$  and  $\phi_{\text{FULL}}$  are the upstream phase with the FONT and full phase reconstruction methods respectively, Mixer is the Mon1 mixer signal,  $A$  is the Mon1 calibration amplitude and  $d$  is the calibration offset needed to take in to account asymmetry in the mixer minimum and maximum output due to cross-talk from the diode (Section 4.2.3).

The difference between the measured phase using these two reconstruction methods is plotted in Figure 6.8, versus the phase offset between the beam phase and the electronics LO phase. For small incoming phases (close to zero Mixer output) the only difference between the two methods is a static offset of  $-d/A$  in the measured phase, and this holds up to  $\pm 10^\circ$  (and is a good approximation up to  $\pm 20^\circ$ ). In this case the corrected downstream phase will

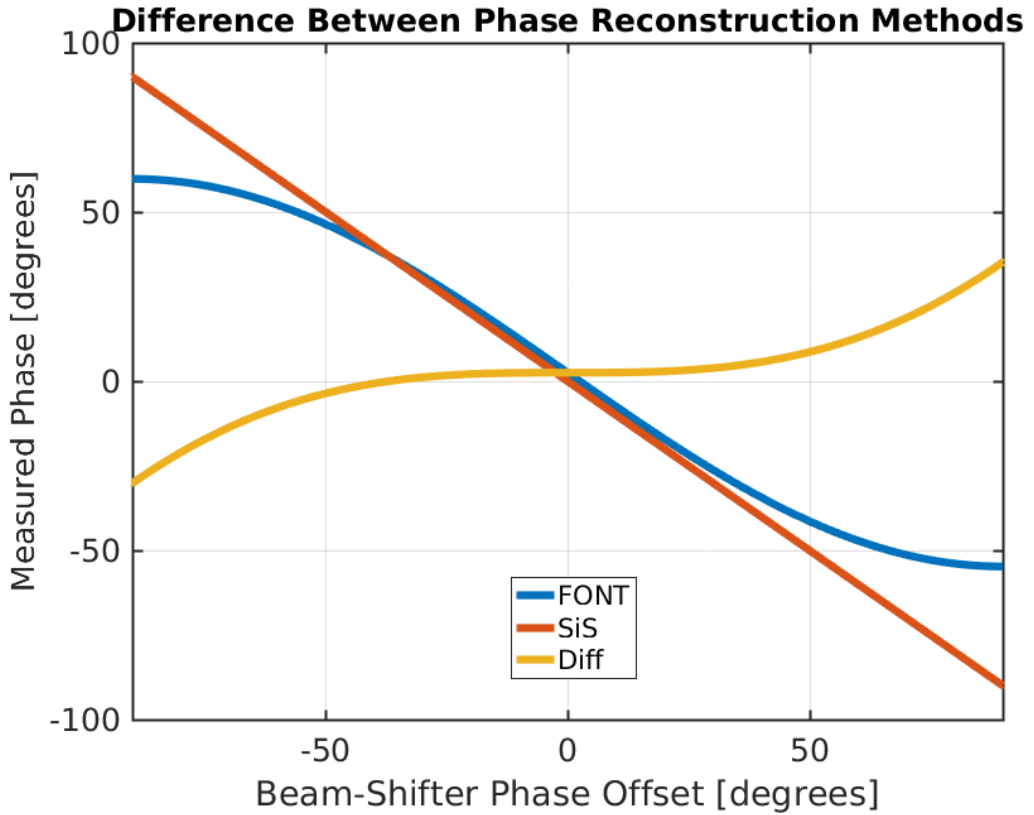


Figure 6.8: Difference between the phase reconstruction method used in the PFF algorithm on the FONT5a board (with the small angle approximation) and the full reconstruction used with data acquired from the SiS digitisers.

contain this constant offset, but the corrected phase jitter, which has been the only focus of the PFF prototype to date, will still be optimal.

With larger offsets between the beam phase and the LO (large Mixer output) the small angle approximation is no longer valid and the difference between the two methods rises to up to  $35^\circ$ . Most importantly the measured phase, and therefore the correction output, is no longer linearly dependent on the incoming beam phase when there is a large offset between the beam and LO phases. In the most extreme case, the measured phase difference between two pulses with a beam-LO phase offset of  $80^\circ$  and  $90^\circ$  would only be  $1^\circ$  with the FONT algorithm instead of the expected  $10^\circ$ , for example. In turn, the difference in the correction applied to the two pulses would only be  $1^\circ$  instead of  $10^\circ$ , degrading the achievable corrected phase jitter.

[TODO: Change legend labels to FONT and FULL, rather than FONT and SiS. And beam-LO rather than Beam-Shifter phase offset]

Figure 6.9 shows a simulation of the theoretical downstream jitter that can be achieved with both phase reconstruction methods with  $0.8^\circ$  initial upstream and downstream phase jitter and an upstream-downstream phase correlation of 97%. These values are chosen to represent the beam conditions that will need to be achieved in order to demonstrate  $0.2^\circ$  phase stability at CTF3. In the  $\pm 10^\circ$  region where the small approximation holds there is

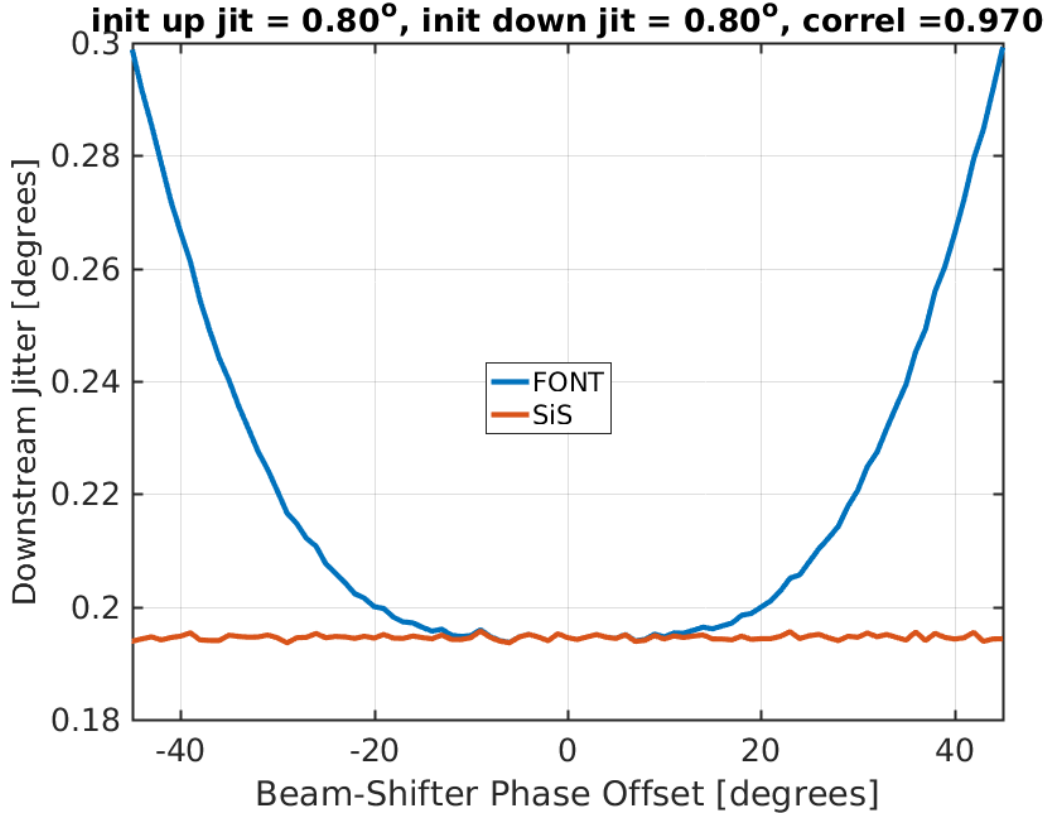


Figure 6.9: Achievable PFF jitter versus phase offset for full phase reconstruction and with the small angle approximation.

no degradation in the achievable corrected phase jitter using the simplified method in the PFF algorithm. Outside this region the jitter is degraded, increasing from below  $0.2^\circ$  to  $0.3^\circ$  for a beam-LO phase offset of  $50^\circ$ .

As the correction range of the PFF system is less than  $\pm 10^\circ$  (Section 6.4.1) there should be no degradation in the PFF performance resulting from the use of the small angle approximation in the PFF algorithm, providing the LO phase shifter in the phase monitor electronics has been set correctly. This highlights the importance to adjust the phase shifters to zero the Mixer output not only in order to maximise the phase monitor resolution (Section 4.6) but also to ensure the correction calculation itself is valid. However, it is perhaps interesting to note that it would not be possible to correct the full CTF3 pulse length to  $0.2^\circ$  jitter with this implementation of the PFF algorithm even if the correction range was large enough to encompass the  $\pm 40^\circ$  phase sag.

## 6.2 Amplifier

Make point that all effects here much smaller than phase monitors/phase propagation and although important to highlight them no attempts yet made to correct them or take them in to account in simulations.

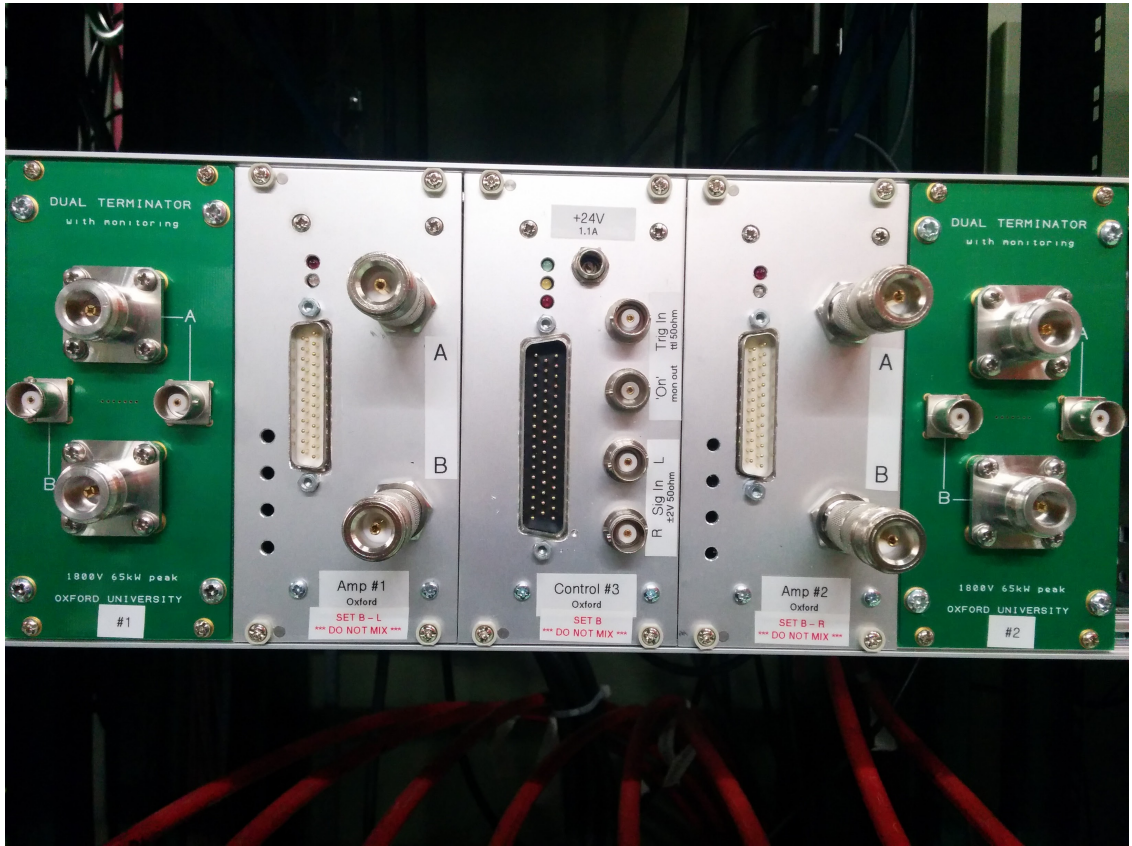


Figure 6.10: Front panel of the amplifier.

Amplifier versions:

First version (nov 2014) 350 V (check)

2nd version (jul 2015) 650 V - double FETs

3rd version: 1200 V with combiner module (?) not pursued

### 6.2.1 Installation

Amplifier inputs:

Trigger from FONT5a board (TRIG OUT DELAY)

DAC1 and DAC2 from FONT5a board

Amplifier outputs:

4 drive signals - one for each strip. Sent to downstream end of kicker

4 terminators

Amplifier on time monitoring

Monitoring of each amplifier output

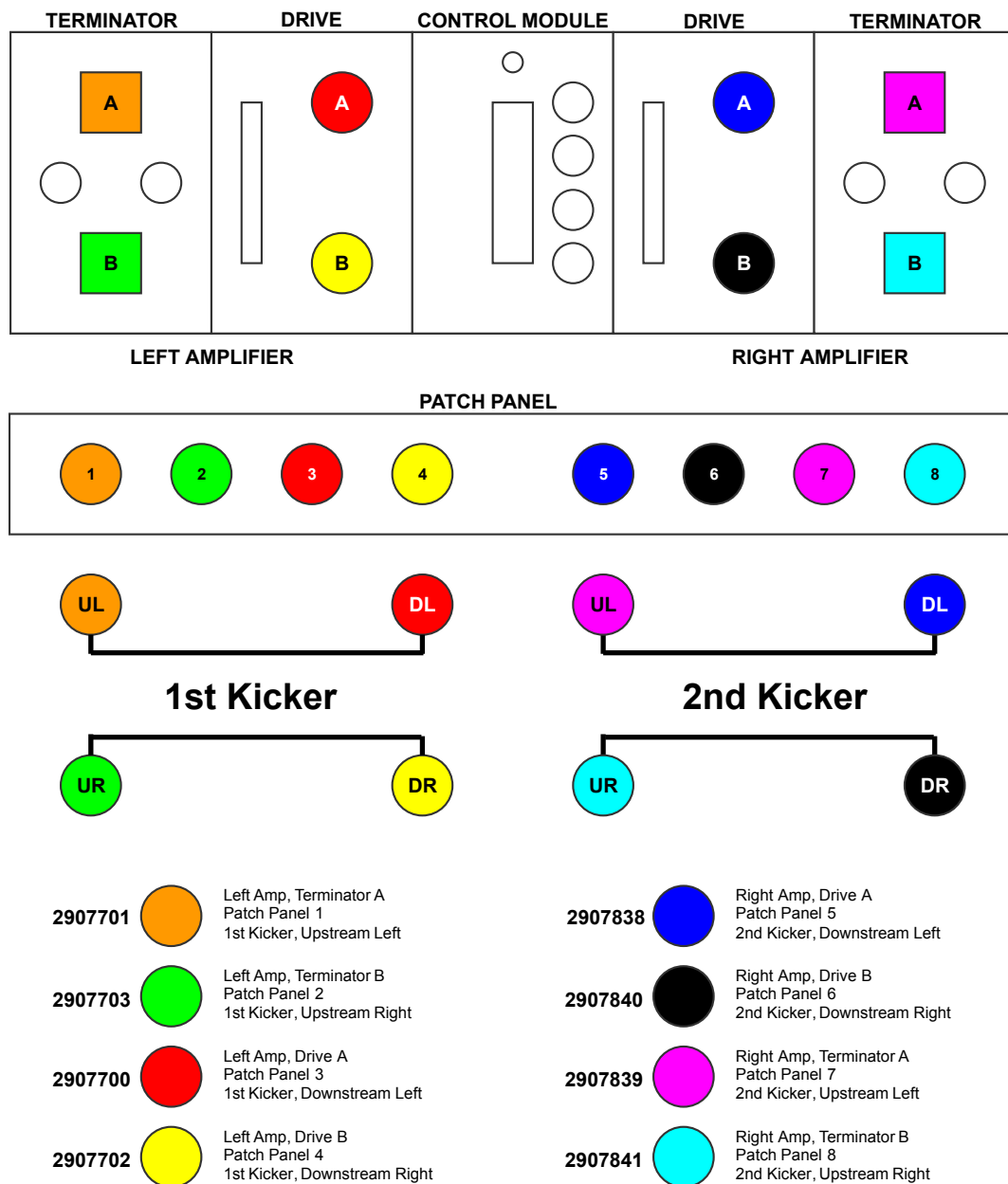


Figure 6.11: Cabling setup for cables between the amplifier and kickers.

### 6.2.2 Linearity

Figure 6.12 shows the amplifier output, as measured by the monitoring signals, at different constant input voltages sent from the FONT5a board between the minimum of -2V (-4096 DAC counts) and maximum of 2V (+4096 DAC counts). The output voltage from the monitoring signals is converted in to the real amplifier output Voltage using the approximate conversion factor of 115. All four amplifier outputs are shown (one for each strip of the two kickers). The plotted values are means taken across a 480 ns central part of the whole 1400 ns output pulse.

The relative polarity of the four outputs is equivalent to what would be sent to the kickers during PFF operation, with opposite polarity of the L and R amplifier outputs sent to each kicker, so that the beam is kicked in opposite directions by each kicker with the second kicker then closing the orbit bump created by the first. Within each side of the amplifier the A and B outputs (sent to each side of the kicker) also have opposite polarity, necessary to create the potential difference across the strips within each kicker that creates the deflecting field for the beam. The relative polarity of the A and B outputs is fixed in the amplifier design and cannot be controlled via the FONT5a board.

The response of the amplifier is highly linear in the region between  $\pm 1.2$  V sent to the amplifier. Outside this range the amplifier clearly begins to enter saturation, in particular above input voltages of  $\pm 1.7$  V. The linear fits shown include only the points between  $\pm 1.2$  V, excluding the first and last three points in the scan of input voltages, in order to not be biased by the effects of saturation.

Figure 6.13 shows the residuals between the linear fit and the real amplifier output across the full range of input voltages. By looking at the residuals a slight deviation from linearity in the  $\pm 1.2$  V range is also visible, although the maximum difference is only 10 V or a 3% relative error. At the maximum input voltage of  $\pm 2$  V the difference between the real output and the amplitude expected if the response was linear across the full range rises above 150 V, or a relative error of more than 25%. For example, the RB output at an input voltage of +2 V is 605 V but the fitted response gives 769 V, a difference of 164 V or 27%.

The effects of amplifier saturation are not taken in to account in the PFF algorithm on the FONT5a board, in which the DAC output is linearly dependent on the input phase (voltage from the phase monitor mixer signal) across the full range. The applied correction to the downstream phase will therefore be non-optimal when the DAC output calculated by the PFF algorithm is above an absolute value of 2500 counts (1.2 V sent to the amplifier). To date the non-linearity of the amplifier as it begins to enter saturation has also not been included in the PFF simulations presented in the following chapters. This may partially explain the small discrepancies seen between the simulated and real results in some datasets, so including the effect will be pursued in the future. In addition, it could be foreseen to incorporate the saturation characteristics in to the PFF algorithm on the FONT5a board, so that calculated outputs above 2500 counts are boosted slightly to compensate for the lower than expected amplifier output.

Discrepancies between the four amplifier outputs are also visible in Figure 6.13 and Ta-

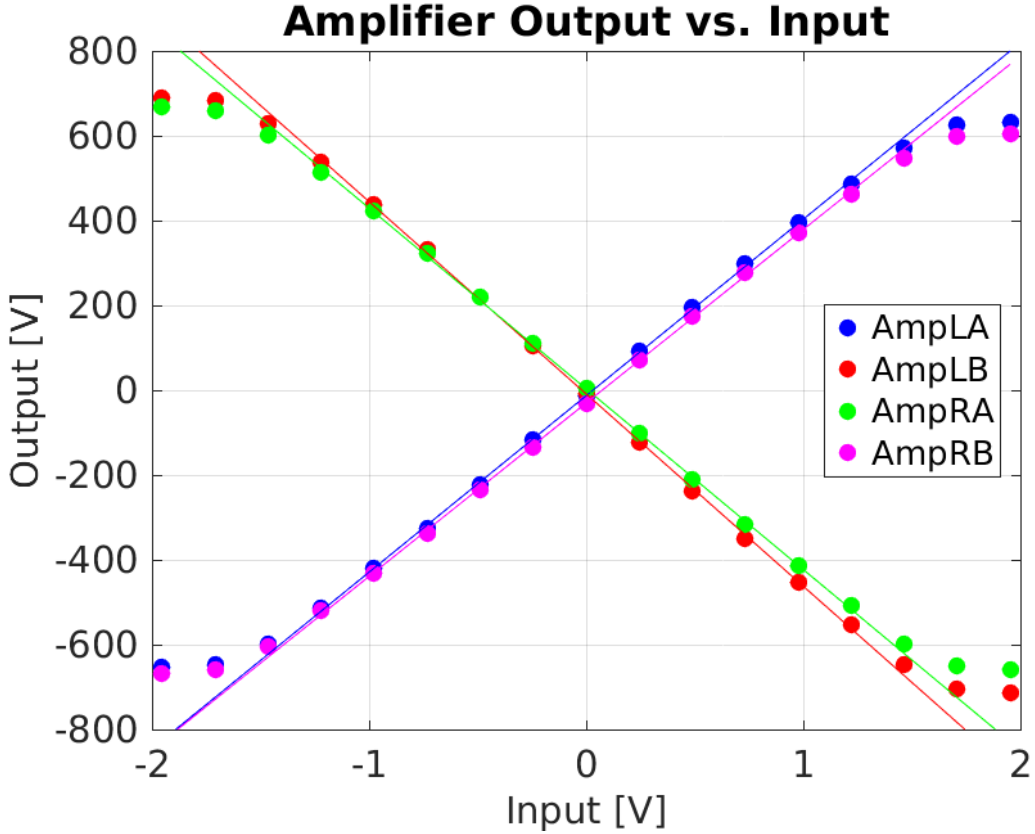


Figure 6.12: Amplifier output vs. input.

ble 6.2, both in terms of gradient and peak output. This can be partially but not completely explained by errors of up to a few percent in the precise calibration of the four monitoring outputs, which do not output exactly 1/115 of the real input voltage [TODO: Ask Colin about errors]. Differences between the A and B outputs sent to each kicker are not an issue for the PFF performance as both are linear (in the  $\pm 1.2$  V range) and the kick experienced by the beam in each kicker is proportional to the difference of the two. Therefore, only the calibration between the output from the FONT5a board sent to the amplifier and the resulting phase shift in the TL2 chicane is affected. However, disparity between the potential difference across each kicker (LA-LB and RA-RB), so that the deflection of the beam in each kicker is different, leads to the orbit bump created by the PFF system not being closed in the chicane, degrading the horizontal beam stability downstream. The fitted potential difference at 1 V input is 869 V for the left amplifier (LA-LB, sent to the first kicker) and 835 V for the right amplifier (RA-RB, sent to the second kicker), a difference of 4%. This can be compensated in the PFF setup on the FONT5a board by using a different gain for each correction output, so that the voltage sent to the right amplifier is higher but the resulting output voltage sent to both kickers is the same. Orbit closure is discussed further in Section 6.4.4.

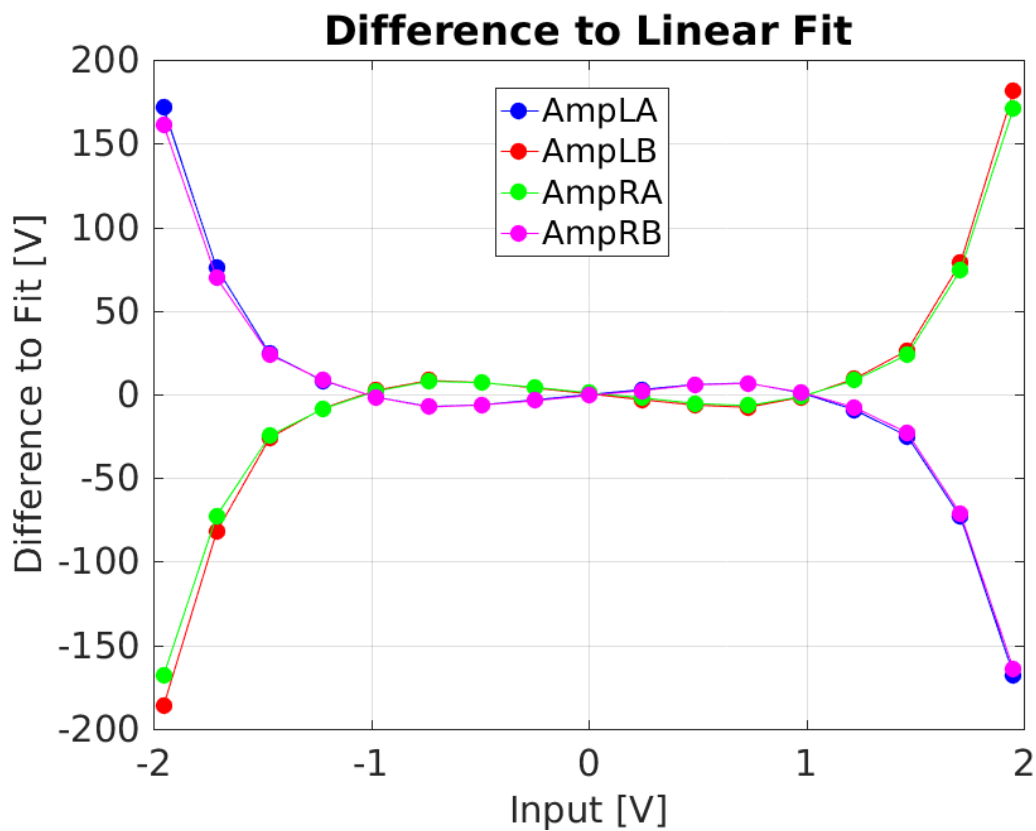


Figure 6.13: Residual between amplifier output and linear fit.

Amplifier Port	Output at +1 V Input
LA	+416 ± 3 V
LB	-453 ± 3 V
RA	-426 ± 3 V
RB	+409 ± 3 V

Table 6.2: Feedforward results using combined data from 20th November 2015.

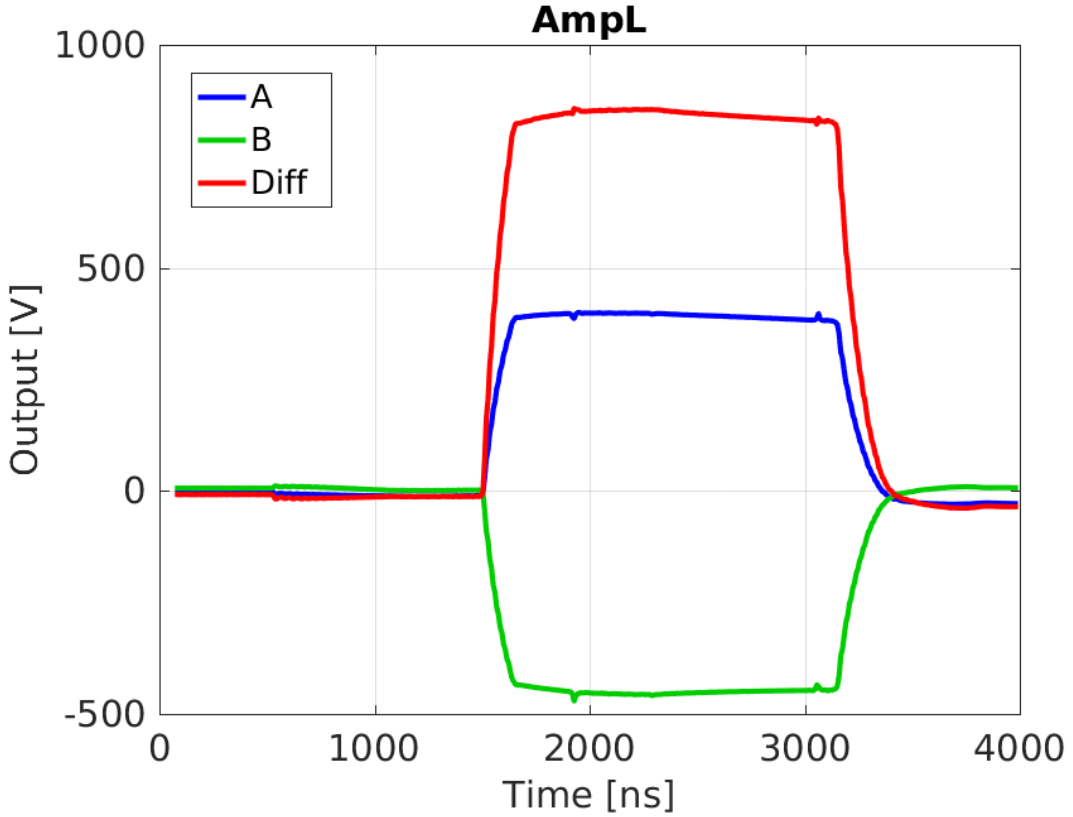


Figure 6.14: Amp L along pulse at 1 V input

### 6.2.3 Shape

In the previous section the linearity of the mean output was considered but the performance of the PFF correction is clearly also sensitive to any variations in output voltage along the amplifier output pulse. Figures 6.14 and 6.15 show the full  $1.4 \mu\text{s}$  amplifier output pulse at a constant  $+1 \text{ V}$  input sent to the left amplifier and a constant  $-1 \text{ V}$  input sent to the right amplifier respectively. Spikes in the signal just prior to 2000 ns and after 3000 ns on the time axis as seen in the plots are beam pickup induced by the beam passing through the kickers. These are therefore not a property of the amplifier performance and are excluded from the analysis in this section. However, the beam pickup is used later in Section 6.5.2 for the purposes of optimising the correction timing.

For each side of the amplifier both the A and B outputs are plotted as well as the difference of the two, which is the relevant quantity in terms of the kick received by the beam as it traverses the kickers. In the ideal case the potential difference should be flat along the full pulse length. However, for both the left and right side variations in the difference are visible, with an initial increase in output across the first 500 ns of the pulse followed by a droop in response across the second half of the pulse. Although not shown here, the shape of the variations along the pulse is consistent across the full range of output voltages, and scale in magnitude with the output voltage. Figure 6.16 shows the peak-to-peak and mean deviation of the output voltage along the pulse across the full range of input voltages. The peak-to-peak deviation refers to the difference between the minimum and maximum output along

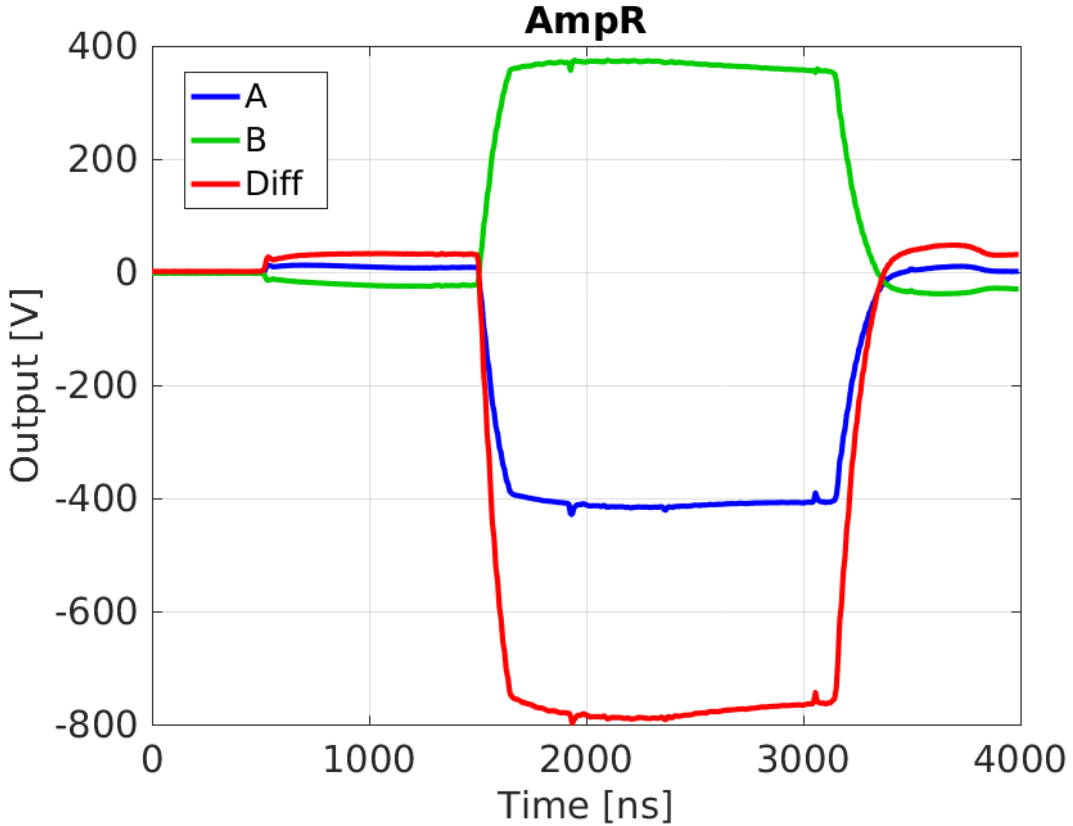


Figure 6.15: Amp R along pulse at 1 V input

the pulse, whilst the mean deviation is the average absolute difference between the mean output and the output at each sample point. For a constant input voltage the output voltage along the pulse varies by up to 88 V peak-to-peak (mean 12 V) for the left amplifier or 93 V peak-to-peak (mean 14 V) for the right amplifier. As a relative difference, this corresponds to approximately a 6 % peak-to-peak, or 1 % mean, variation along the pulse.

The PFF algorithm on the FONT5a board uses a single gain value across the whole pulse length for each correction output, thus making the approximation that the amplifier response is flat along the pulse. The variations along the amplifier pulse therefore directly translate in to discrepancies between the intended phase shift as calculated and the real phase shift experienced by the beam. As the region of interest for the correction is a few hundred nanoseconds about the central part of the pulse, as opposed to the full pulse length, the 1 % mean variation is more indicative of the resulting error than the 6 % peak-to-peak variation. With a correction range (Section 6.4.1) of  $\pm 6^\circ$ , the effects of the non-flat amplifier output should be below  $0.06^\circ$  and not measurable considering the phase monitor resolution of  $0.14^\circ$ . Nevertheless, it could be foreseen to implement a droop correction in the PFF algorithm on the FONT5a board, taking the variations in the amplifier output along the pulse in to account.

As for the mean output voltage, the second way variations in the amplifier output along the pulse can impact the PFF performance is via the orbit closure in the chicane. For this the relevant quantity is the sum of the potential difference sent to each kicker, or

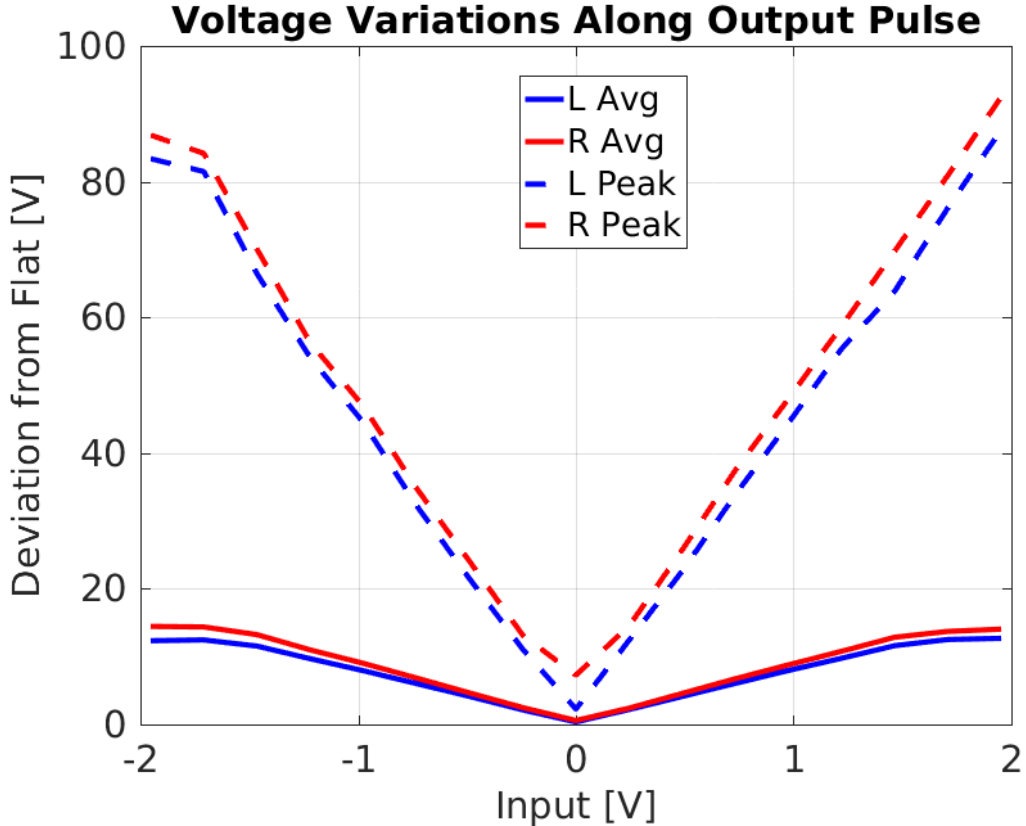


Figure 6.16: Flatness of potential difference sent to kickers.

$(LA - LB) + (RA - RB)$ . To ensure orbit closure this quantity, named the residual kick here, should be zero across the whole pulse length for all input voltages. Figure 6.17 shows the residual kick along the pulse for all the input voltages in the scan. Clearly they are not all centred around zero, but this is expected due to the differences in the mean output voltage of the four amplifier outputs seen in the previous section. As already stated, the overall mean offset can be removed by using a different gain for the two correction outputs. However, any variations along the pulse cannot be compensated for in the PFF algorithm. The magnitude of the effect is summarised in Figure 6.18, showing the peak-to-peak and average deviation of the residual kick from flat. The overall residual kick is very flat and effect is smaller than any of those previously shown — only up to 2 V on the mean or 21 V peak-to-peak. Whether this has any measurable effect on the orbit closure is discussed in Section 6.4.4.

#### 6.2.4 Bandwidth

[TODO: ask Colin if he has any plots?]

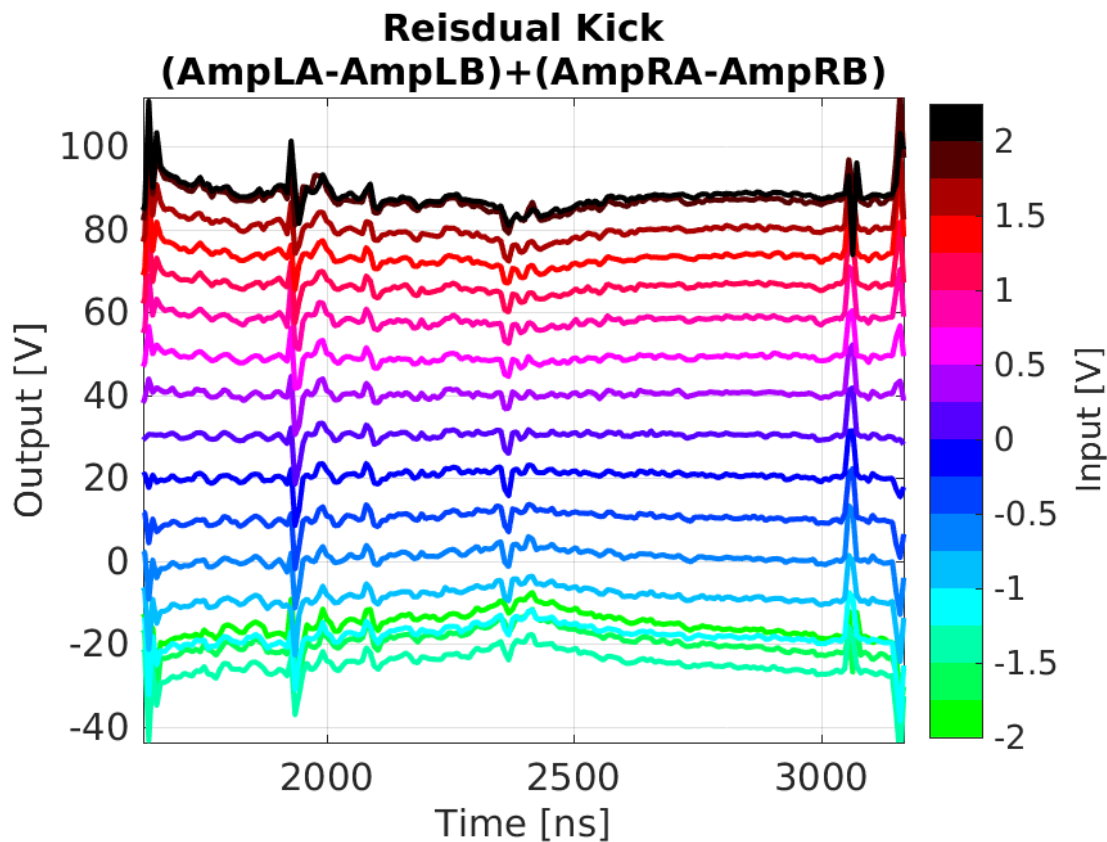


Figure 6.17: Residual kick along pulse.

## 6.3 Data Acquisition and Signal Processing

### 6.3.1 SiS Digitiser Setup

(already discussed in ph mon chapter)

### 6.3.2 Acquisition Tools

### 6.3.3 Monitoring Tools

Online display

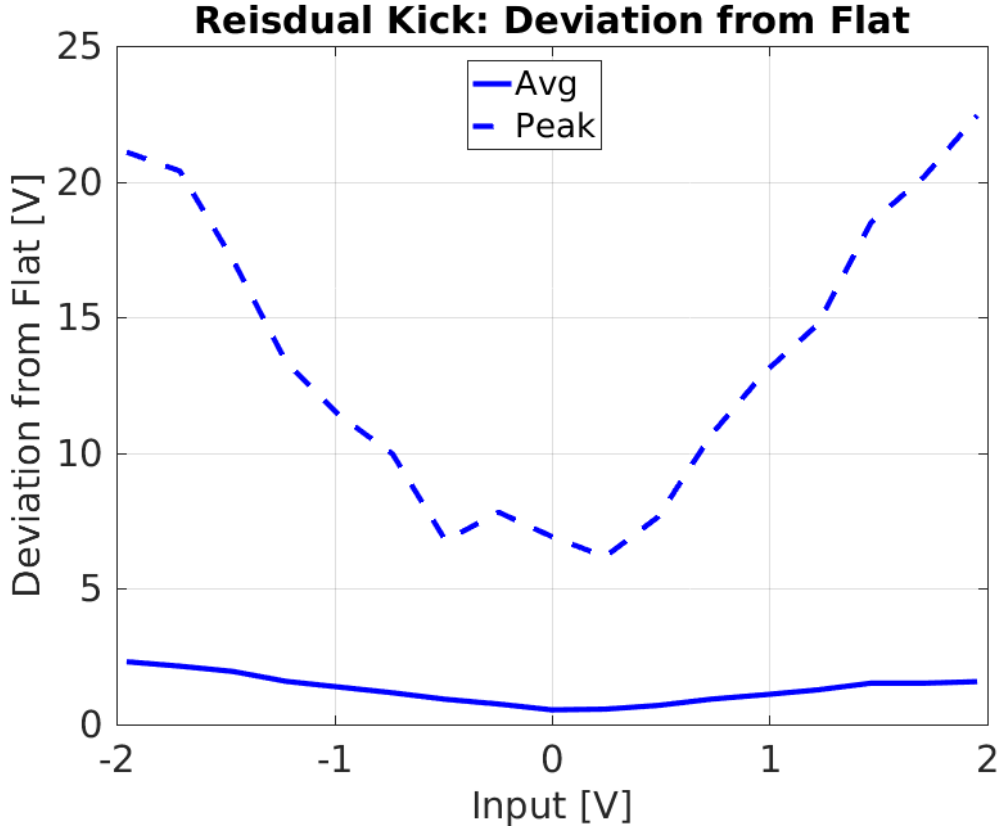


Figure 6.18: Residual kick along pulse: deviation from flat.

### 6.3.4 Time Alignment of Signals

### 6.3.5 Definition of Zero Phase

## 6.4 Kicker and Optics Performance Verification

### 6.4.1 Correction Range

Knowledge of the correction range of the PFF system, or more specifically the relationship between the voltage sent to the amplifier and the phase shift in the chicane, is critical for the PFF setup. The first checks of the ability to shift the phase in the TL2 chicane using the new phase feedforward optics were performed with magnetic correctors prior to the PFF amplifier being available (these correctors can be used to implement a secondary “Slow Correction” to complement the PFF system, as discussed in Section 9.2). Aside from their use for the PFF correction, these tests and the clear variation with beam phase versus voltage sent to the PFF kickers shown in this section are already a significant achievement and a verification of the extensive work to improve the MADX model of TL2 presented in Chapter 3.

Figure 6.19 shows the mean phase shift after the chicane (in the downstream phase monitor) across the full  $\pm 2$  V input range of the amplifier. Constant DAC outputs from the FONT5a board were sent to the amplifier in 17 steps between -4096 counts (-2 V) and +4096

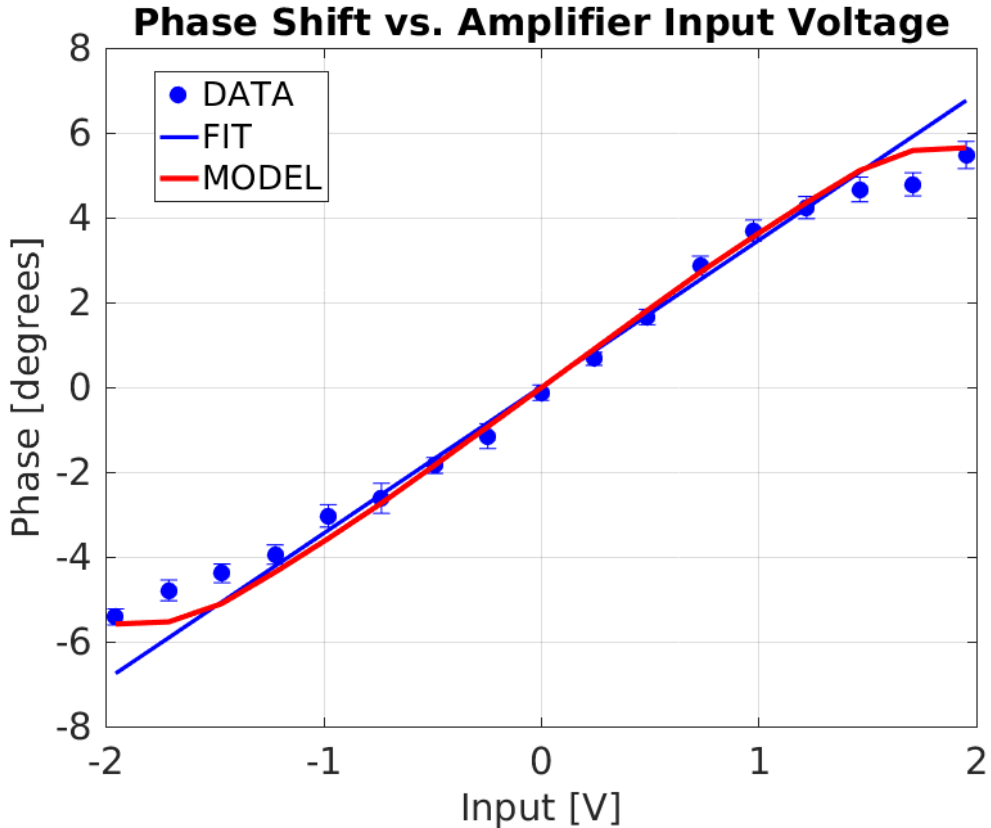


Figure 6.19: Phase shift versus amplifier input voltage.

	Phase Shift at +1 V Input	Max Phase Shift
Data	$3.5 \pm 0.1^\circ$	$5.5 \pm 0.3^\circ$
Model	$3.6^\circ$	$5.6^\circ$

Table 6.3: Phase shift at +1 volt input to the amplifier.

counts (+2 V). In order to reduce the sensitivity to any drifts in the beam phase between data points the scan was taken in interleaved mode, alternating between pulses with no drive sent to the amplifier and a constant non-zero DAC output. The phase plotted in Figure 6.19 is therefore the difference between 50 kicked beam pulses and 50 “nominal” pulses taken at the same time for each amplifier input voltage.

At the maximum amplifier input voltage of 2 V the phase after the chicane is shifted by  $5.5 \pm 0.3^\circ$ . The fitted phase shift per Volt sent to the amplifier is  $3.5 \pm 0.1^\circ$  in the  $\pm 1.2$  V linear range of the amplifier (excluding the first and last three points, blue “FIT” line in Figure 6.19). This fitted gradient is required and was previously introduced for the conversion between the PFF gain in the units on the FONT5a board and the real applied gain in Section 6.1.4. In Section 6.1.4 it was quoted in terms of the phase shift in radians per DAC count output from the FONT5a board, rather than degrees per Volt as shown here. The value of  $30\mu\text{rad}/\text{count}$  is easily derived using the conversion factors between degrees and radians and knowing that a DAC output of 4096 counts corresponds to 2 V sent to the amplifier. [TODO: Calculated factor is 29.827 microradians/count here. One I actually used

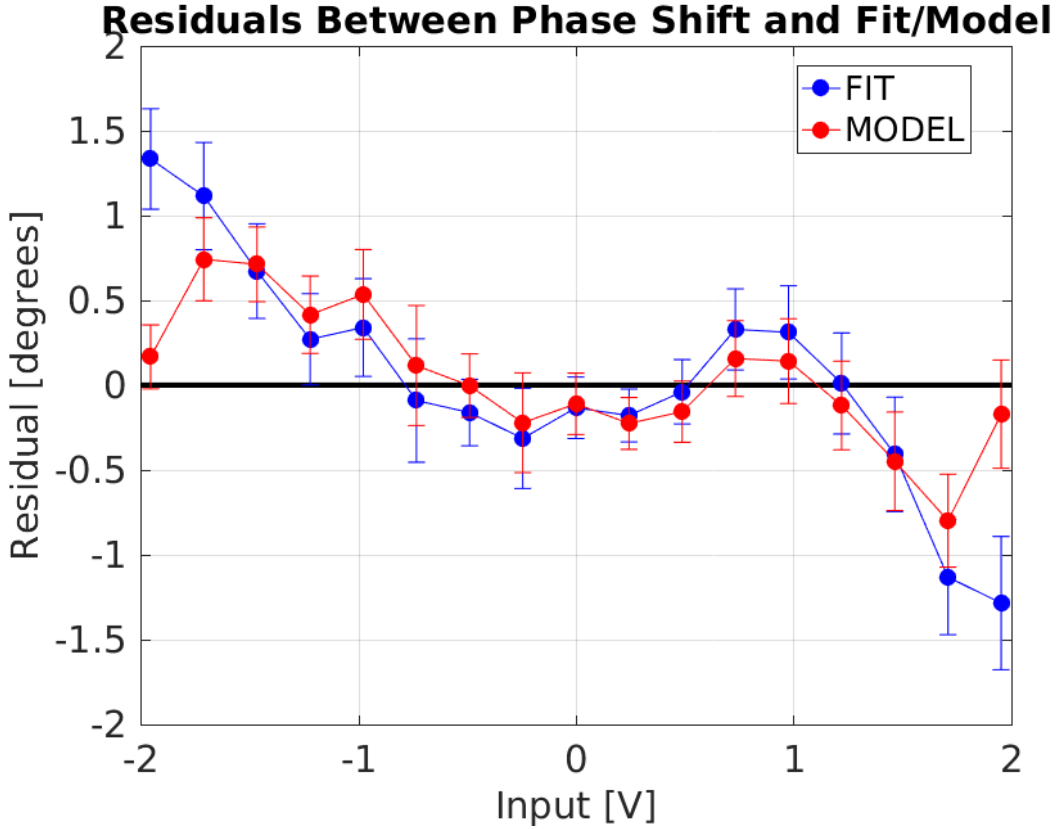


Figure 6.20: Phase shift versus amplifier input voltage.

for gain conversion, simulations etc. was 26.18 (used full range rather than linear range)]

Given knowledge of the amplifier output characteristics (Section 6.2.2), the kicker specifications (Section 2.3.4) and the chicane optics (Section 3.4.3) the real phase shift seen in the scan can be compared to the expected phase shift based on the system parameters. The predicted phase shift,  $\Delta\phi$ , in degrees is given by:

$$\Delta\phi = V_{amp}[V_{font}].K.R_{52} \cdot \frac{360}{\lambda_{12\text{GHz}}}$$
 (6.12)

Where  $V_{amp}[V_{font}]$  is the amplifier output Voltage at an input voltage of  $V_{font}$  sent from the FONT5a board,  $K$  is the angular deflection of the beam per Volt applied to each kicker strip,  $R_{52}$  is the  $R_{52}$  value between the kickers in the PFF optics and  $\frac{360}{\lambda_{12\text{GHz}}}$  converts the calculated orbit length difference in to an equivalent 12 GHz phase using the 12 GHz wavelength  $\lambda_{12\text{GHz}}$ . The value of most of these parameters has already been derived in the sections previously mentioned. They are:

$$V_{amp}[1 \text{ V}] = 435 \text{ V}$$

$$K = 0.8 \text{ } \mu\text{rad/V}$$

$$R_{52} = -0.7 \text{ m}$$

$$\lambda_{12\text{GHz}} = 2.5 \text{ cm}$$

The value of  $V_{amp}[1 \text{ V}]$  is given as a representative value in the linear range of the amplifier but the real amplifier output at all input voltages is used in the predictions to include the

effects of saturation in the calculated phase shift values. Also, the output sent to the first kicker (from the left side of the amplifier) is used as this is most relevant for the phase shift in the chicane (the orbit should be closed after the second kicker with no further phase shift in the chicane after that point). The value of  $K$  is derived from the kicker design, in which 1.4 kV applied to each strip gives a 1 mrad kick for a 150 MeV beam [TODO: REF]. The actual CTF3 beam energy at this time was approximately 135 MeV (calculated based on the dipole currents used in the machine setup), so the value of  $K$  above is scaled by a factor 150/135.

In Figure 6.19 the red line “MODEL” shows the predicted phase shifts using Equation 6.4.1. Table 6.3 compares the fitted gradients and maximum phase shift for the model and real data. The overall agreement between the two is good, with the residuals between both the model and the data, as well as the linear fit to the data and the data, generally consistent with zero within error bars in the  $\pm 1.2$  V linear range of the amplifier as shown in Figure 6.20.

Outside the linear range some discrepancies appear, although at the maximum  $\pm 2$  V output the agreement is good so the effect is largest where the amplifier is entering saturation but before hard saturation is reached. However, most amplifier effects can be excluded as the analysis in this section uses the same dataset that was used to characterise the amplifier performance in Section 6.2. This could hint at possible remaining higher order errors in the TL2 chicane optics, or unexpected behaviour from the kickers or amplifier. Although subtracting alternating, interleaved pulses should remove the sensitivity to drifts in the machine it is possible that some residual effect remains. To determine whether the discrepancies are reproducible further scans of this type will need to be completed in the future. The residuals between between the data and the linear fit between  $\pm 1.2$  V would also be of significance for the PFF correction should they not converge to zero with additional measurements, as they are of similar magnitude to the  $0.2^\circ$  downstream jitter target.

However, the overall conclusion is as expected — the phase shift in the chicane linearly depends on the amplifier input in the  $\pm 1.2$  V ( $\pm 2500$  DAC counts) region thus a close to optimal correction can be applied in this range, corresponding to a  $\pm 4.2 \pm 0.1^\circ$  phase shift. However, when the calculated optimal correction is between an absolute input voltage of 1.2 V and 2.0 V, 2500 to 4096 DAC counts, or  $\pm 4.2 \pm 0.1^\circ$  to  $\pm 7.0 \pm 0.2^\circ$ , the actual phase shift in the chicane is lower, only up to  $\pm 5.5 \pm 0.3^\circ$ , due to the amplifier entering saturation (and possibly other effects to be determined). Any calculated correction outside  $\pm 5.5 \pm 0.3^\circ$  receives a static phase shift of  $\pm 5.5 \pm 0.3^\circ$  in the chicane. In the limit where all pulses are outside this range the PFF system can only induce a static shift in the mean phase and makes no improvement to the phase jitter. Understanding the impact of the limited correction range on the PFF results was particularly critical for interpreting the early correction attempts with the first version of the amplifier, giving approximately half the ranges shown in this section. This is discussed using simulations of the PFF system in Chapters 7 and 8.

<http://accelconf.web.cern.ch/accelconf/ipac2011/papers/tupc007.pdf> 1.4 kV to each strip  
 $= 1$  mrad kick at 150 MeV 1.26 kV to each strip  $= 1$  mrad kick at 135 MeV

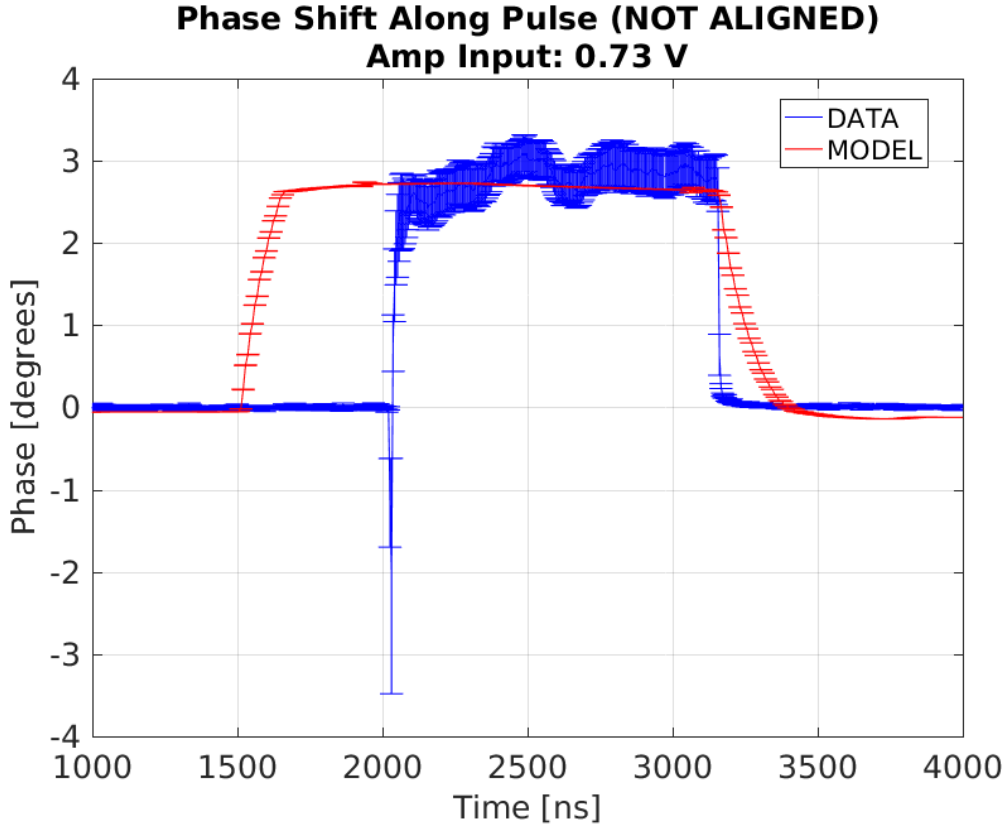


Figure 6.21: Traces relative timing scan.

#### 6.4.2 Variations Along Pulse

[TODO: In this section I intended to check the stability of the constant kick along the pulse, as I did for the "Shape" section with the amplifier above. The results from the constant kick data do not look good, though - the errors are quite large and there are some nasty oscillations along the pulse, such as in the example Figure 6.21. With the phase stability downstream a much longer scan would probably be needed to draw conclusions here, though even on longer time scales I think it needs to be checked that the difference between odd and even pulses converges to zero. As it is I would probably choose to skip this section, or possibly just show one of the better plots.]

#### 6.4.3 Shape

[TODO: The purpose of this section is to compare the shape of the given kick to the upstream phase - i.e. compare the upstream phase to the amplifier monitoring output and the difference in the downstream phase with PFF off and on. Again here my first attempts produced results that were not as I'd like, without particularly good agreement between the difference in the downstream phase and the upstream phase shape. Looks kind of like the two are rotated with respect to each other. More analysis needed here to check more thoroughly. I think this section should definitely be included, but I need either an explanation for the differences or to find datasets where the agreement is much better.]

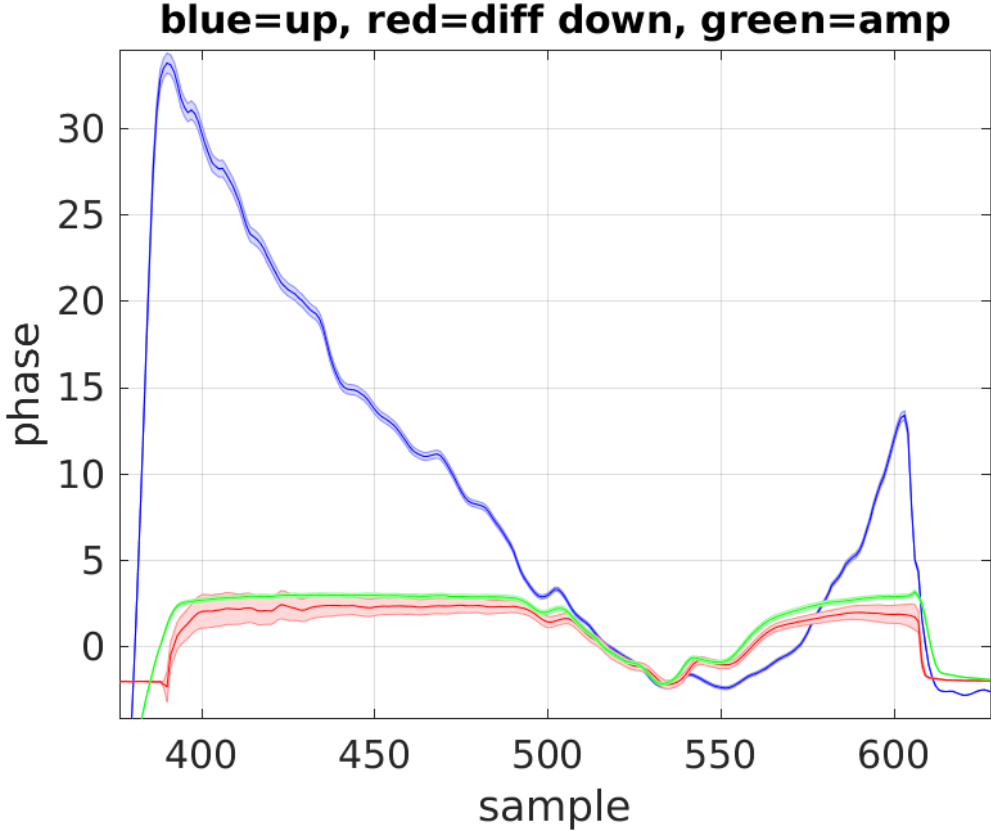


Figure 6.22: Traces relative timing scan.

#### 6.4.4 Orbit Closure

At CLIC the PFF system must not degrade the transverse beam stability. This means for any voltage sent to the kickers the horizontal beam orbit after the PFF chicane must be unchanged, or closed, despite the different orbits inside the chicane. As such, the PFF optics for the TL2 chicane at CTF3 is also designed to give a closed kick, as presented in Section 3.4.3. However, up until now the main focus during PFF operation has been the primary goal of reducing the downstream phase jitter and ensuring good beam transmission to the downstream phase monitor. As a result orbit closure after the TL2 chicane has not yet been strictly enforced during PFF operation as will be seen in this section, but the current status is shown here as an additional cross-check of the PFF optics and to highlight where improvements are needed for future tests.

Using the same constant kick data as Section 6.4.1 Figure 6.23 shows mean the horizontal orbit before, inside and after the TL2 chicane across the full  $\pm 2$  V range of inputs sent to the amplifier. The vertical black lines on the plot mark the approximate location of the entry to the chicane (index CC.500) and the exit of the chicane (index CC.800), with the two kickers being located at CC.480 and CC.780. Two BPMs before and after the chicane, as well as the four inside the chicane, are included. The plotted positions are the difference between the kicked and nominal (non-kicked) orbit at each BPM, thus removing any misalignment in the BPM centres. Before the chicane and the first kickers there is no significant effect on the orbit as expected. Inside the chicane the PFF system induces an orbit offset of up to

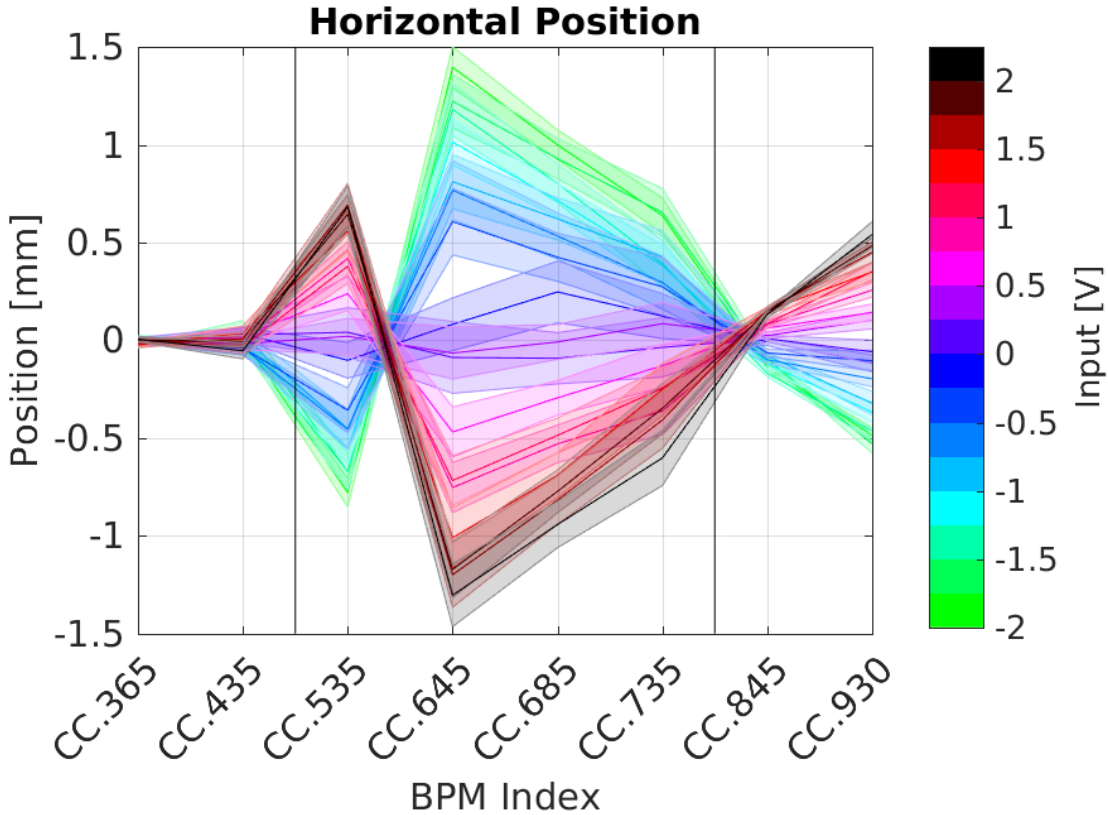


Figure 6.23: Horizontal orbit offset in and around the TL2 chicane at different input voltages sent to the amplifier.

$1.4 \pm 0.1$  mm. After the chicane, in BPMs CC.845 and CC.930, the orbit should return to zero in the ideal case. However, a clear residual offset can be seen, up to  $0.5 \pm 0.1$  mm in CC.930.

During this scan the input sent to both sides of the amplifier was the same magnitude. However, in Section 6.2.2 it was seen that the right side of the amplifier, sent to the second kicker, gave 4% lower output than the left side. This could explain why the orbit after the chicane was not closed during this scan, and during PFF operation which has typically used equal gain for both correction outputs to date. Figure 6.24 shows the expected orbit in the TL2 chicane in the case where both kickers are driven with the same voltage (“nominal optics”) and with the 2nd driven with a 4% lower voltage (“real amplifier ratio”).<sup>1</sup> The full MADX orbit propagated through all elements is shown, with the eight real measured BPM offsets also included at their respective positions. Each BPM point represents the gradient of a linear fit using the variation with input voltage seen previously in Figure 6.23. Before and inside the chicane the agreement between the BPM data and the model is excellent. As seen before, the BPM orbit is not closed after the chicane, unlike the nominal optics. If the actual kicker voltage ratio is taken in to account the MADX orbit after the chicane is not closed either, but the offset has opposite polarity to the real data in the last BPM.

<sup>1</sup>The term “nominal optics” is used in this section to refer to the nominal PFF optics, not the nominal optics created in Chapter 3 to use when the PFF system is not under operation.

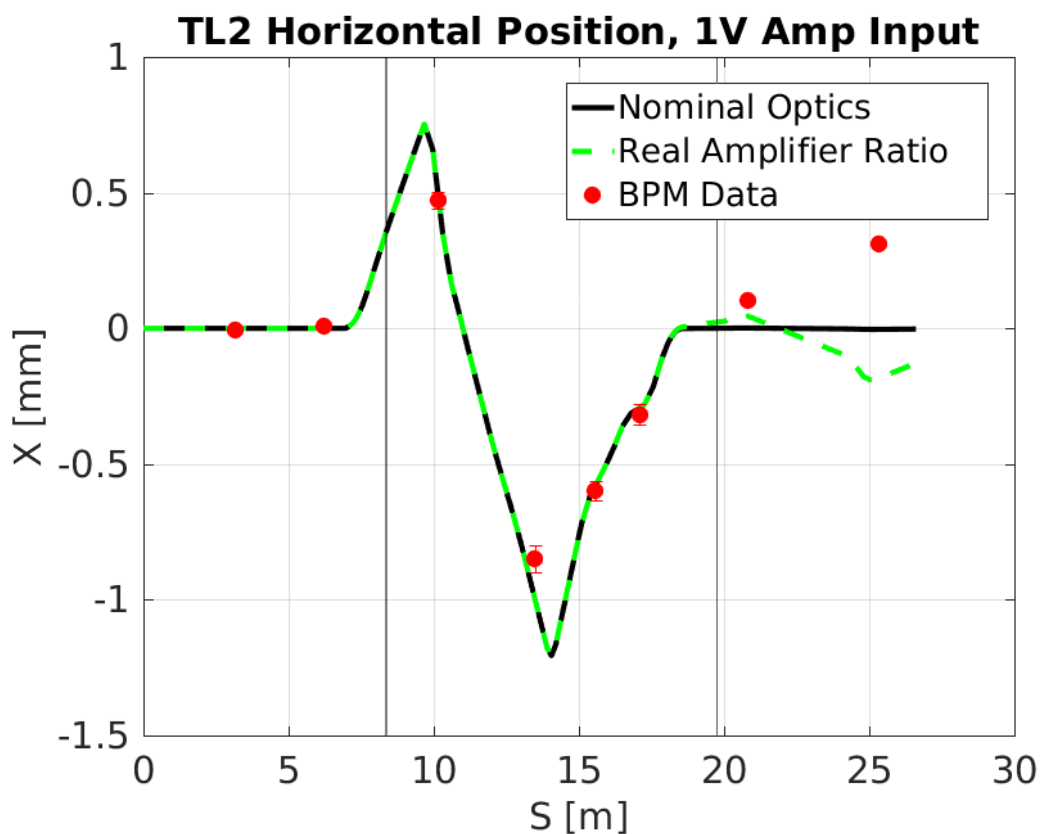


Figure 6.24: Orbit in the TL2 chicane at 1 V amplifier input for the BPM data, nominal model and model taking in to account the difference in amplifier output voltage to each kicker.

The true explanation for the non-closed orbit is that the quadrupole strengths used in the machine setup are not exactly nominal. Although every effort has been made to keep the TL2 optics as close to nominal as possible, particularly inside the chicane, it is an extremely sensitive area for the setup of CTF3 and beam transport in to the CLEX area downstream of TL2 (including the location of the downstream phase monitor in the TBL line) is always difficult. Minor modifications have therefore been necessary in order to achieve full beam transmission to the downstream area, both for PFF and other experiments at CTF3. The largest changes have been made to the four quadrupoles following the chicane but one quadrupole inside the chicane, CC.IQFL0730 (just prior to the 2nd kicker) has a set value 10% lower than the nominal optics, as well as differences up to 2% in the other quadrupoles. Using the real quadrupole strengths used in the machine gives the result shown in Figure 6.25. In this case the agreement between the model and the data is also extremely good after the chicane. It may still be possible to compensate for these differences by outputting different voltages to each kicker and this will be investigated. Alternatively, a completely nominal optics can be set in the chicane purely for the purposes of verifying orbit closure, reverting back to non-nominal optics and closure if needed to achieve good beam transmission for normal PFF operation.

[TODO: Not enough detail r.e. why beam transport there is difficult etc.?]

[TODO: Do have data with different ratios of kicker strengths. Can analyse to see effect on closure. Considering quad currents don't think it adds anything to discussion here, though.]

[Comment for Piotr: With these quad currents also expect to see some dispersion leaking out of the chicane. Up to 0.3 m in girder 9.]

## 6.5 Correction Output Timing

All the results based on the amplifier outputs and kicked beam presented so far have used a constant output voltage sent from the FONT5a board across the full  $1.4 \mu\text{s}$  time window that the amplifier is powered for. As the  $1.4 \mu\text{s}$  amplifier output sent to the kickers is much longer than the  $1.1 \mu\text{s}$  CTF3 beam pulse it is easy to ensure that the full length of the pulse experiences the constant kick with this setup. However, for operation of the PFF system precise control of the correction output timing becomes critical. In order to remove phase variations along the pulse with the PFF system the output correction signal, shaped by the upstream phase, must arrive at the kickers exactly in sync with the beam. Any timing misalignment between the beam and correction signal arrival will result in residual oscillations along the pulse in the downstream phase, even in the case where the upstream-downstream phase propagation is perfect. Approximating the phase sag along the pulse to be quadratic,  $\phi_u(t) \sim \phi_d(t) \sim t^2$ , a misaligned correction would yield a corrected downstream phase with a linear increase in phase along the pulse with time,  $\phi_{PFF}(t) \sim \phi_d(t) - \phi_u(t + \delta) \sim -2\delta t - \delta^2$ , for example, where  $\phi_{PFF}$  is the corrected phase,  $\phi_d$  the uncorrected downstream phase,  $\phi_u$  the upstream phase,  $t$  the time and  $\delta$  the time misalignment in the applied correction. Also, the effect is particularly significant for any higher frequency variations in phase along the

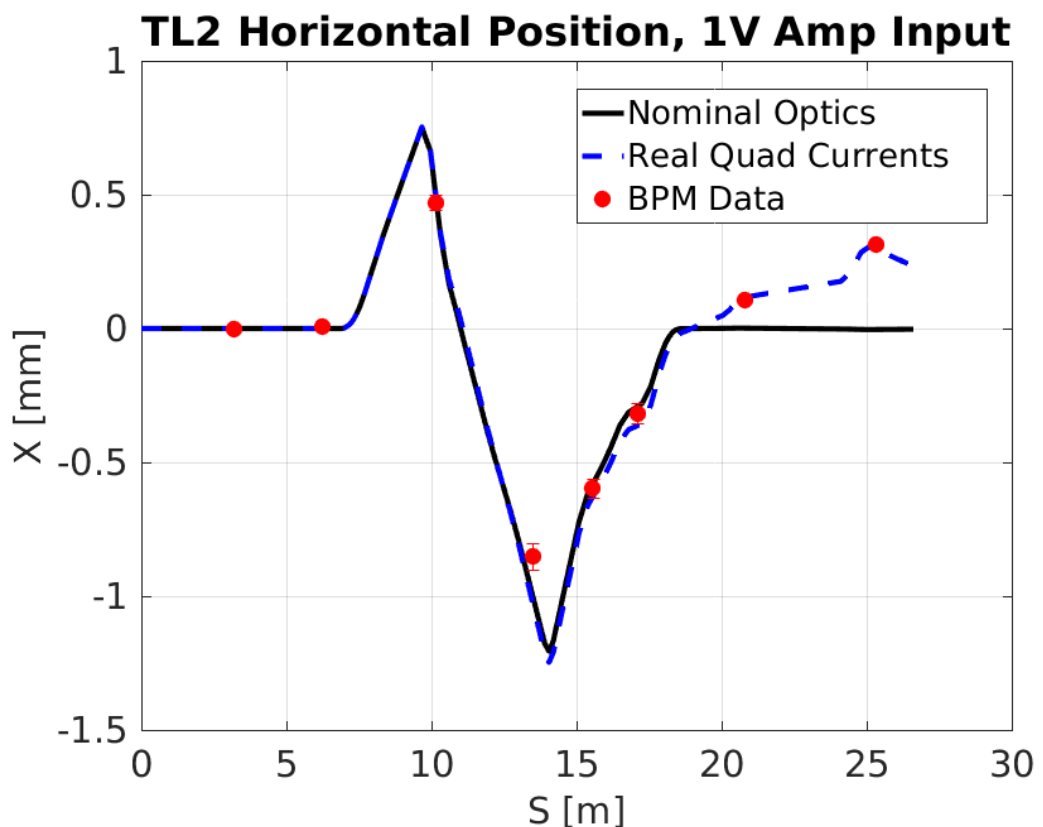


Figure 6.25: Orbit in the TL2 chicane at 1 V amplifier input for the BPM data, nominal model and model taking in to account the quadrupole currents in the real machine setup.

pulse. If a 40 ns oscillation is present in the upstream phase but the correction is applied with a 50 ns delay, for example, a second 40 ns oscillation with opposite sign would be introduced to the “corrected” downstream phase at a later time with no change to the initial oscillation. Although the effects are most visible along the pulse, any timing delay will also degrade the achievable mean phase jitter. This section gives an overview of the main methods that have been used to ensure that the correction output to the two kickers arrives in time with the beam.

### 6.5.1 Kicker Cable Lengths

The cables carrying the correction signal between the PFF amplifier and the kickers in the TL2 chicane are the single largest contributor to the overall system latency. They must be routed from the PFF electronics racks (in the klystron gallery, one floor and directly above the location of the upstream phase monitors), down in to the machine hall and across the width of the CTF3 facility to the TL2 chicane. The initial kicker cables installation used pre-existing cable trays and gave a signal transit time of 260 ns, with a signal speed of  $0.66 c$  and approximate lengths of 50 m. This is more than two thirds the overall PFF latency budget, which must be lower than the 380 ns beam time of flight between the upstream phase monitor and the first kicker. Considering the latencies of the various pieces of hardware in the PFF system chain as well as the cables between the upstream phase monitors and the PFF electronics (Section 2.2.2), the overall PFF system latency would have been in excess of the 380 ns beam time of flight with this setup. By re-routing the cables on to a dedicated pathway and trimming any remaining slack it was possible to reduce the cable lengths by up to 90 ns, bringing the system within the latency budget as will be seen in the following sections. Precise measurements of the cable lengths with this setup are presented in this section, as well as their significance beyond ensuring the system is within the latency requirements.

With two kickers, two strips per kicker and two ends of each strip a total of eight cables are needed. The drive from the amplifier is sent to the downstream end of each kicker strip, traverses the kicker, and is then terminated back at the amplifier after leaving the upstream end. Drive is sent to the downstream end of each kicker (meaning it propagates through the kicker in the opposite direction to the beam) so that the electric and magnetic fields between the strips are in the same direction, as discussed in Section 2.3.4. Rather than being connected directly to the amplifier, the eight kicker cables are connected to a patch panel below the amplifier in the PFF electronics racks. Eight additional cables, around 70 cm in length, are used to connect the amplifier outputs to the patch panel. This is in order to create a tidier cabling setup in the rack as well as making changes to the amplifier cabling easier, when necessary. [TODO: Picture]. The kicker cables are of type [TODO: REF] with HN-type connectors and the patch panel cables of type [TODO: REF] with N-type connectors to match the amplifier.

The length of the eight kicker cables and eight patch panel cables has been measured using time domain reflectometry (TDR) on a network analyser [TODO: REF?]. The network analyser is used to send a short pulse down the cable, with one end of the cable connected

Label	Length	Amplifier Port	Patch Panel Port
2907701B	$2.99 \pm 0.05$ ns	LAT	1
2907703B	$3.03 \pm 0.05$ ns	LBT	2
2907700B	$3.03 \pm 0.05$ ns	LAD	3
2907702B	$3.01 \pm 0.05$ ns	LBD	4
2907838B	$3.03 \pm 0.05$ ns	RAD	5
2907740B	$3.05 \pm 0.05$ ns	RBD	6
2907739B	$3.03 \pm 0.05$ ns	RAT	7
2907741B	$3.03 \pm 0.05$ ns	RBT	8

Table 6.4: Lengths of cables between the amplifier and the patch panel.

to the network analyser and the other end disconnected so it is not correctly terminated. As the signal reaches the (non-terminated) end of the cable the discontinuity in impedance creates a reflected signal that propagates back to the network analyser. The time difference between when the signal was output and when the reflected signal arrives back at the network analyser therefore corresponds to double the one-way signal transit time in the cable. [TODO: Example TDR plot?]

Table 6.4 shows the patch panel cable lengths and Table 6.5 the kicker cable lengths that were determined with this method. Quoted errors of  $\pm 0.05$  ns are estimated based on the sampling rate of the measurement. The amplifier port, patch panel port and kicker strip that the cables are connected to are also shown in the table, as well as their corresponding CTF3 identifying number for reference. For the amplifier port labels the three letters correspond to:

- Whether the cable is connected to the **L**evel or **R**ight side of the amplifier.
- Whether the cable is connected to the amplifier **A** or **B** outputs on that side.
- Whether the cable is connected to the amplifier **D**rive or **T**erminator.

And for the kicker strip labels the three letters correspond to:

- Whether the cable is connected to the first (**1**) or second (**2**) kicker.
- Whether the cable is connected to the **U**pstream or **D**ownstream end of the kicker strip.
- Whether the cable is connected to the **L**evel or **R**ight kicker strip, as viewed looking at the upstream end of the kicker.

Finally, the patch panel connectors are simply labelled from 1 to 8 from left to right, as viewed from the front of the rack. All of the cable connections between the amplifier, patch panel and kickers are shown in Figure 6.11.

The patch panel cables all have lengths of around 3 ns, with the lengths of each matched to within the measurement error. After the re-routing and shortening of the kicker cables

Label	Length	Patch Panel Port	Kicker Strip
2907701A	$171.28 \pm 0.05$ ns	1	1UL
2907703A	$171.30 \pm 0.05$ ns	2	1UR
2907700A	$171.29 \pm 0.05$ ns	3	1DL
2907702A	$171.30 \pm 0.05$ ns	4	1DR
2907838A	$205.45 \pm 0.05$ ns	5	2DL
2907740A	$205.62 \pm 0.05$ ns	6	2DR
2907739A	$205.15 \pm 0.05$ ns	7	2UL
2907741A	$204.49 \pm 0.05$ ns	8	2UR

Table 6.5: Lengths of cables between the patch panel and the kickers.

the cables connected to the first kicker have a length of around 170 ns, whilst the cables for the downstream kicker are longer at around 205 ns. For the downstream kicker the latency requirements are slightly relaxed due to the additional 36 ns beam time of flight between the kickers. Rather than also shortening the downstream kicker cables as much as possible some additional slack was left so that the difference in lengths is similar to the difference in the beam time of flight between the two. This means the two correction outputs (one for each kicker) can be sent from the FONT5a board at, or close to, the same time as discussed in Section 6.5.3.

Although all the upstream kicker cables are matched within the measurement error there are some differences in the downstream kicker cable lengths, with cable 2907741A more than 1 ns shorter than cable 2907740A, for example. If there is a difference between the lengths of the cables connected to the downstream left and downstream right strips of a kicker (the driven end) there will be a time offset in the voltage applied to each side of the kicker, which would degrade the quality of the PFF correction. However, there is no need for the cables connected to the upstream ends of the kickers to be of matched lengths, the only requirement is that they are terminated correctly at the amplifier. The shorter 2907741A cable is therefore connected to the upstream end of the second kicker, and the cables 2907838A and 2907740A, with lengths matched to within 200 ps, are used to carry the amplifier output to the downstream end of the strips.

[TODO: Tolerances for cable length matching?]

### 6.5.2 Absolute Timing

#### Using Beam Pickup

[TODO: Kicker pick-up theory. In particular, is time between pickup exactly the beam pulse length or is it longer by double the kicker length?]

Figure 6.26 shows the beam pickup at the start and end of the pulse from the PFF kickers at CTF3, as seen on one of the amplifier monitoring outputs (each of the four amplifier monitoring outputs, one for the upstream end of each strip prior to the signal being terminated at the amplifier, gives a similar response). The separation of the peaks in the beam pickup

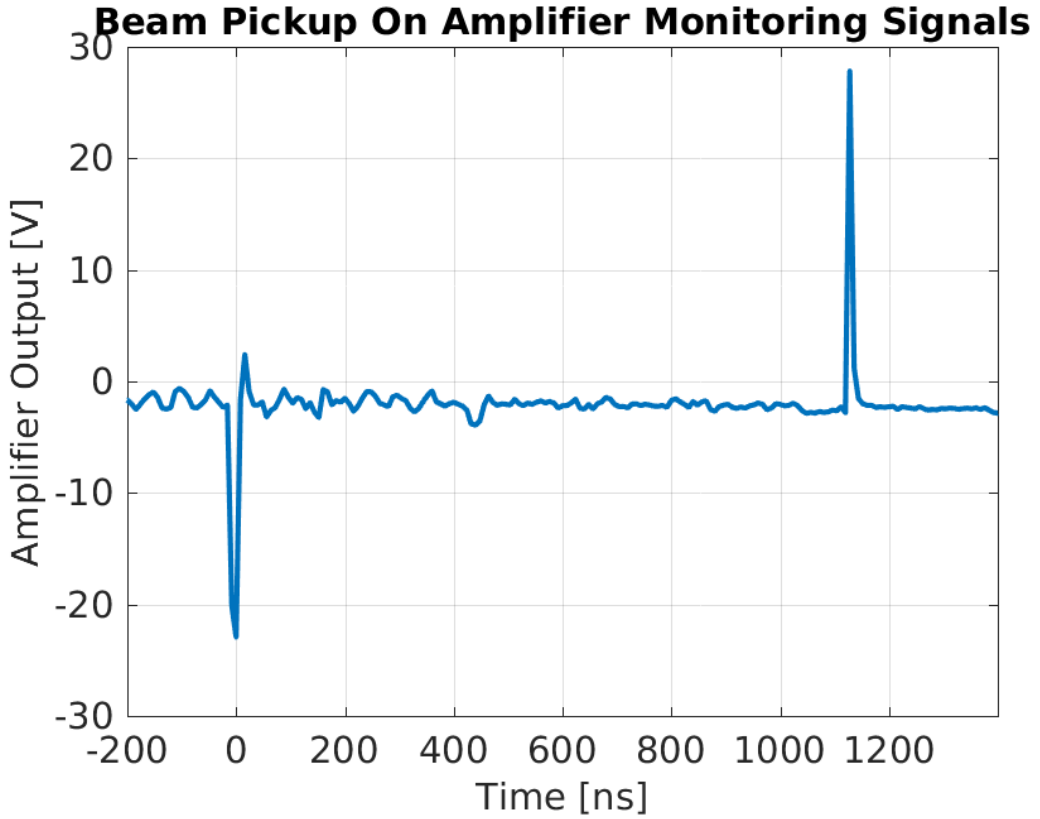


Figure 6.26: Beam pickup on kicker strips as seen on amplifier monitoring signals.

is  $1.1 \mu\text{s}$ , thus the same as the CTF3 pulse length as expected. By comparing the timing of these peaks with respect to the start and end of the amplifier output pulse, using the same amplifier monitoring signal, it is possible to ensure that the correction output arrives in sync with the beam.

An example of this is shown in Figure 6.27. A constant DAC output is sent from the FONT5a board to the amplifier and both this output pulse and the beam pickup, at samples 275 and 493, are visible in the figure. Importantly, the DAC output is gated using the upstream phase monitor diode signal (in other words, the constant DAC output is only sent during the time when the diode is non-zero) and this has two consequences. Firstly, the amplifier output pulse has the same length as the beam pulse in the upstream phase monitor. Secondly, the timing of the output is identical to what it would be in normal PFF operation. In the case of Figure 6.27 the drive to the amplifier is sent as quickly as possible after the arrival of the upstream diode signal at the FONT5a board. It can be seen that the amplifier pulse arrives before the beam pickup, thus with the PFF system setup this way the correction would be applied slightly early. This result therefore proves that the PFF system just meets the latency requirements, with the overall time needed to transport and process all the relevant signals a few tens of nanoseconds less than the 380 ns time of flight of the beam between the upstream phase monitor and the first kicker. However, what is also clear in the figure is that the time offset between the start of the amplifier pulse and the first beam pickup spike is much larger than the time difference between the end of the amplifier pulse and the second beam pickup spike. This is due to the energy transient across the first 100 ns

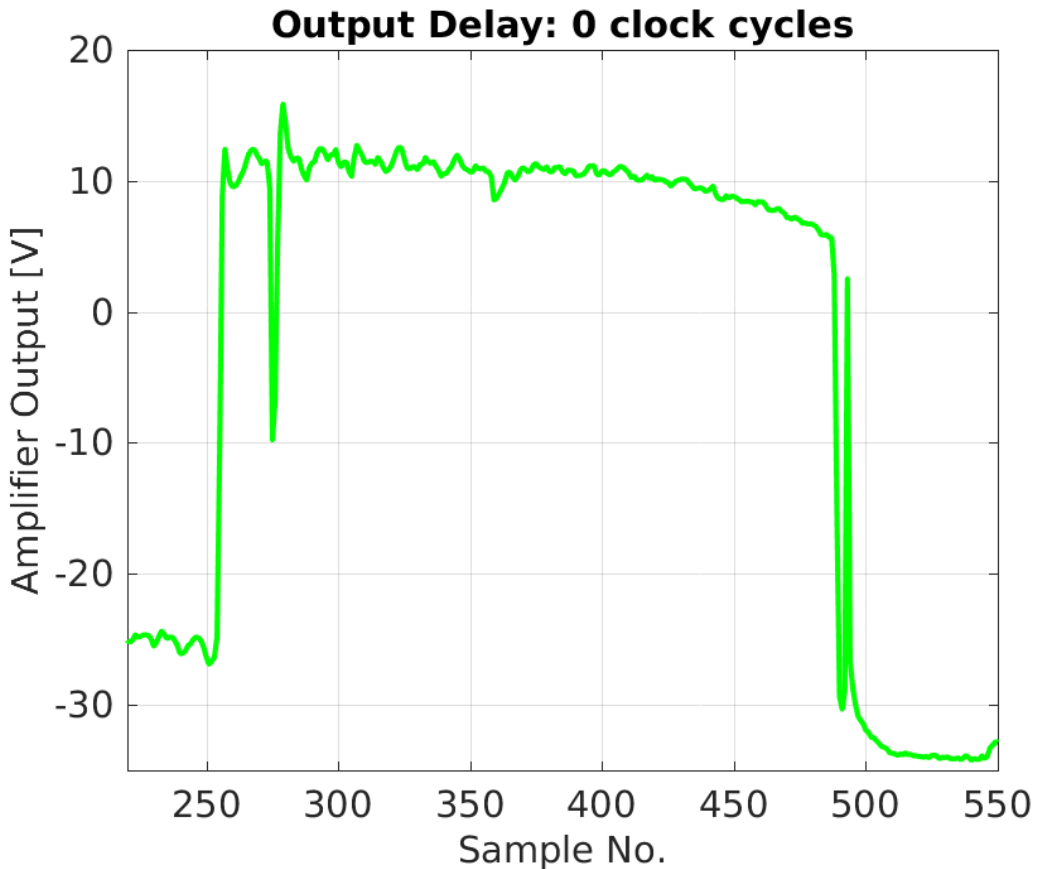


Figure 6.27: Output delay of 0 clock cycles. Full pulse.

of the CTF3 beam pulse which is present in the upstream phase monitor but is then lost prior to the TL2 chicane, predominantly in TL1. As a result the downstream beam pulse is shorter than the upstream beam pulse which defines the length of the correction output. Therefore, in order to align the correction output with the beam the signals from the end of the amplifier and beam pulses must be used, not the start.

The firmware for the FONT5a board includes an output delay parameter that can be used to fine-tune the timing of the correction output sent to the amplifier. This can be done independently for each of the two correction outputs so that it can be ensured the correction arrives in sync with the beam in each kicker individually (the relative timing of the two kickers is discussed in the next section). The delay can be varied between 0 and 31 clock cycles in integer steps, with one clock cycle corresponding to one period of the 357 MHz ADC clock frequency, or 2.8 ns. A delay of up to 86.8 ns can therefore be added to the correction outputs. Figure 6.28 shows the effect of varying the output delay across the full range of possible values, zoomed in on the end of the pulse. For all output delays the beam pickup remains at sample 493, as expected. Meanwhile, the end of the amplifier pulse is moved from before the beam pickup (output too early) to after the beam pickup (output too late). To achieve the optimal correction timing the end of the amplifier pulse must be aligned with the beam pickup and this is achieved with a delay of 7 clock cycles, or 19.6 ns, as shown in Figures 6.29 and 6.30. This delay has been used for the latest PFF runs presented in Chapter 8. Due to ambiguity in which point along the falling edge of the amplifier pulse the

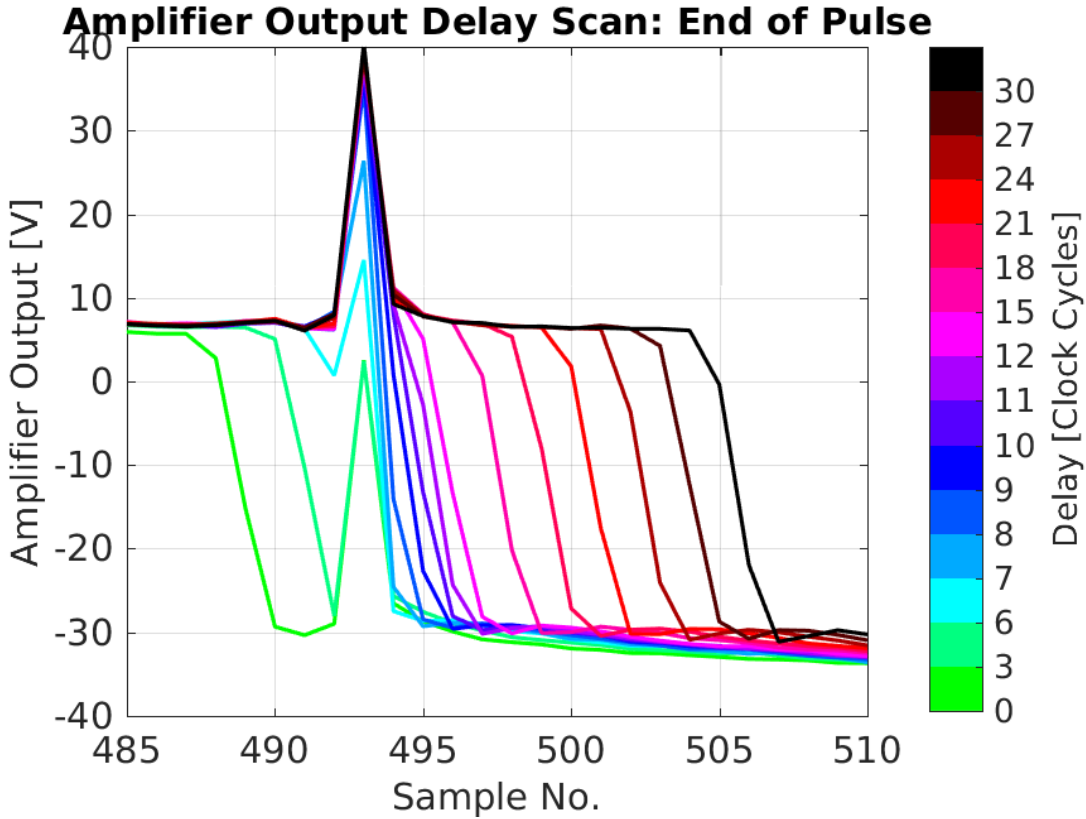


Figure 6.28: Output delay scan, end of pulse.

beam pickup should be aligned to there may be a remaining error of up 3 clock cycles in the exact alignment, and this can only be verified by beam based measurements (not using the amplifier monitoring outputs).

### Using BPMs

This section presents one way in which the correction output timing can be determined using a combination of the phase monitor measurements and a BPM signal downstream of the TL2 chicane. The results shown here were performed with the first, lower power version of the amplifier and the FONT5 rather than the later FONT5a board, and because of this the optimal output delay calculated here does not agree with the value of 7 clock cycles from the beam pickup based measurement above. The newer hardware has the same latency as the previous versions, thus the difference does not come from hardware changes but rather associated changes to cabling between the phase monitor electronics, FONT5a board and amplifier. The measurement will be repeated in the future to verify that both methods give consistent results when the same hardware and cabling setup is used.

The FONT5 (and FONT5a) board firmware provides the functionality to be able to change the gain of each PFF correction output independently. This means it is possible to apply the correction to only one kicker, or to kick the beam in the same direction in each kicker (i.e. to use the same sign for the gain in each kicker, rather than gains with equal magnitude but opposite sign). In both of these cases the kicked PFF orbit in the chicane

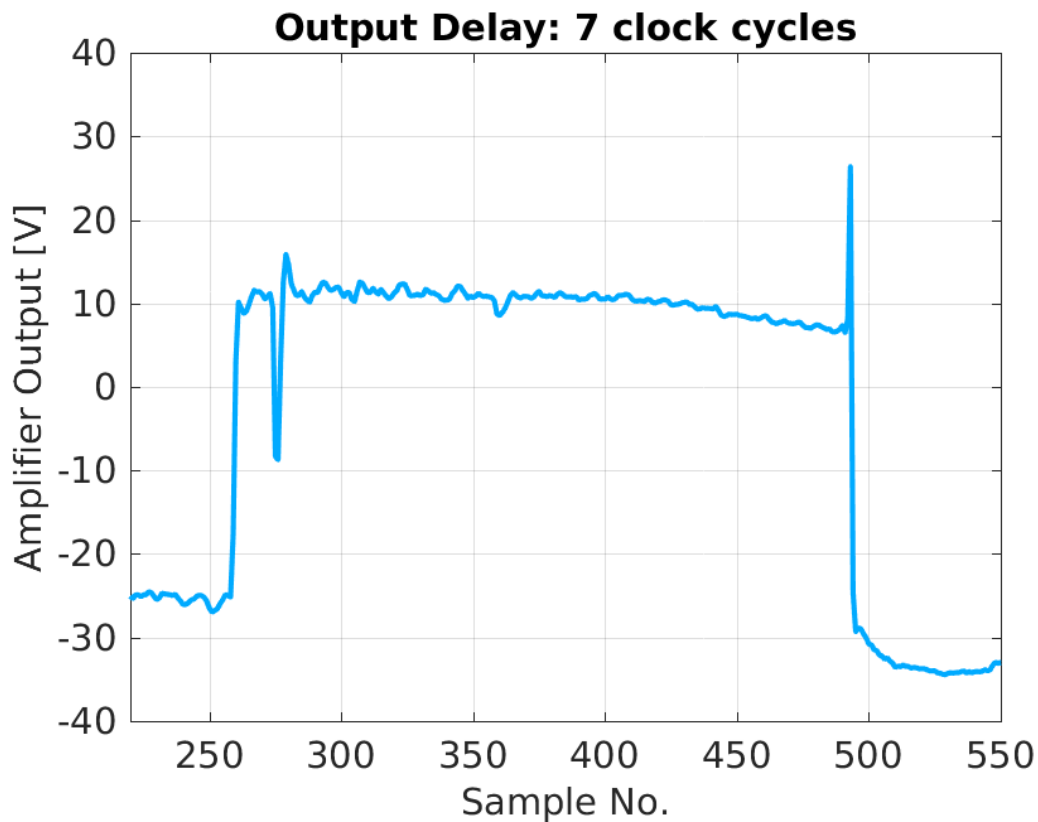


Figure 6.29: Output delay of 7 clock cycles. Full pulse.

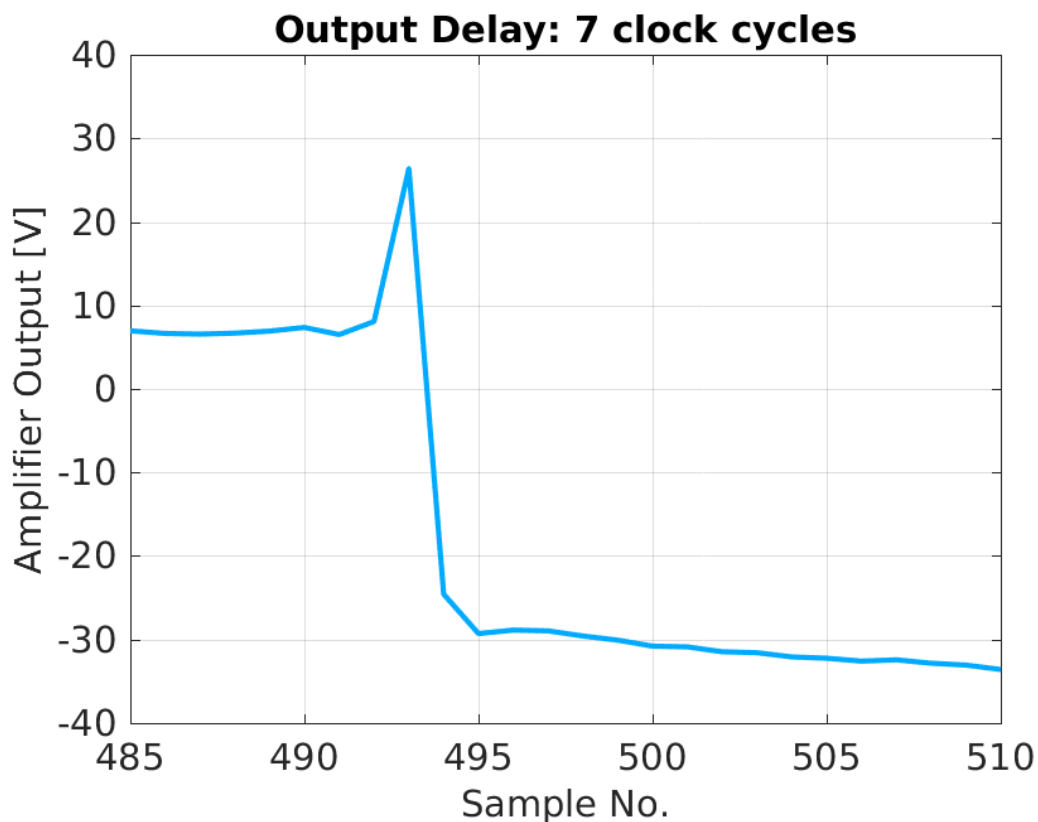


Figure 6.30: Output delay of 7 clock cycles. End of pulse.

is not closed, thus the horizontal position along the beam pulse in a BPM after the chicane depends on the shape and timing of the applied correction.<sup>2</sup>

Figure 6.31 compares the upstream phase, downstream phase and horizontal position (in a BPM after the TL2 chicane) along the pulse in the case where the PFF correction is applied with gains set to kick the beam in the same direction in each kicker, and with no output delay applied in the FONT5 board. The data is taken in interleaved mode, with the plotted phases shown using the PFF off data and the BPM trace being the difference between the PFF on and PFF off data. Each signal is scaled and sign flipped where necessary to give variations along the pulse with the same magnitude and sign, in arbitrary units. The BPM and phase monitor signals are acquired with the same sampling frequency of 192 MHz, with each aligned so that the end of the pulse is at the same sample number.

By taking the difference of the PFF off and PFF on data in the BPM any residual orbit variations along the pulse not related to the PFF system are removed, thus the remaining shape should match that of the PFF correction output, which in turn is linked to the upstream phase. The downstream phase should also have the same shape as the upstream phase with the PFF system off, within the limits of the upstream-downstream phase correlation achieved at this time. During this measurement many oscillations along the upstream phase were present, which usually are not desired but for this measurement are perfect points of reference to check the time alignment of the signals. As expected the overall shape of the residual horizontal position in the BPM along the pulse and the two phase signals is very similar. The largest feature in the upstream phase that is present in all three signals occurs at sample 671 in the upstream phase, with the location of the peak of this oscillation in the phase signals and the BPM marked by vertical black lines in the figure. The peak as seen in the BPM signal is clearly before the peak in the phase monitor signals thus in this case the correction was applied early, with a measured offset of -36 ns between the peaks.

This measurement was repeated with four different correction output delays applied in the FONT5 board, at delays of 0, 10, 20 and 30 clock cycles (0 to 84 ns), which includes points where the correction is applied both early and late. Fitting the measured time offset between the peaks in the BPM and the phase in the same way as before yields an optimal correction output delay to apply of  $39 \pm 7$  ns (Figure 6.32), or  $14 \pm 3$  clock cycles. Applying this delay in data analysis gives the result shown in Figure 6.33, in which the similarity of the three signals becomes clear.

### 6.5.3 Relative Kicker Timing

For the phase correction the absolute output timing sent to the first kicker, as derived above, is the most critical as this defines the alignment of the applied phase shift in the chicane with the beam. The second kicker's main purpose is then to close the kick created by the first, ensuring the orbit after the chicane is closed (with the caveats already mentioned in Section 6.4.4). For the purposes of orbit closure it is also important to ensure that the

---

<sup>2</sup>In Section 6.4.4 it was shown that the corrected orbit is not perfectly closed in normal PFF operation either. However, in this case no attempt at orbit closure is made so the measured effect seen in the BPMs is much larger.

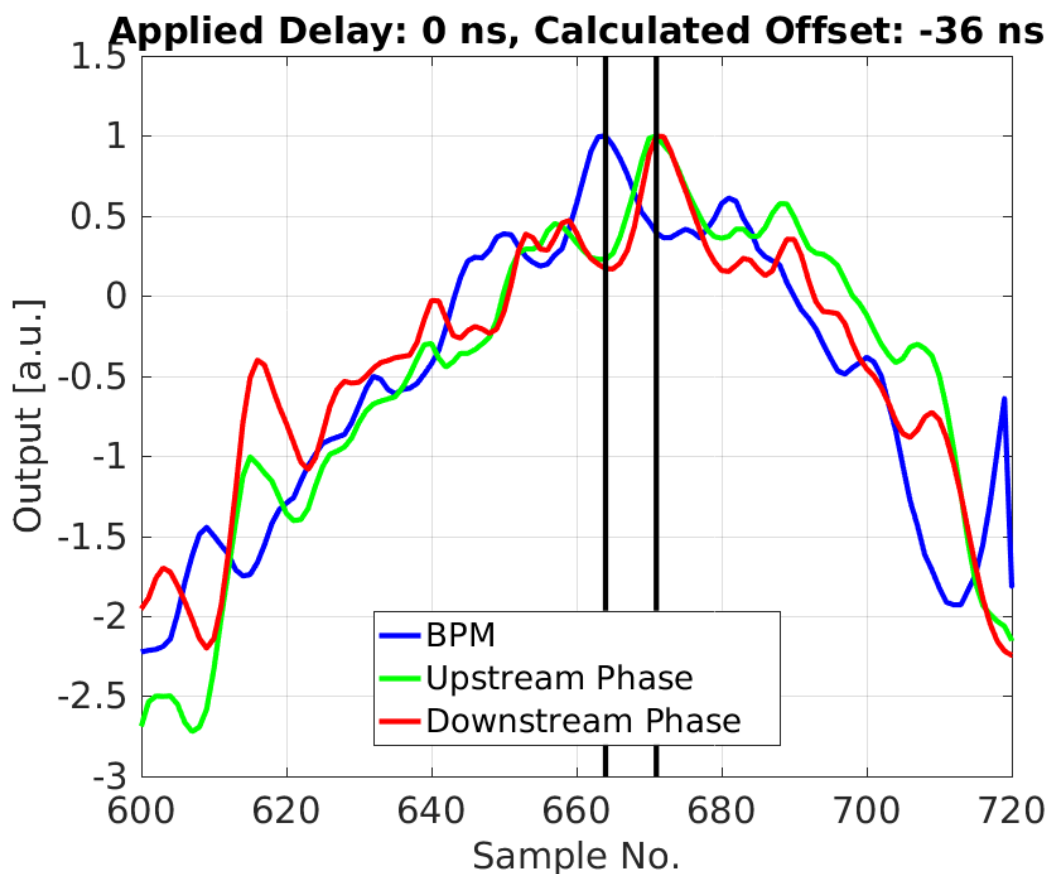


Figure 6.31: Kick output with no delay as seen on BPM and phase signals.

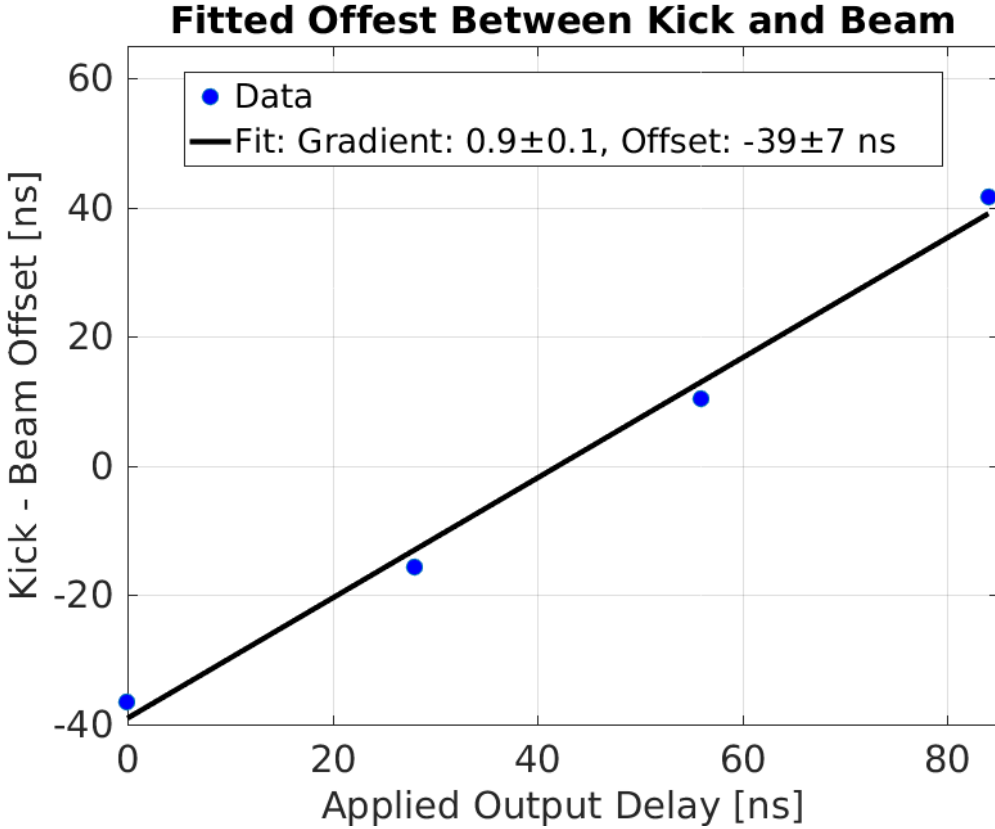


Figure 6.32: Fit time offset between kick and beam at different output delays.

correction arrives at the second kicker in time with the beam. As discussed in Section 6.5.1 the beam time of flight between the kickers is about 36 ns, thus the correction must arrive at the second kicker 36 ns later than the first kicker. Most of this difference should be accounted for by the longer cable lengths for the second kicker, but the precise relative timing is checked here. In this context the relative timing means the additional output delay that must be applied to the FONT5a correction output for the second kicker with respect to the first in order to ensure the correction is aligned in time with the beam in both kickers.

Figure 6.34 shows a simulated example of the expected effect of kicking the beam with a relative time offset in each kicker, in this case with the output to the second kicker arriving later than the first kicker (with respect to the beam pulse). The kickers are driven with opposite polarity in the same way as the PFF system, and the first kicker is shown with a larger output than the second. The total kick received in the chicane is given by the sum of the two, shown in black. In the ideal case the total/residual kick in the chicane should be zero so that the orbit is closed after the chicane. However, with a timing offset between the two kickers there are large peaks in the residual kick at the start and end of the pulse, where only one of the two kickers receives its full drive. Due to the different amplitude of the two kickers the residual kick is also non-zero in the central part of the pulse. With well-aligned timing the residual kick would be constant along the full pulse length, or zero across the full pulse length if the kicks had matched amplitudes.

By varying the relative timing of the two correction outputs on the FONT5a board

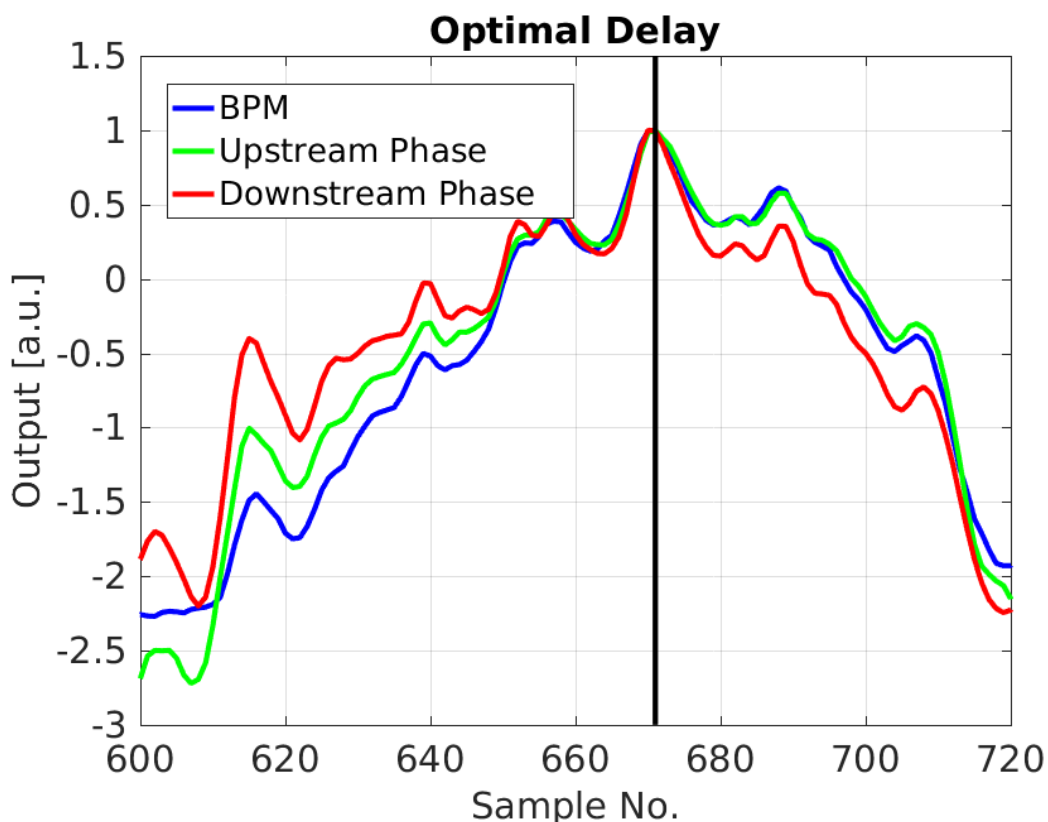


Figure 6.33: Alignment between BPMs and phase signals with optimal delay applied in analysis.

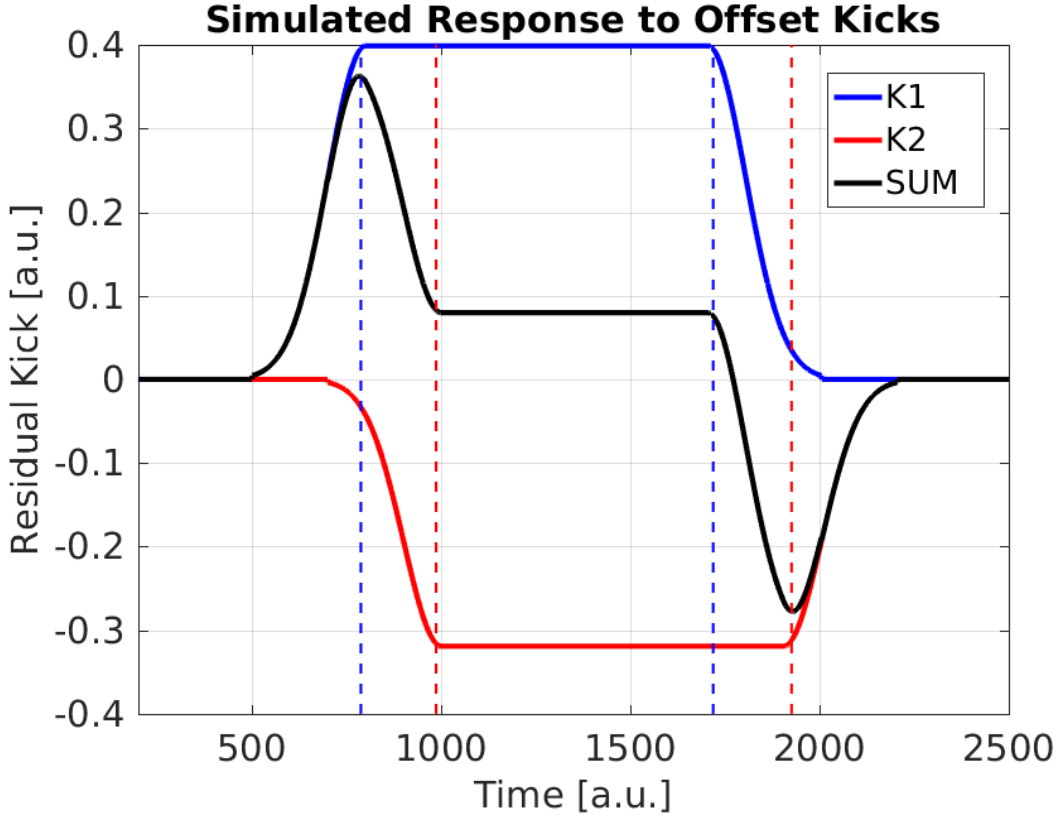


Figure 6.34: Simulated response to offset kicks.

(K1 and K2 delay) and using a BPM after the TL2 chicane to measure the size of the peaks at the start and end of the pulse resulting from the offset kicks (in the same way as Figure 6.34) the optimal relative delay can be determined. The optimal relative delay is the point that minimises the size of the peaks on the rising/falling edge of the pulse, with the peak magnitude approximately linearly dependent on the delay. Figure 6.35 shows the result of doing this, using a constant DAC output from the FONT5a board applied across a 168 ns portion of the pulse. The horizontal position in a BPM after the TL2 chicane is plotted for relative K2 delays ranging between -10 (K1 output delayed with respect to K2) to +10 (K2 output delayed with respect to K1) clock cycles. Aside from the asymmetry between the size of the peaks at the start and end of the pulse the result is as expected from the example previously discussed. [TODO: Why asymmetry? Differences in output along pulse?]. Note the non-zero position offset in the central part of the pulse. Based on the orbit closure results in Section 6.4.4 this is predominantly due to optics differences leading to a non-closed orbit, rather than the small difference in amplifier output voltage to each kicker.

Figure 6.36 then shows the peak beam offset in the BPM versus the relative K2 delay using the falling edge of the pulse. The peak beam offset is defined as the difference between the maximum and minimum beam position after the chicane between sample 458 and 477 (as seen in Figure 6.35 [TODO: Add vertical lines to show ranges?]). As the K2 delay approaches the optimal value the difference in beam position in this range converges to the 0.3 mm offset in the flat central part of the kicked pulse. The point of intersection between the two linear fits shown (one for the points with a positive peak position and the other for points with a

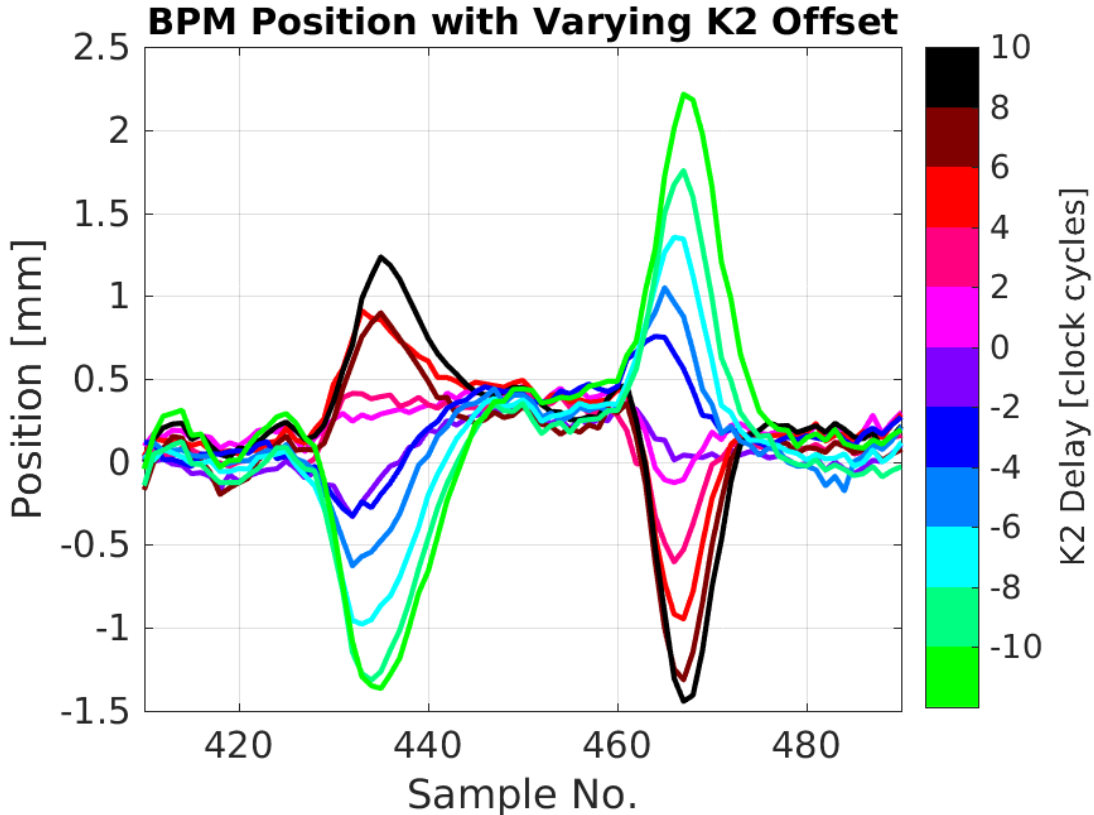


Figure 6.35: Measured BPM offset for different relative kick delays.

negative peak) gives the optimal relative K2 offset to be  $0.1 \pm 0.5$  clock cycles. Repeating the procedure for the peaks at the rising edge of the pulse gives a result of  $1.9 \pm 2.0$  clock cycles, and the two results combine to give an optimal value of  $0.5 \pm 0.6$  clock cycles.

Relative K2 delays of both 0 and 1 clock cycles have been used during PFF operation, with no measurable difference in the PFF results between the two to date although this will have to be verified with further orbit closure tests. Adding the absolute delay of 7 clock cycles derived in Section 6.5.2, the final delays to apply in the FONT5a board are:

- **K1 delay:** 7 clock cycles.
- **K2 delay:** 7 or 8 clock cycles.

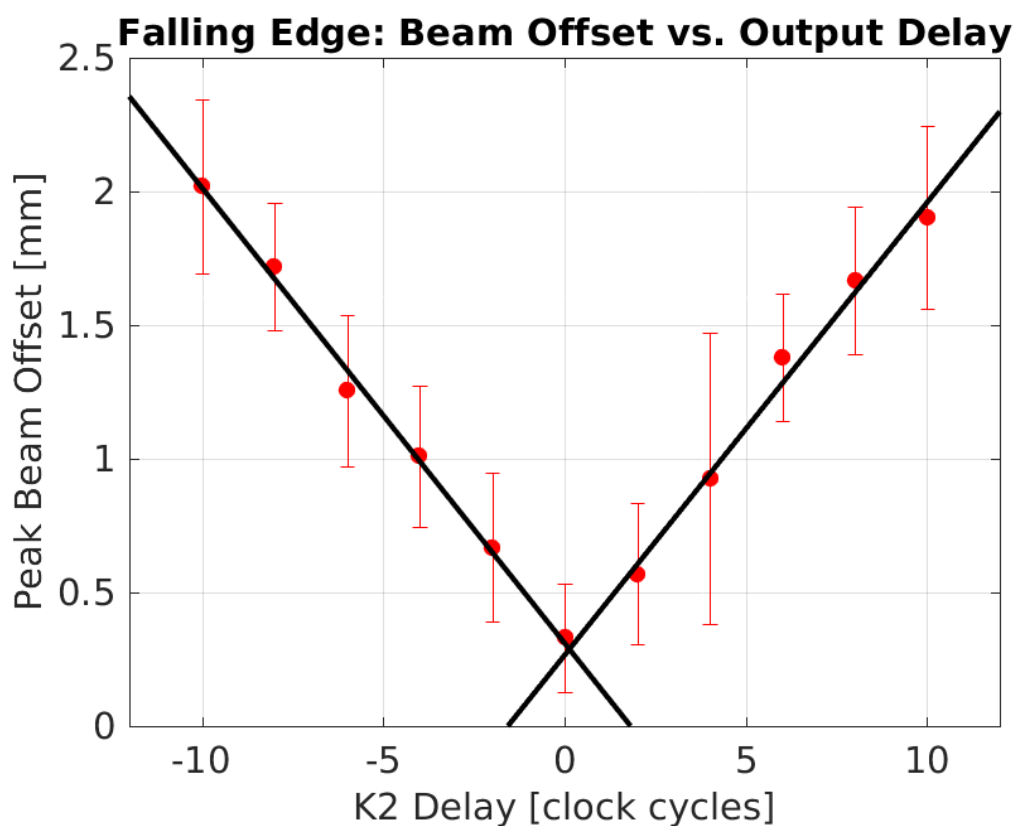


Figure 6.36: Fitted peak BPM offset vs. relative kick delay.

# Chapter 7

## Early Phase Feedforward Attempts and Simulations

This is the introductory text.

### 7.1 Gain Scans

### 7.2 Simulation Method

### 7.3 Effect of Limited Correction Range

### 7.4 Effect of Timing Offsets

### 7.5 Effect of Limited Bandwidth

### 7.6 Effect of Variations Along the Pulse

correlation, jitter

### 7.7 Effect of Amplifier Non-linearities

# Chapter 8

## Best Achieved Phase Stabilisation

Over the course of 2014 and 2015 much experience has been gained with the PFF system and vast improvements have been made to the system setup, hardware performance and beam conditions as discussed in previous chapters. Many datasets have been taken, in particular in December 2014, July 2015 and November 2015, and in all cases a reduction in downstream phase jitter has been achieved. The purpose of this chapter is to present and discuss the downstream phase stability that was accomplished on the 20th November 2015, the day during which the best overall conditions to date for the PFF correction were obtained.

### 8.1 Lowest Achieved Phase Jitter

The results presented in this section show the best downstream phase jitter currently achieved at CTF3 with the PFF correction. Naturally, this dataset was taken during the best beam conditions currently achieved at CTF3 in terms of phase propagation, taken just after a series of R56 and beam energy optimisations using the same methods discussed in Chapter 5. In particular, the first attempt to smooth the upstream phase along the pulse by adjusting the waveform of the first klystron in the CTF3 injector (MKS02) as described in Section 5.5.3 yielded the highest upstream-downstream phase correlation achieved to date in normal conditions (higher correlations can be achieved by adding an additional jitter source upstream, as seen in Section 9.1). November 2015 also represents the first time the PFF system was operated with the improved phase monitor resolution after switching to mechanical phase shifters (Section 4.5) and with the latest version of the amplifier which doubled the correction range compared to earlier tests (Section 6.2).

The dataset was taken on the 20th November 2015 as one of a sequence of short measurements fine-tuning the gain around the optimal value. Results from the other datasets in this sequence are discussed in the following section to demonstrate the phase stability achieved on longer time scales. The individual dataset shown here comprises 150 pulses taken in interleaved mode, with the correction applied to the 75 odd indexed pulses and no correction applied to the remaining 75 even indexed pulses. The used gain in FONT5a units was 800, corresponding to an actual applied correction of 1.13 times the upstream phase

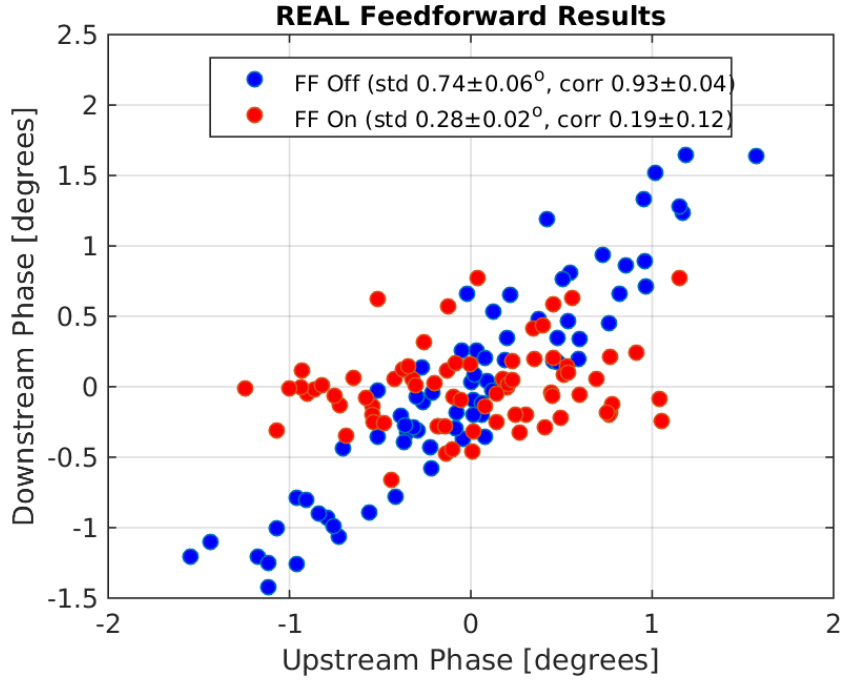


Figure 8.1: Mean phase.

using the conversion factor calculated in Section ?? [TODO: Scale based on new conversion factor].

### 8.1.1 Mean Phase Jitter

Initially considering the mean pulse phase, the correlation with the PFF correction off in this dataset, as shown by the blue distribution of points in Figure 8.1, is  $0.93 \pm 0.04$ . This gives a theoretical limit of a factor  $2.7 \pm 0.4$  reduction in the downstream jitter using Equation 2.1. The achieved uncorrected downstream mean phase jitter of  $0.74 \pm 0.06^\circ$  and downstream-upstream jitter ratio of  $1.1 \pm 0.1$  are also the lowest achieved at CTF3 to date. With this initial jitter and the theoretical reduction factor of  $2.7 \pm 0.4$  the lowest corrected downstream jitter that could be achieved is then  $0.27 \pm 0.05^\circ$ . The aforementioned correlation and jitter ratio combine to give an optimal gain of  $1.0 \pm 0.1$  (Equation 2.2). The actual system gain of 1.1 [TODO: update based on new conversion factor] and the optimal gain therefore agree within the error bars, thus the theoretical corrected downstream jitter of  $0.27 \pm 0.05^\circ$  should also be possible with the actual system.

The red distribution of points in Figure 8.1 then shows the effect of the PFF correction on the phase distribution. The downstream phase jitter is reduced from  $0.74 \pm 0.06^\circ$  to  $0.28 \pm 0.02^\circ$ , a reduction of a factor  $2.6 \pm 0.3$ . Within the error this does indeed agree perfectly with the theoretical limit derived previously given the beam conditions in this dataset, as expected. The correction acts to remove all correlation between the upstream and downstream phase, rotating the distribution as seen in the plot. The correlation is reduced from  $0.93 \pm 0.04$  to  $0.19 \pm 0.12$ .

Correction Status	Upstream Jitter	Downstream Jitter	Correlation
FF Off	$0.69 \pm 0.06^\circ$	$0.74 \pm 0.06^\circ$	$0.93 \pm 0.04$
FF On	$0.57 \pm 0.05^\circ$	$0.28 \pm 0.02^\circ$	$0.19 \pm 0.12$
FF Simulated	$0.69 \pm 0.06^\circ$	$0.27 \pm 0.02^\circ$	$0.06 \pm 0.12$

Table 8.1: Best PFF results.

In terms of the achieved downstream phase jitter it should be noted, however, that the measured upstream jitter of  $0.57 \pm 0.05^\circ$  across the pulses with the PFF correction on in this dataset is lower than the  $0.69 \pm 0.06^\circ$  measured with the PFF system off (Table 8.1). This is assumed to be a statistical fluctuation rather than being a systematic difference between the odd and even pulses at CTF3 or an effect of the correction (which can only influence the downstream phase) [TODO: calculate how likely this fluctuation is/check there is no systematic difference between odd/even]. Assuming the PFF on upstream jitter propagated downstream with the same ratio as the PFF off data, the true ‘natural’ downstream jitter without the correction applied would have been  $0.61 \pm 0.09^\circ$  and the true factor reduction in the corrected jitter achieved with the PFF system would be decreased to  $2.2 \pm 0.4$ . Assuming the upstream-downstream phase correlation was also not affected by this statistical fluctuation (so that the theoretical jitter reduction of a factor  $2.7 \pm 0.4$  still holds), a corrected jitter of  $0.23 \pm 0.05^\circ$  would have been theoretically possible for the PFF on pulses in this dataset.

[TODO: Distribution of points at around 0.5 degrees downstream?]

With interleaved data it is also possible to simulate the expected effect of the correction empirically, as an additional point of comparison between the achieved and expected results plus to verify that the complete behaviour of the system is understood. The distribution of simulated corrected phases is shown in green on Figure 8.2. It is derived by taking the initial distribution with the PFF system off (blue points) and subtracting the upstream phase, multiplied by a gain factor, from the downstream phase. This exactly mimics what the feedforward system would have done if it had been applied to the even pulses in this dataset, and can be directly compared to the odd pulses taken at the same time with the actual correction applied. In this example the simulation shown is the ideal case, considering a correction with infinite range and bandwidth applied with the optimal gain. As expected the simulated corrected downstream jitter of  $0.27 \pm 0.02$  agrees perfectly with the theoretical prediction of  $0.27 \pm 0.05^\circ$  previously derived. The achieved jitter of  $0.28 \pm 0.02$  matches both the theoretical and simulated jitter predictions within the error, giving confidence that the overall PFF setup in this dataset (after all the commissioning steps discussed in Chapter 6) was close to optimal. There is perhaps some room for improvement due to the difference between the upstream jitter in the PFF on and off data, as mentioned previously, and this will be elaborated on in Section 8.2 below. Nevertheless, this result clearly demonstrates stability on the mean phase approaching the CLIC target of 0.2 degrees at 12 GHz and demonstrates that achieving this stability with a PFF system is feasible.

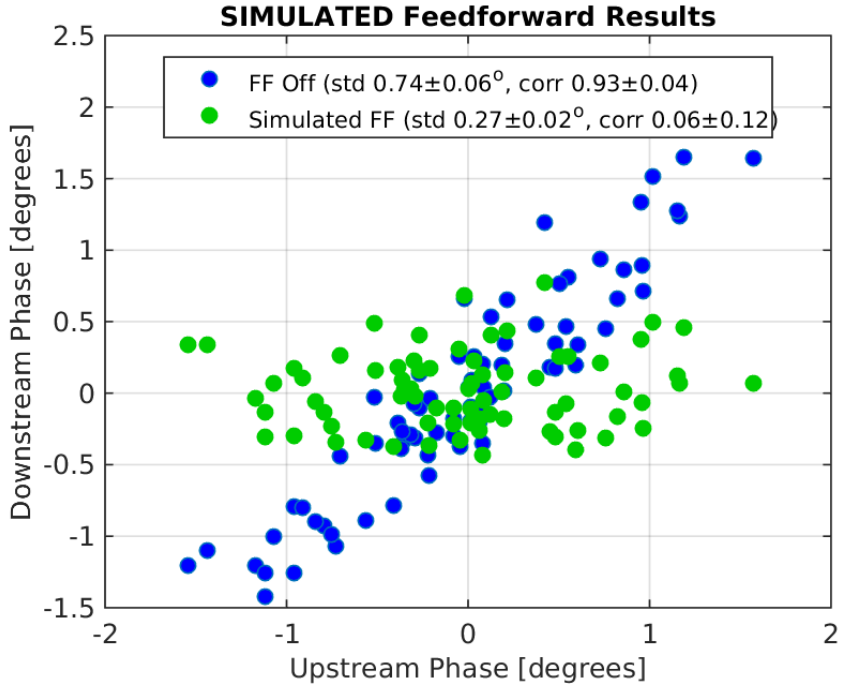


Figure 8.2: Simulated PFF.

### 8.1.2 Correction of Pulse Shape

Moving on to the stabilisation of the phase along the pulse, Figure 8.3 shows the mean phase along the pulse upstream, downstream with the PFF system off and downstream with the PFF system on. The vertical black lines mark the sample range that was used to calculate the mean phase results presented previously. This range is chosen to cover the maximal proportion of the pulse within which the the correction is not being saturated as a result of the phase sag (plus jitter) exceeding the  $\pm 6^\circ$  correction range. It covers a total of 81 samples at 5.2 ns per sample, giving a total time span of 422 ns. The demonstration of  $0.28 \pm 0.01^\circ$  mean phase stability is therefore already on a much longer pulse than is needed for CLIC, where the combined pulse length is only 240 ns. [TODO: Any significant reduction in measured jitter by using 240ns window?]

With the optimised phase propagation in place the overall shape of the upstream and (uncorrected) downstream phase, in green and blue respectively, along the pulse are very similar, although small uncorrelated variations are still visible. These uncorrelated differences are then visible in the corrected downstream phase (in red), although the overall ability of the PFF system to flatten the CTF phase sag within the sample range is strikingly clear. The original peak-to-peak variation in the mean downstream phase along the pulse of  $5.76 \pm 0.14^\circ$  with the correction off is reduced to  $0.65 \pm 0.07^\circ$  degrees with the correction applied within the indicated range. Outside the central region of the pulse, where the amplifier is saturated, the PFF system can no longer correct the shape of the phase along the pulse. The only effect is to shift the phase by the maximum possible correction of  $5.5^\circ$ .

Figure 8.4 expresses the effect of the PFF system on the phase along the pulse within the central region in terms of the distribution of ‘flatness’ values for each pulse in the data

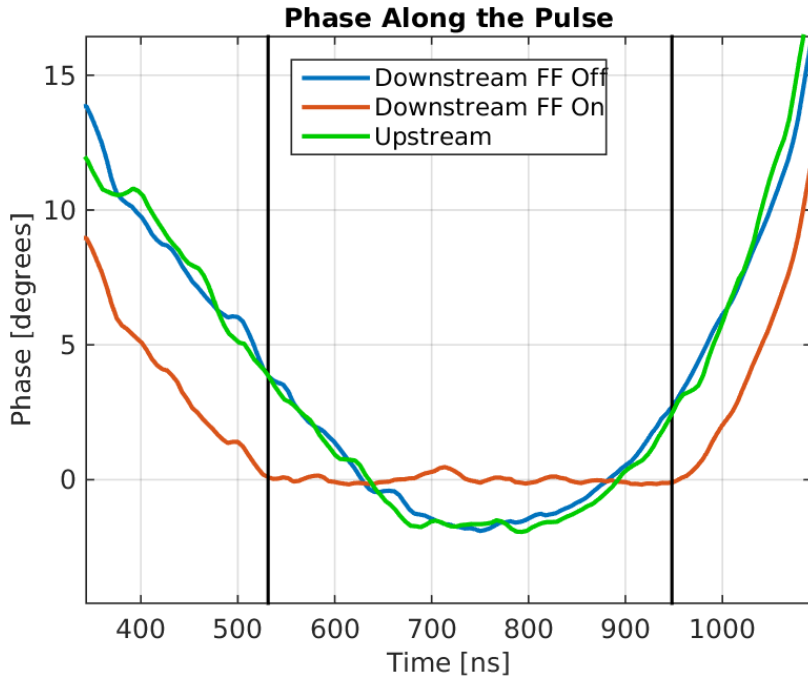


Figure 8.3: Mean phase along.

set with PFF system off and on. For each pulse the flatness value is defined as the standard deviation of phase values about the mean across the sample range. In this case the flatness value of each pulse therefore corresponds to the standard deviation of 81 values (the length of the sample range). A pulse with a flatness value of zero would have constant phase across the whole sample range, with no small variations such as those seen in Figure 8.3. The value is also insensitive to the jitter on the overall mean pulse phase seen earlier in Figure 8.1. In Figure 8.4, the initial uncorrected downstream pulse flatness, dominated by the phase sag at CTF3, of  $1.68 \pm 0.02^\circ$  is reduced to  $0.26 \pm 0.01^\circ$  with the correction applied. On average, the corrected pulses are  $6.5 \pm 0.3$  times ‘flatter’ than the uncorrected pulses.

### 8.1.3 Phase Jitter Along the Pulse

Finally, Figure 8.5 shows the overall phase jitter at each sample along the pulse upstream and downstream with the PFF system off and on. These jitter values contain components coming from both the jitter on the overall mean pulse phase discussed initially and from the variations along the pulse (the non-zero flatness of each pulse). These jitter values are therefore larger and taking the mean sample jitter within the sample range an initial downstream jitter of  $0.72 \pm 0^\circ$  is reduced to  $0.36 \pm 0^\circ$  by the correction in this case, a factor 2 reduction. There are also variations of up to a factor 2 in the jitter that was achieved at each sample point, the lowest jitter being  $0.27 \pm 0^\circ$  at time 797 ns on the x-axis and the worst  $0.52 \pm 0^\circ$  at time 552 ns. The achieved jitter along the pulse within the central sample range also agrees with the simulated result of  $0.38 \pm 0^\circ$  using the interleaved pulses without the correction applied, as shown in Figure 8.6.[TODO: Error bars] Again, outside the sample range the actual system can not match the unlimited range simulation as the phase sag along

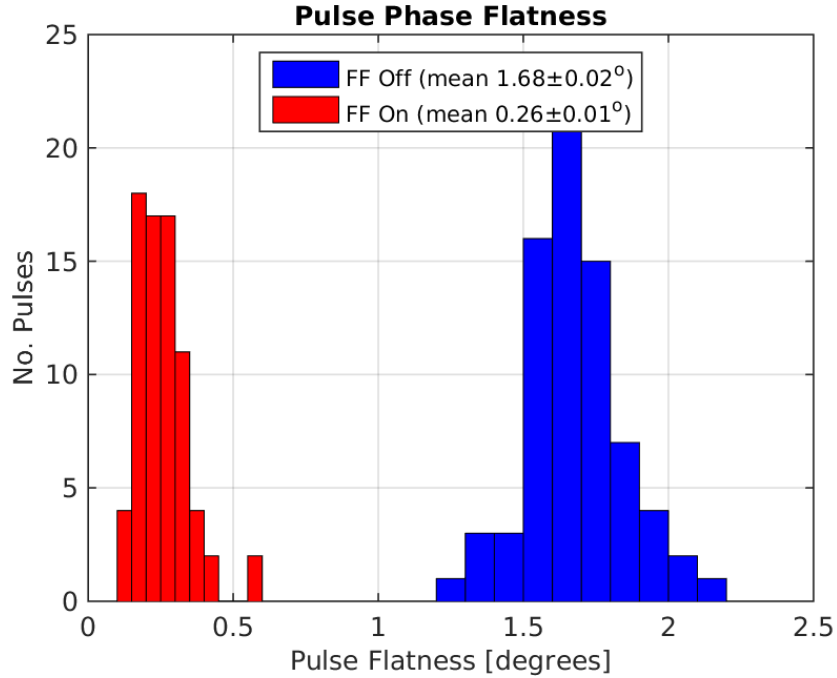


Figure 8.4: Flatness.

the pulse saturates the correction.

The sample by sample phase jitter along the pulse is the true figure of merit which must be reduced to 0.2° at CLIC. Although the largest component of phase jitter at CTF3 is on the pulse mean, effects such as energy variations along the pulse cause differences in the jitter and upstream-downstream phase correlation at each sample point [TODO: sec ref]. This leads to the variations in the achievable corrected downstream jitter along the pulse seen here, which can only be improved by further fine-tuning of the CTF3 injector stability and optics. [TODO: More details. Maybe correlation plot?]

## 8.2 Correction on Longer Time Scales

The remainder of this chapter focuses on remaining operational issues for the PFF system largely resulting from drifts in the CTF3 beam conditions. This section therefore discusses the status of the correction across longer time scales, presenting both the level of corrected phase jitter that can currently be achieved routinely and to highlight areas where improvements are still needed both in the PFF setup itself and the beam conditions. Being able to regularly demonstrate and maintain corrected downstream phase jitters at the level achieved in the best dataset shown previously (below 0.3°) on the mean phase, is one of the key goals for the PFF prototype in 2016. To be concise this section focuses on the mean phase jitter, though exactly the same arguments can be applied to the correction of the jitter along the pulse and the pulse shape.

The data used is from around 15:25 to 18:05 on the 20th November 2015, the same day as the record result previously shown which was taken during this period at 15:38. The

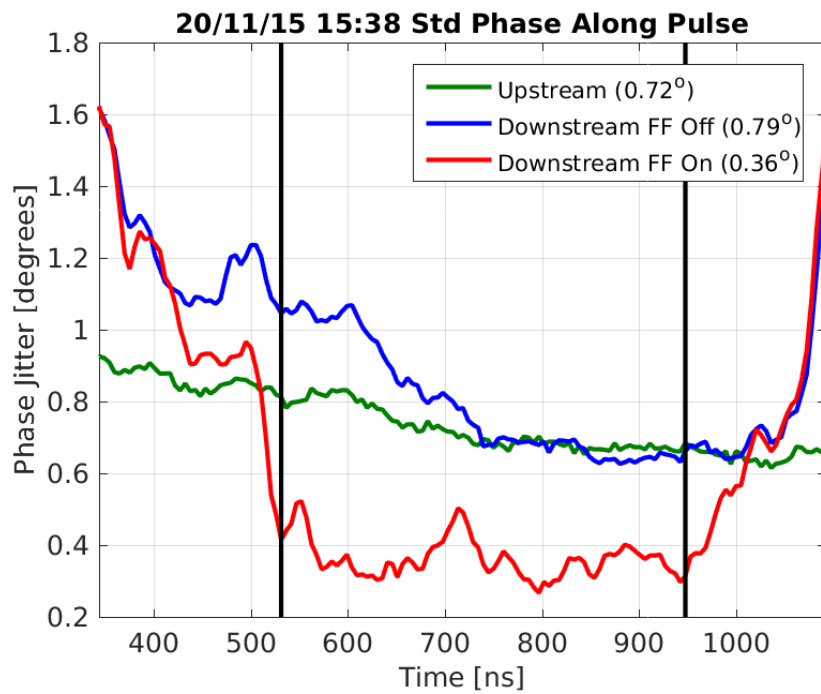


Figure 8.5: Std phase along.

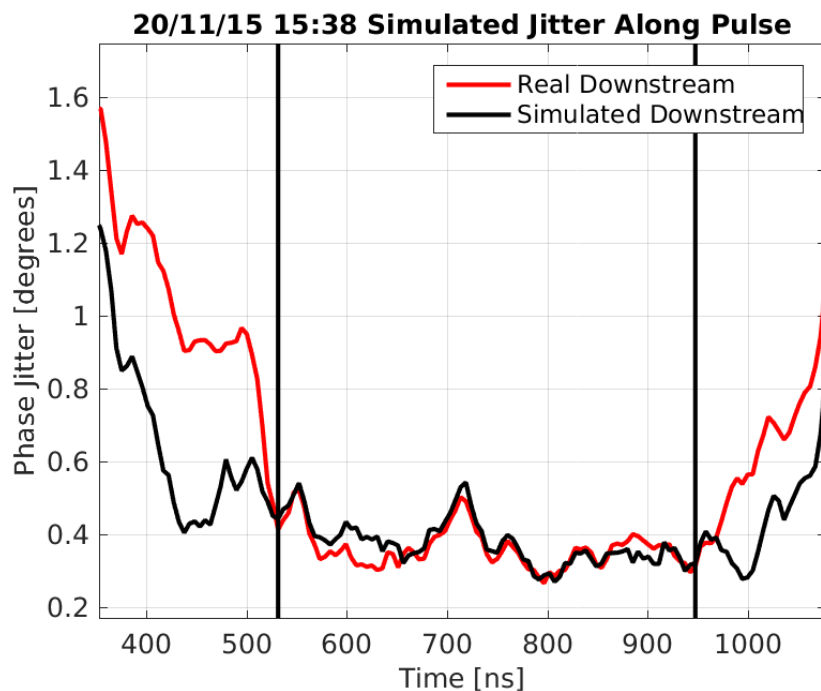


Figure 8.6: Std phase along.

PFF system was not operated continuously throughout this two and a half hour window but 15 individual datasets of a few hundred pulses each were taken and these results have been combined to create a large sample of 3083 interleaved pulses (1541 with the correction on and 1542 with the correction off). The raw history of the mean phases upstream and downstream with the correction on and off in the combined data are shown in Figure 8.7. The time span of each individual dataset is marked by vertical black lines and the times displayed on the plot represent the start time of each dataset. [TODO: Pulse no. from 1-3083 rather than 1-1500 and offset odd/even by one]. Note that the large jump in the downstream phase between the 16:00 and 16:04 datasets was caused by changes made to magnetic correctors in the TL2 chicane in order to re-optimize the beam orbit and transmission to the downstream phase monitors at this time. In Figure 8.17 the mean phase is subtracted (separately for the upstream, downstream PFF off and downstream PFF on phase) from each dataset to remove this effect, making a comparison between datasets easier. It is important to emphasise that, apart from this jump in the downstream phase, the overall picture is a fair reflection of the (uncorrected) phase stability at CTF3 in optimal conditions.

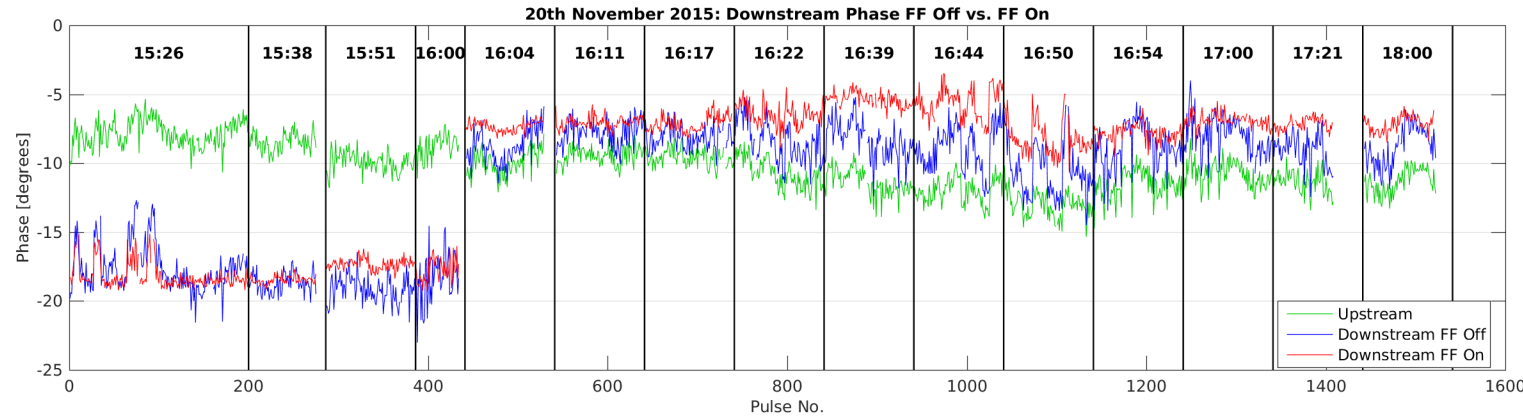


Figure 8.7: History of mean phase across datasets.

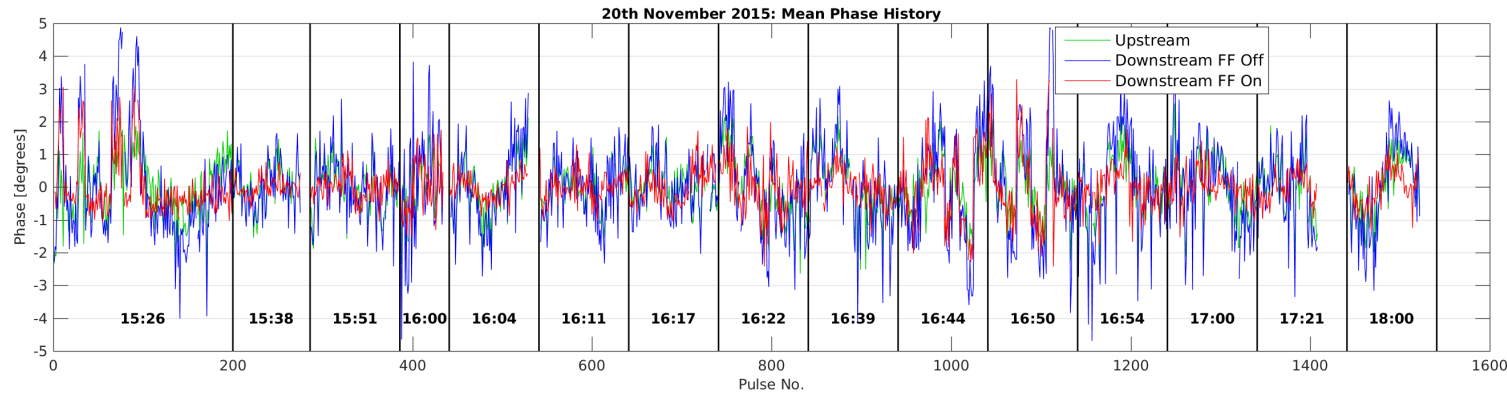


Figure 8.8: History of mean phase across datasets, with mean subtraction.

### 8.2.1 Upstream Phase Drifts

Over the course of the data taking period the mean upstream phase, in green, varies by ten degrees peak-to-peak or  $1.75 \pm 0.02^\circ$  in terms of jitter (Figure 8.7). [TODO:Source of drift, comment on feedbacks]. Small drifts of up to a few degrees in the upstream phase are not an issue for the performance of the PFF correction providing the correlation between the upstream and downstream phase is not degraded. In some cases upstream phase drifts may lead to a loss in correlation, this could be the case if the source of the drift is a variation in beam energy due to the issues discussed in Chapter 5, for example. The variation of the correlation between datasets is discussed later in this section.

Larger changes in the upstream phase such as the ten degree fluctuation seen here may also impact the PFF performance purely via the limited correction range of  $\pm 6^\circ$  combined with the phase sag along the CTF pulse. Indeed the PFF prototype's main purpose is not to remove any large, slow phase drifts but rather the faster pulse-to-pulse jitter and high frequency variations along the pulse. The phase offset applied by the PFF correction at each sample along the downstream phase,  $\Delta\phi_d(t)$ , is given by:

$$\Delta\phi_d(t) = \begin{cases} -6^\circ, & \text{if } g\phi_u(t) \geq +6^\circ. \\ +6^\circ, & \text{if } g\phi_u(t) \leq -6^\circ. \\ -g\phi_u(t), & \text{otherwise.} \end{cases} \quad (8.1)$$

Where  $\phi_u(t)$  is the upstream phase at each sample point and  $g$  is the gain factor used. As the optimal gain (Section 2.5.2) for the correction is typically larger than one due to the slight amplification in the downstream phase jitter with respect to the upstream jitter the range of the PFF system in terms of the upstream phase is less than  $\pm 6^\circ$  (for example  $\pm 5.3^\circ$  for the 15:38 jitter record dataset with a gain of 1.13). Any point along the upstream phase with  $|g\phi_u(t)| > 6^\circ$  receives the maximum  $6^\circ$  phase shift downstream but can not be corrected to zero, with this remaining residual degrading the corrected phase jitter that can be achieved. Samples with  $|g\phi_u(t)| > 5^\circ$  will also receive a slightly non-optimal correction due to the effects of the amplifier entering saturation, shown in Section ??, although this effect is assumed to be small and is not yet considered in the discussion here [TODO: Calculate how significant].

Figure 8.9 shows the fraction of pulses for which the optimal correction is within the correction range in the combined dataset. During the setup of the PFF system it is necessary to choose the zero point for the correction, i.e. the incoming upstream phase at which the correction output to the kickers is 0 V. This is done in the PFF firmware on the FONT5a board by varying a channel offset applied to the raw digitiser data from the ADC to which the upstream phase monitor mixer signal is connected [TODO: ref sec]. In terms of equation 8.1 this is equivalent to adding a constant offset to  $\phi_u$  across the full pulse length. The optimal channel offset zeroes the mean phase (ADC output) taken across the part of the pulse where the best correction is desired (usually the flatter central part of the pulse at CTF3). In this case the effects of limited correction range are minimised, as the full  $\pm 6^\circ$  range can be used to remove variations about the mean phase, rather than also having to

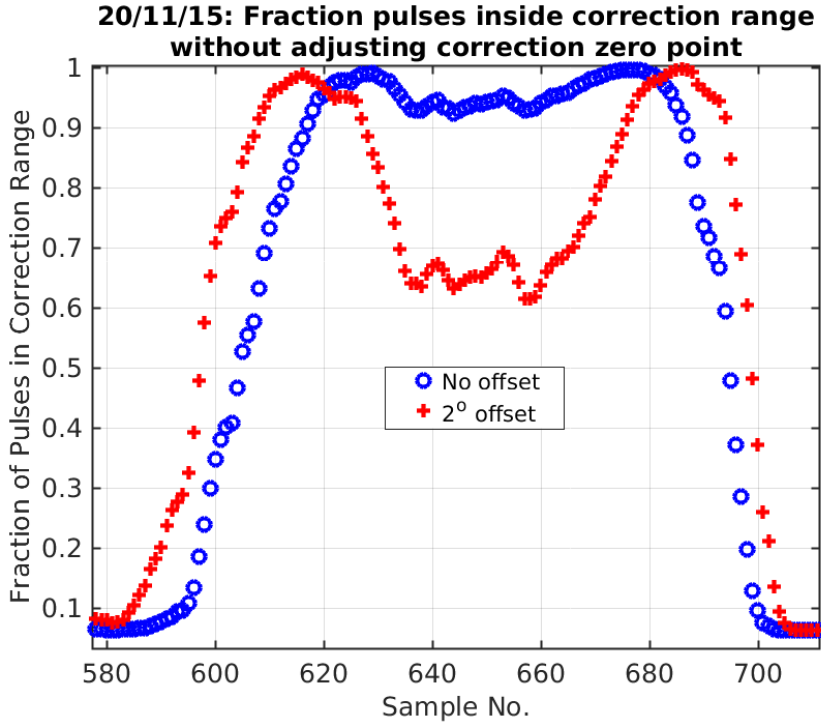


Figure 8.9: Fraction of pulses outside the correction range along the pulse. [TODO: Add line using real dataset offsets]

remove a static phase offset in the overall mean. In this case the ideal correction across a 310 ns portion of the pulse is within the  $\pm 6^\circ$  range 96% of the time.

However, as to date this offset has been set up manually small deviations from the ideal case are possible. Figure 8.9 also shows the fraction of pulses within the correction range if there is a static two degree offset in the upstream phase. In this case as many as 39% of pulses are outside the correction range within the normally correctable central region of the pulse. To mitigate these effects and to get the largest reduction in jitter possible within each individual dataset the centring of the upstream phase in the correction range on the FONT5a board is normally adjusted between datasets. As a consequence of this differences in the upstream phase between datasets are not removed in the corrected downstream phase, as the zero point for the PFF correction is effectively moving with the phase drifts during the data taking period. These remaining slow drifts could be removed at CTF3 using a secondary “slow phase feedback”, also utilising the TL2 chicane, which is the focus of Section 9.2.

The accuracy to which the channel offset for the upstream phase has been set can be inferred by comparing the mean downstream phase in each dataset with the correction on (red) and off (blue) in Figure 8.7. In the ideal case the mean phase should be identical with the PFF system on and off, so that the full correction range is being used to correct jitter about the mean as mentioned previously. Although this is the case for some datasets, such as the 15:38 dataset, a clear offset between the two is often present, most visible in the datasets between 16:39 and 16:50 in which the corrected phase is clearly shifted several degrees with respect to the uncorrected phase. The offset in each dataset is plotted in Figure 8.10 [TODO: Change to table?]. In the region between 16:39 and 16:50 the offset falls below

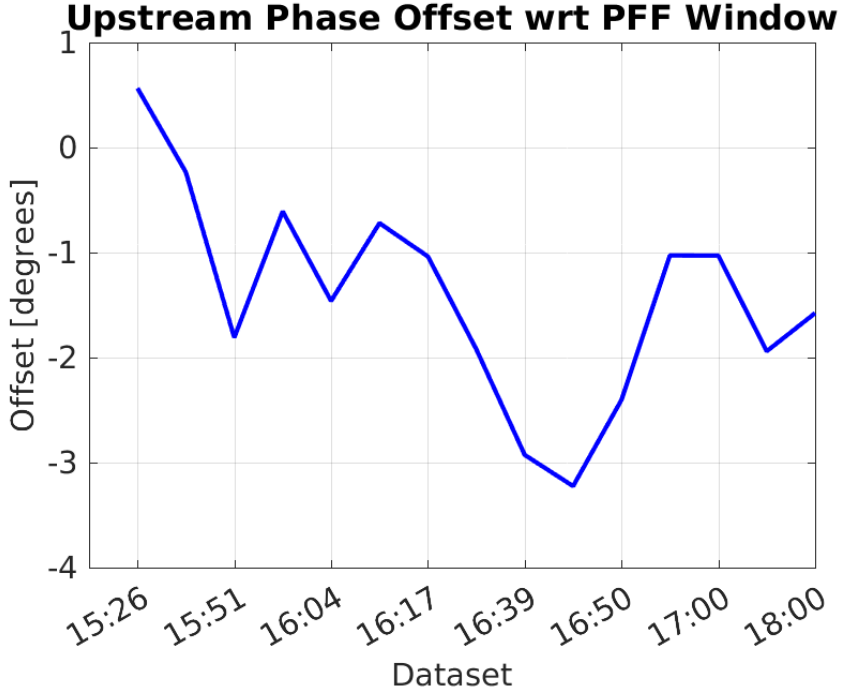


Figure 8.10: Offset between downstream phase with FF off and FF on.

$-3^\circ$ . The mean offset across the combined dataset is  $-1.4^\circ$  [TODO: Calc error, weight by datset lengths]. In the following sections it will be shown that the effect of the non-optimal set point for the offset is small overall, although there is a noticeable degradation in the jitter that can be achieved in the datasets with the largest offsets. In any case, implementing an automatic procedure to set the zero point for the correction optimally in the FONT5a DAQ would be a useful improvement to the PFF setup procedure and this will be pursued for future PFF attempts in 2016.

### 8.2.2 Gain Stability

Another PFF parameter that has been set up largely empirically to date is the correction gain. Historically, the gain set point for the PFF prototype has been determined by a combination of viewing the results of gain scans (Section 7.1) and by observing the flatness of the corrected downstream phase in online displays of the phase monitor signals. If the applied gain is too large this can be quickly seen in the online monitors as the PFF system will act to invert the original phase sag along the pulse, for example. In this way it is relatively simple to find approximately the correct gain set point and further fine-tuning is done by varying the gain in small steps between datasets. In later PFF attempts this approach was complimented by implementing an online display of the optimal gain given the current measured upstream and downstream phase jitters and correlation (Section 6.3.1), although this only gives a representative value when the PFF system is turned off (otherwise the calculated gain value is based on the corrected jitters and correlation). However, in this section it will be shown that due to drifts in the beam conditions at CTF3 there are large variations in the optimal gain between datasets, and these variations are rarely accurately followed in the PFF setup when

using this empirical approach. An automatic gain optimisation procedure is therefore another area of improvement for future PFF attempts. Particularly if the gain was automatically updated in real time during long datasets a significant reduction in jitter could be achieved, as will be seen in the remainder of this chapter. Of course, in the ideal case the stability of beam conditions at CTF3 would be improved so that the variations in optimal gain over the course of a few hours are much smaller than those shown here.

The optimal gain depends on the downstream-upstream phase jitter ratio and the downstream-upstream phase correlation (Section 2.5.2). In Figures 8.7 and 8.8 large differences in the phase stability in each dataset are clearly visible, comparing for example the large phase jumps in the 15:26 and 16:50 datasets to the comparatively calm periods at 15:38 and 16:17. This is summarised in Figure 8.11, which shows the upstream and downstream (with PFF off) phase jitter across the 5–10 minute time period of each dataset. Over the course of the data taking period the mean upstream and downstream phase jitter both vary by around a factor two — the upstream jitter between  $0.6 \pm 0^\circ$  in the 16:17 dataset and  $1.1 \pm 0^\circ$  at 16:22, and the downstream jitter between  $0.7 \pm 0^\circ$  at 15:38 and  $2.2 \pm 0^\circ$  at 16:50. [TODO: error] Given the same correlation, a factor two increase in the uncorrected downstream jitter also doubles the corrected downstream phase jitter that can be achieved with the PFF system. [TODO: explain why double jitter means double corrected jitter/refer back to prev sec].

Also of key importance for the PFF correction is that not only are there large variations in jitter between datasets but additionally in the downstream-upstream jitter ratio (dashed line in Figure 8.11). In fact, the only dataset in which the upstream and downstream jitter are comparable is the record 15:38 dataset (with a ratio of 1.1). In all other datasets the downstream jitter is more than 1.3 times larger than the upstream jitter, reaching a maximum amplification of 2.2 in the 16:50 dataset. The mean ratio across the 15 datasets is 1.5 with a standard deviation of 0.3. [TODO: errors]

As well as the jitter ratio, the upstream-downstream phase correlation also varies between datasets, as shown in Figure 8.12. The worst correlation is  $0.80 \pm 0.04$  in the 15:26 dataset and the best  $0.96 \pm 0.03$  in the 16:54 dataset. Although this has a much smaller 20% effect on the optimal gain than the factor 2 variation in jitter ratio, it has a large effect on the theoretical jitter improvement that can be achieved with the PFF system due to the dependence on the correlation squared in Equation 2.1. With 80% phase correlation only a theoretical factor 1.7 reduction in the downstream phase jitter can be achieved, whereas with 96% correlation this is increased to a factor 3.6.

There is no observed dependence of the phase jitter ratio on the phase correlation, as shown in Figure 8.13, so the effects of varying correlation and jitter ratio on the optimal gain are independent. [TODO:why?]. They combine to give the optimal gain plotted in Figure 8.14 (red line). As it is dominated by the differences in jitter ratio, the gain also varies by close to a factor two, varying from 1.00 in the 15:38 dataset to 1.95 in the 16:00 dataset. The real gain factor that was actually used in the dataset is also plotted, in blue. Although in places the empirically derived gain that was used follows the trend of the optimal gain, the changes are much smaller and it is clear that the real gain was systematically lower than the optimal gain. The smallest gain actually used was 1.06 (at 15:51) and the largest 1.34 (15:26 and 16:00), with an overall mean across the data taking period of 1.16 compared

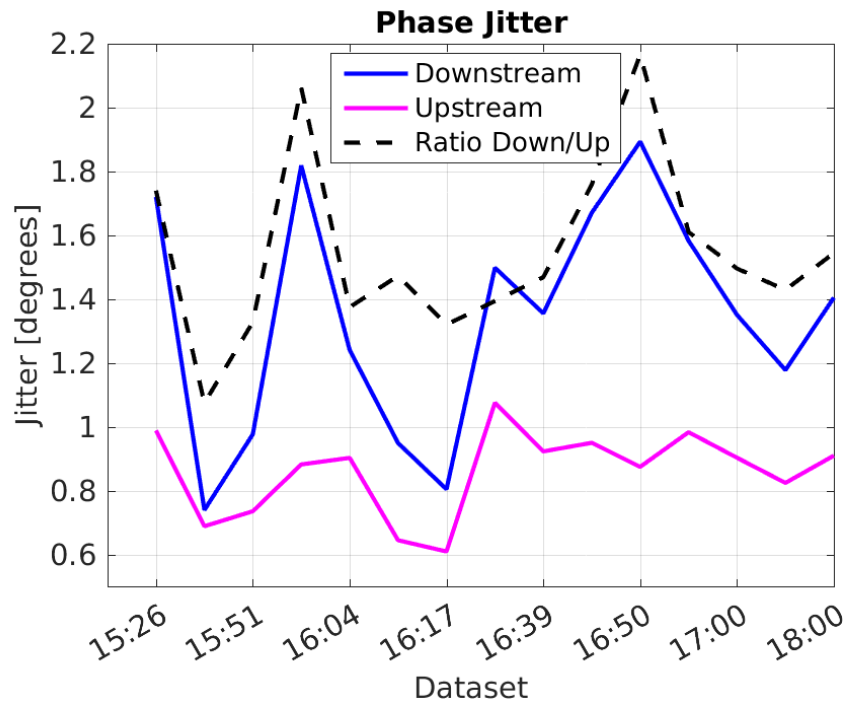


Figure 8.11: Upstream and downstream phase jitter in each data set.

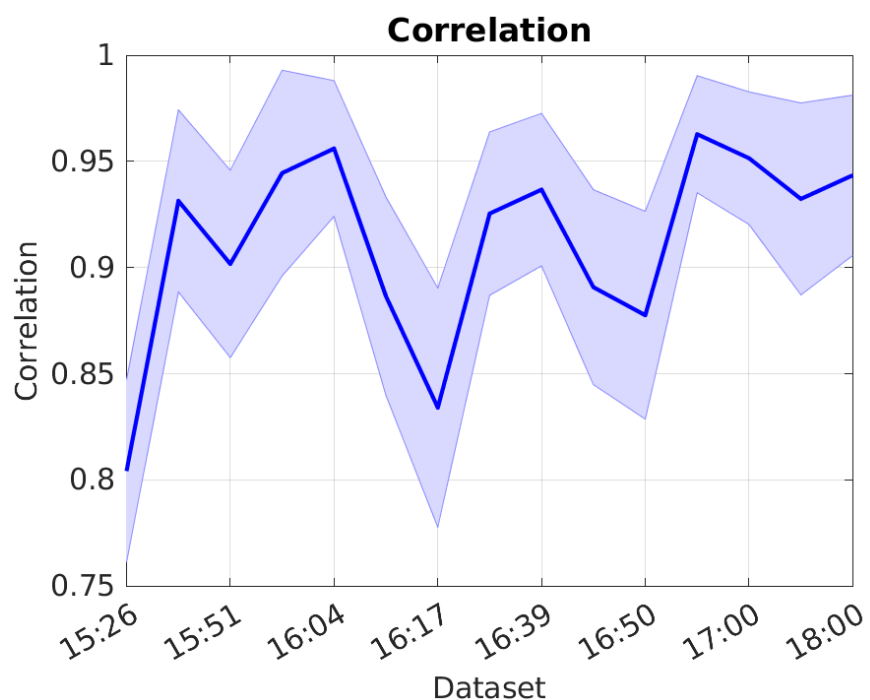


Figure 8.12: Upstream-downstream mean phase correlation in each dataset with PFF off.

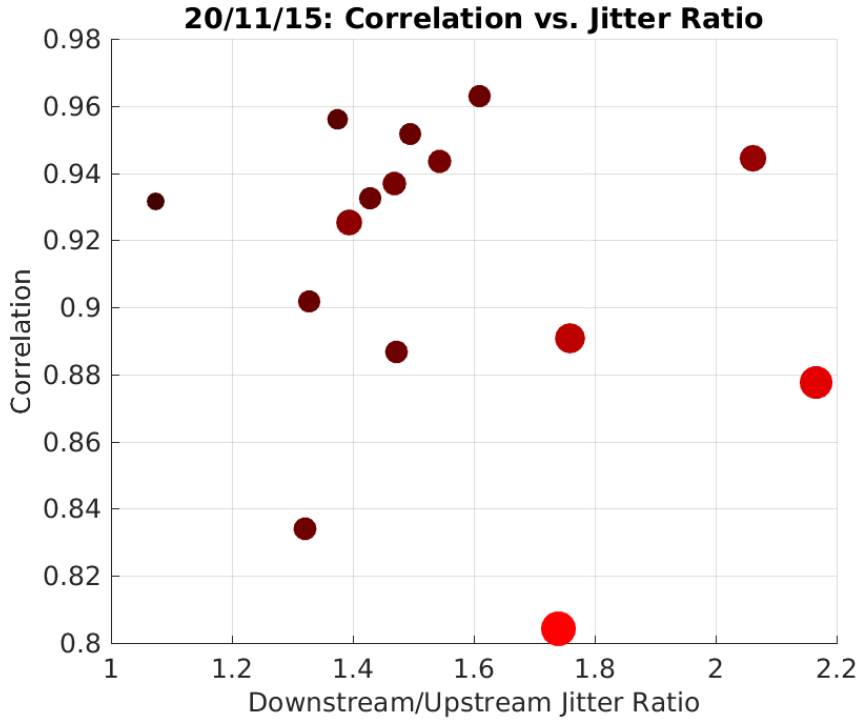


Figure 8.13: Correlation vs. phase jitter ratio.

to the optimal value of 1.41. The impact of the real system generally under-correcting the downstream phase as a result of lower than optimal gain is discussed in the next sections.

### 8.2.3 Results

It has been shown that the frequent drifts in both phase and downstream-upstream phase jitter ratio have not been optimally taken in to account in the PFF setup in terms of the used offset and gain. Nevertheless, even with a sub-optimal setup a large reduction in the downstream phase jitter can be achieved in all datasets. In the remainder of this section it will be shown that considering these constraints the PFF system is achieving close to peak performance, as well as highlighting the benefit that more accurate gain and offset control would have.

Firstly referring back to Figure 8.13, the size (area) and colour of the markers in the plot depend on the corrected downstream jitter that could be achieved in that dataset using the optimal gain. Small, black markers correspond to the lowest theoretical jitter and large, red markers to the largest theoretical jitter. This is to emphasise again that it is a compromise between high correlation and low initial downstream jitter (and by extension low downstream-upstream jitter ratio) that gives the best conditions for the PFF correction. There are seven datasets with an achieved correlation of above the 93% seen in the 15:38 record result, for example, but they yield worse theoretical corrections as 15:38 remains the only dataset in which a high correlation and low upstream-downstream jitter amplification have been achieved at the same time.

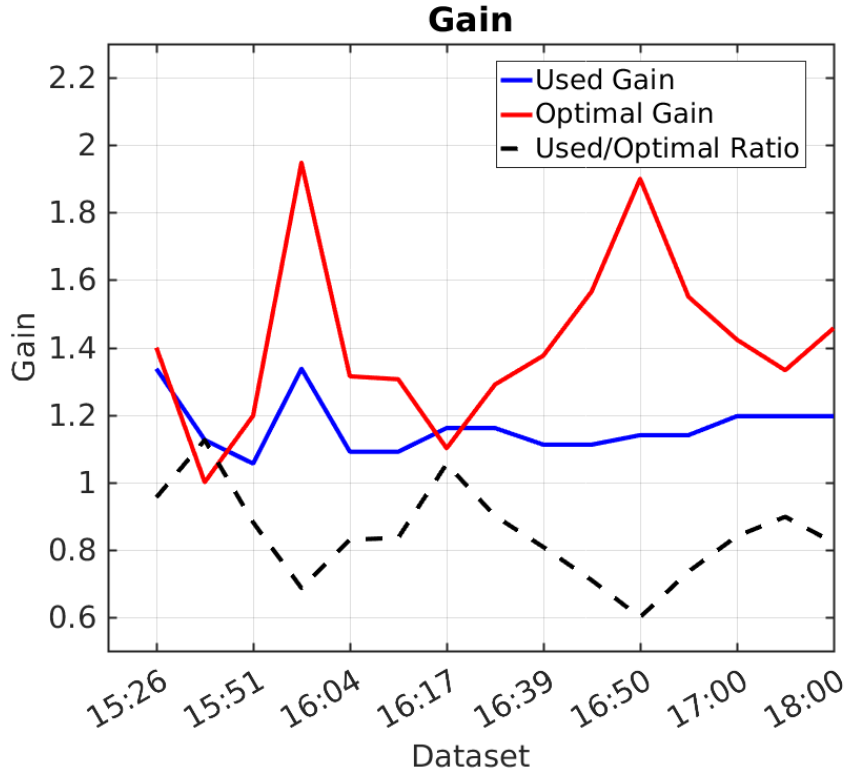


Figure 8.14: Gain used in each dataset compared to the optimal gain.

Figure 8.15 and Table 8.2 then show the simulated corrected downstream jitter chronologically for each dataset with five different simulation setups:

- **Unlimited:** With unlimited correction range and the optimal gain (theoretical limit).
- **6deg Range:** With  $\pm 6^\circ$  correction range and the optimal gain.
- **Real Gain:** With  $\pm 6^\circ$  correction range and the real gain used by the actual PFF system.
- **Real Offset:** With  $\pm 6^\circ$  correction range and the real offset in the actual PFF setup.
- **All effects:** With  $\pm 6^\circ$  correction range, the real gain, and the real offset in the actual PFF setup.

[TODO: Simulations should use 5.5 degree range instead AND I used FONT gain conversion factor of 711 but correct value is 624]

By comparing the results of these five simulations it is possible to identify which PFF parameters are most critical for the correction performance. Later, by comparing the most restricted simulation, including the real offset and gain, to the phase jitter actually achieved it can be determined whether the PFF system is behaving as expected or whether there are remaining effects that need to be understood.

With the ideal PFF setup the  $\pm 6^\circ$  range set by the amplifier power is sufficient to be able to optimally correct almost all the natural phase jitter, thus the difference between the

unlimited and 6deg range simulation is small. The only visible effect is in datasets with the largest incoming phase jitter, with a maximal  $0.05^\circ$  degradation in the achievable phase jitter in the 16:00 dataset with an incoming uncorrected phase jitter of 1.8 degrees, for example. The correction range is therefore not a limiting factor for the PFF performance in normal conditions, although it may become significant if the PFF system were operated on longer time scales without updating the offset or when trying to demonstrate a factor 10 reduction in jitter (Section 9.1).

Depending on the dataset, the effects of using non-optimal gain and non-optimal offset are much larger. In the 15:26, 15:38, 15:51 and 16:17 datasets where both the gain and offset are close to optimal all five simulations give close to the same result, as expected. For most the other datasets the largest effect on the achievable corrected jitter comes from the non-optimal gain, with a difference of up to  $0.24^\circ$  in the simulated phase jitter (16:00). However, in the period between 16:22 and 16:50 where the offset in the PFF setup was largest its influence can be similar to that of the non-optimal gain, or in some cases larger, with a maximal degradation in the achievable downstream jitter of  $0.16^\circ$  (16:50) coming from the offset alone. With the effects of limited correction range, non-optimal offset and non-optimal gain combined the achieved corrected jitter is expected to be up to  $0.29^\circ$  worse than the theoretical limit (16:50), although in most datasets the effect is much smaller than this, with no significant difference between the unlimited and all effects simulations in the previously mentioned 15:26, 15:38, 15:51 and 16:17 datasets, for example.

Only the 15:38 dataset has a theoretical (and in all simulation scenarios) corrected downstream jitter of below  $0.3^\circ$  but in 10 out of 15 datasets below  $0.5^\circ$  jitter could have been achieved with an optimal PFF setup (or in 6 out of 15 with the actual setup). Further improvements not only in the peak phase propagation conditions achieved so far but also clearly on the stability of the phase propagation are therefore needed to demonstrate CLIC level phase stability both on short and long time scales at CTF3.

The achieved downstream jitter with the actual PFF system are presented in Figure 8.16 and Table 8.3, along with the uncorrected downstream and upstream jitter and the most realistic "all effects" simulation of the expected performance. Overall the agreement between the downstream jitter achieved with the actual PFF system and the simulation is very good. This gives confidence that the PFF system is behaving as expected and all the effects limiting the current performance are understood and in principle can be improved to yield lower jitter in future PFF attempts. However, there is a region between 16:17 and 16:44 where differences between the simulation and actual system can be seen. In particular, the  $0.58 \pm 0.04^\circ$  and  $0.82 \pm 0.06^\circ$  downstream jitter in the 16:17 and 16:22 datasets, respectively, are noticeably worse than the simulated results of  $0.45 \pm 0.03$  and  $0.65 \pm 0.05$ . The source of this is not yet understood and possibly hints at additional areas for improvement in the PFF setup.

Nevertheless, despite highlighting where the PFF setup and beam conditions are non-optimal during this discussion the overall benefit of the PFF system is clear - the downstream phase jitter is reduced in every dataset, with a maximum reduction factor of 3.2 in the 16:05 dataset (in which the highest correlation of 96% was achieved). Attempts to demonstrate a larger reduction factor, closer to the CLIC specification of an order of magnitude, are

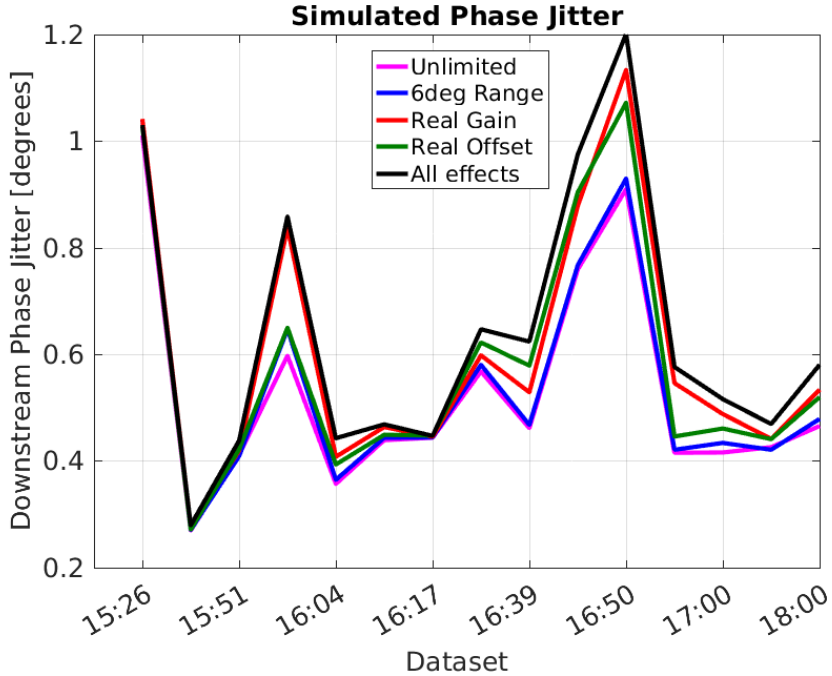


Figure 8.15: Theoretical corrected downstream jitter with optimal and used gain.

presented in Section 9.1.

Rather than showing each individual dataset, Figures 8.17—8.21 and Table 8.4 present the upstream-downstream phase distribution and overall jitter improvement with all the datasets combined. In order to yield meaningful results the mean upstream and downstream phase (both with FF on and FF off) are subtracted separately for each dataset. The effect of this can be seen by comparing Figure 8.7 (with no mean subtraction) and Figure 8.8. Without this subtraction any calculated jitter and correlation values across the combined dataset would be dominated by changes in the downstream phase resulting from changing the zero point (offset) for the correction between datasets, plus the large step in the downstream phase between the 16:00 and 16:04 datasets due to a beam setup change.

Overall, the actual system is able to reduce an initial downstream jitter of  $1.40 \pm 0.03^\circ$  by a factor of two, down to  $0.72 \pm 0.01^\circ$  (Figures 8.17, 8.18 and 8.19). Due to the non-optimal setup in some datasets as shown the PFF system does not remove all correlation between the upstream and corrected downstream phase, with the initial correlation of  $0.89 \pm 0.01$  reduced only to  $0.48 \pm 0.02$ . With a completely optimal setup and unlimited correction range all the correlation would be removed and the jitter could have been reduced further to  $0.61 \pm 0.01^\circ$  (Figure 8.20). To achieve better than this improved beam conditions are required, including more stable and higher upstream-downstream phase correlation and lower and more stable phase jitters. Considering the constraints of the actual system and non-optimal setup, the achieved downstream jitter and residual correlation are as expected (Figure 8.21).

## 8.3 Possible Areas for Future Improvement

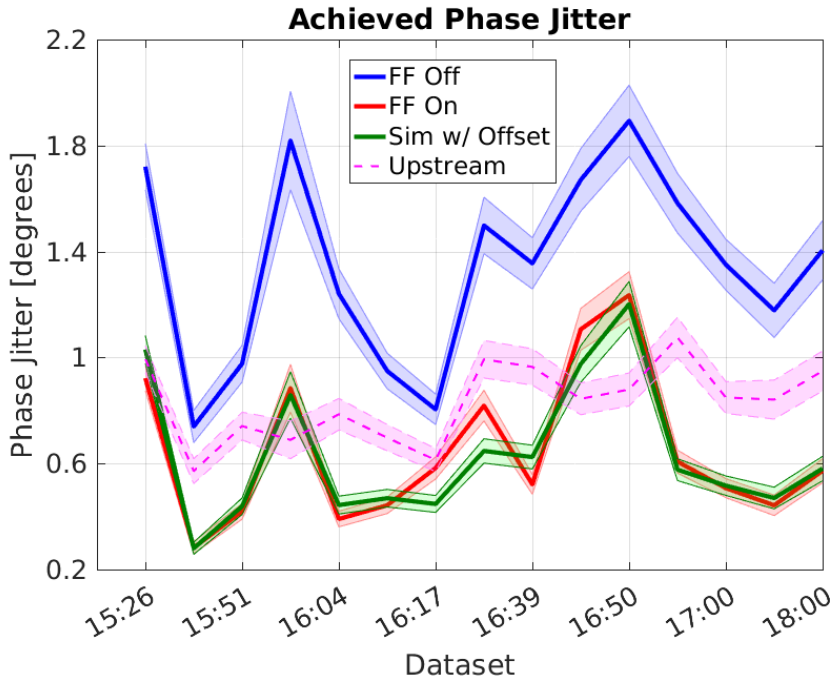


Figure 8.16: Corrected downstream jitter with the actual PFF system.

Time	Unlimited	6deg Range	Real Gain	Real Offset	All Effects
15:26	$1.01 \pm 0.05^\circ$	$1.04 \pm 0.05^\circ$	$1.04 \pm 0.05$	$1.03 \pm 0.05^\circ$	$1.03 \pm 0.05^\circ$
15:38	$0.27 \pm 0.02^\circ$	$0.27 \pm 0.02^\circ$	$0.28 \pm 0.02$	$0.27 \pm 0.02^\circ$	$0.28 \pm 0.02^\circ$
15:51	$0.41 \pm 0.03^\circ$	$0.41 \pm 0.03^\circ$	$0.42 \pm 0.03$	$0.42 \pm 0.03^\circ$	$0.44 \pm 0.03^\circ$
16:00	$0.60 \pm 0.06^\circ$	$0.65 \pm 0.07^\circ$	$0.84 \pm 0.09$	$0.65 \pm 0.07^\circ$	$0.86 \pm 0.09^\circ$
16:04	$0.36 \pm 0.03^\circ$	$0.36 \pm 0.03^\circ$	$0.41 \pm 0.03$	$0.39 \pm 0.03^\circ$	$0.44 \pm 0.03^\circ$
16:11	$0.44 \pm 0.03^\circ$	$0.44 \pm 0.03^\circ$	$0.46 \pm 0.03$	$0.45 \pm 0.03^\circ$	$0.47 \pm 0.03^\circ$
16:17	$0.44 \pm 0.03^\circ$	$0.44 \pm 0.03^\circ$	$0.45 \pm 0.03$	$0.45 \pm 0.03^\circ$	$0.45 \pm 0.03^\circ$
16:22	$0.57 \pm 0.04^\circ$	$0.58 \pm 0.04^\circ$	$0.60 \pm 0.04$	$0.62 \pm 0.04^\circ$	$0.65 \pm 0.05^\circ$
16:39	$0.46 \pm 0.03^\circ$	$0.47 \pm 0.03^\circ$	$0.53 \pm 0.04$	$0.58 \pm 0.04^\circ$	$0.62 \pm 0.04^\circ$
16:44	$0.76 \pm 0.05^\circ$	$0.77 \pm 0.05^\circ$	$0.88 \pm 0.06$	$0.90 \pm 0.06^\circ$	$0.98 \pm 0.07^\circ$
16:50	$0.91 \pm 0.07^\circ$	$0.93 \pm 0.07^\circ$	$1.13 \pm 0.08$	$1.07 \pm 0.08^\circ$	$1.20 \pm 0.09^\circ$
16:54	$0.42 \pm 0.03^\circ$	$0.42 \pm 0.03^\circ$	$0.55 \pm 0.04$	$0.45 \pm 0.03^\circ$	$0.58 \pm 0.04^\circ$
17:00	$0.42 \pm 0.03^\circ$	$0.43 \pm 0.03^\circ$	$0.49 \pm 0.03$	$0.46 \pm 0.03^\circ$	$0.52 \pm 0.04^\circ$
17:21	$0.43 \pm 0.04^\circ$	$0.42 \pm 0.04^\circ$	$0.44 \pm 0.04$	$0.44 \pm 0.04^\circ$	$0.47 \pm 0.04^\circ$
18:00	$0.47 \pm 0.04^\circ$	$0.48 \pm 0.04^\circ$	$0.53 \pm 0.04$	$0.52 \pm 0.04^\circ$	$0.58 \pm 0.05^\circ$

Table 8.2: Simulated feedforward results from 20th November 2015.

Time	Up Jitter	Down Jitter FF Off	Correlation FF Off	Down Jitter FF On	Down Jitter Sim
15:26	$0.99 \pm 0.05^\circ$	$1.72 \pm 0.09^\circ$	$0.80 \pm 0.04$	$0.92 \pm 0.05^\circ$	$1.03 \pm 0.05^\circ$
15:38	$0.57 \pm 0.05^\circ$	$0.74 \pm 0.06^\circ$	$0.93 \pm 0.04$	$0.28 \pm 0.02^\circ$	$0.28 \pm 0.02^\circ$
15:51	$0.74 \pm 0.05^\circ$	$0.98 \pm 0.07^\circ$	$0.90 \pm 0.04$	$0.42 \pm 0.03^\circ$	$0.44 \pm 0.03^\circ$
16:00	$0.69 \pm 0.07^\circ$	$1.82 \pm 0.19^\circ$	$0.94 \pm 0.05$	$0.88 \pm 0.09^\circ$	$0.86 \pm 0.09^\circ$
16:04	$0.79 \pm 0.06^\circ$	$1.24 \pm 0.09^\circ$	$0.96 \pm 0.03$	$0.39 \pm 0.03^\circ$	$0.44 \pm 0.03^\circ$
16:11	$0.70 \pm 0.05^\circ$	$0.95 \pm 0.07^\circ$	$0.89 \pm 0.05$	$0.44 \pm 0.03^\circ$	$0.47 \pm 0.03^\circ$
16:17	$0.61 \pm 0.04^\circ$	$0.80 \pm 0.06^\circ$	$0.83 \pm 0.06$	$0.58 \pm 0.04^\circ$	$0.45 \pm 0.03^\circ$
16:22	$0.99 \pm 0.07^\circ$	$1.50 \pm 0.11^\circ$	$0.93 \pm 0.04$	$0.82 \pm 0.06^\circ$	$0.65 \pm 0.05^\circ$
16:39	$0.96 \pm 0.07^\circ$	$1.36 \pm 0.10^\circ$	$0.94 \pm 0.04$	$0.52 \pm 0.04^\circ$	$0.62 \pm 0.04^\circ$
16:44	$0.84 \pm 0.06^\circ$	$1.67 \pm 0.12^\circ$	$0.89 \pm 0.05$	$1.11 \pm 0.08^\circ$	$0.98 \pm 0.07^\circ$
16:50	$0.88 \pm 0.06^\circ$	$1.89 \pm 0.13^\circ$	$0.88 \pm 0.05$	$1.24 \pm 0.09^\circ$	$1.20 \pm 0.09^\circ$
16:54	$1.08 \pm 0.08^\circ$	$1.58 \pm 0.11^\circ$	$0.96 \pm 0.03$	$0.61 \pm 0.04^\circ$	$0.58 \pm 0.04^\circ$
17:00	$0.85 \pm 0.06^\circ$	$1.35 \pm 0.10^\circ$	$0.95 \pm 0.03$	$0.51 \pm 0.04^\circ$	$0.52 \pm 0.04^\circ$
17:21	$0.84 \pm 0.07^\circ$	$1.18 \pm 0.10^\circ$	$0.93 \pm 0.05$	$0.44 \pm 0.04^\circ$	$0.47 \pm 0.04^\circ$
18:00	$0.95 \pm 0.08^\circ$	$1.40 \pm 0.11^\circ$	$0.94 \pm 0.04$	$0.57 \pm 0.05^\circ$	$0.58 \pm 0.05^\circ$

Table 8.3: Feedforward results from 20th November 2015.

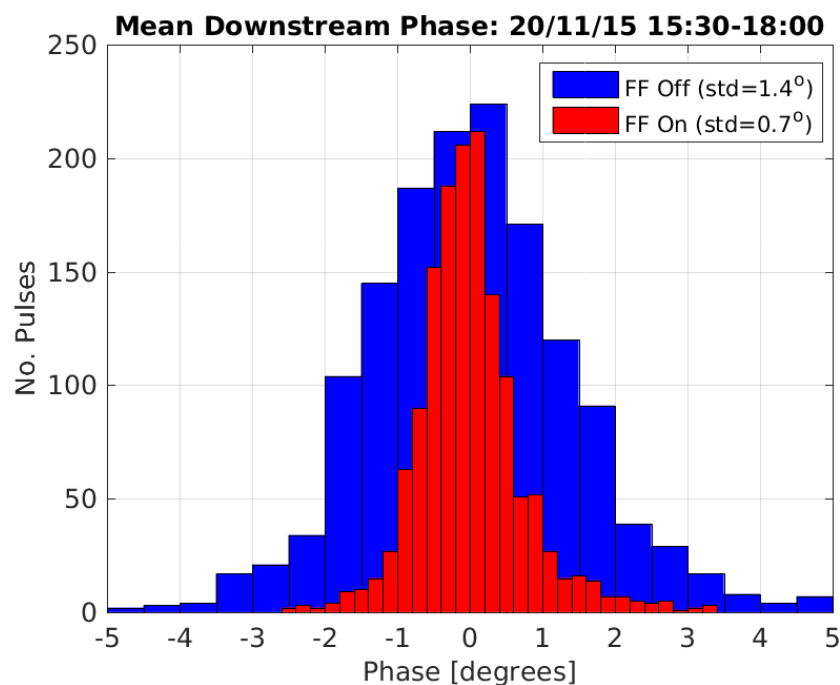


Figure 8.17: Histogram showing overall distribution of downstream phase with FF off and on.

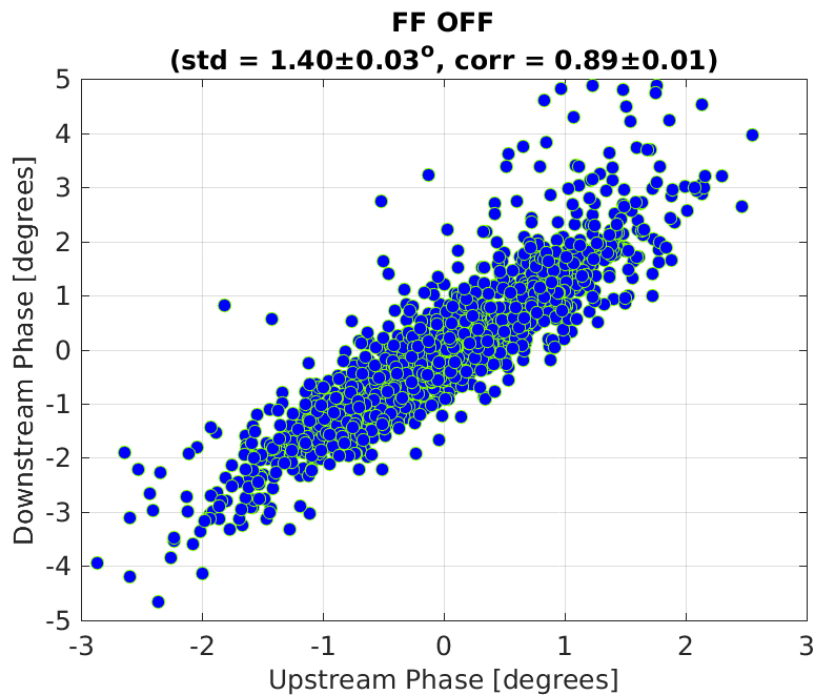


Figure 8.18: Downstream phase vs. upstream phase with FF off.

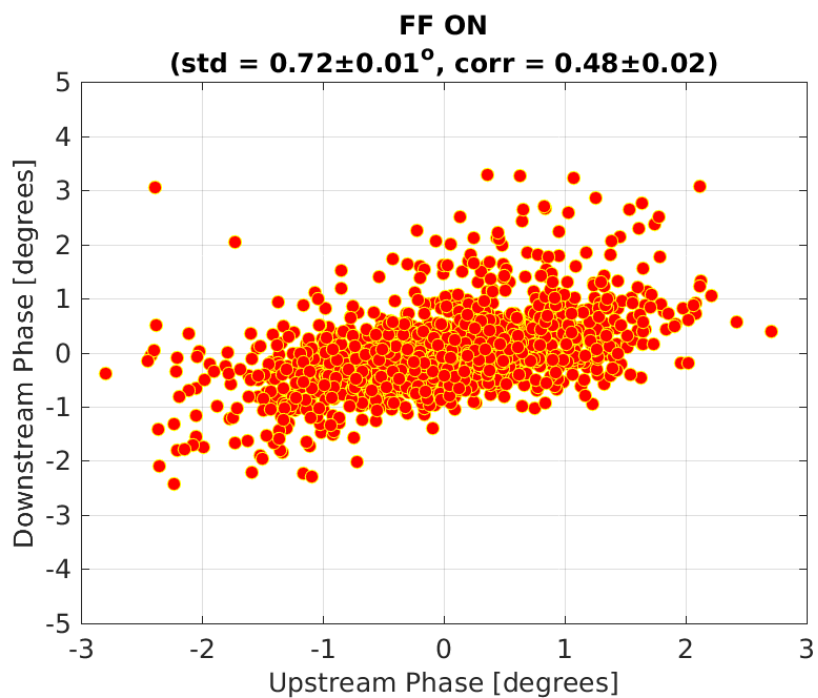


Figure 8.19: Downstream phase vs. upstream phase with FF on.

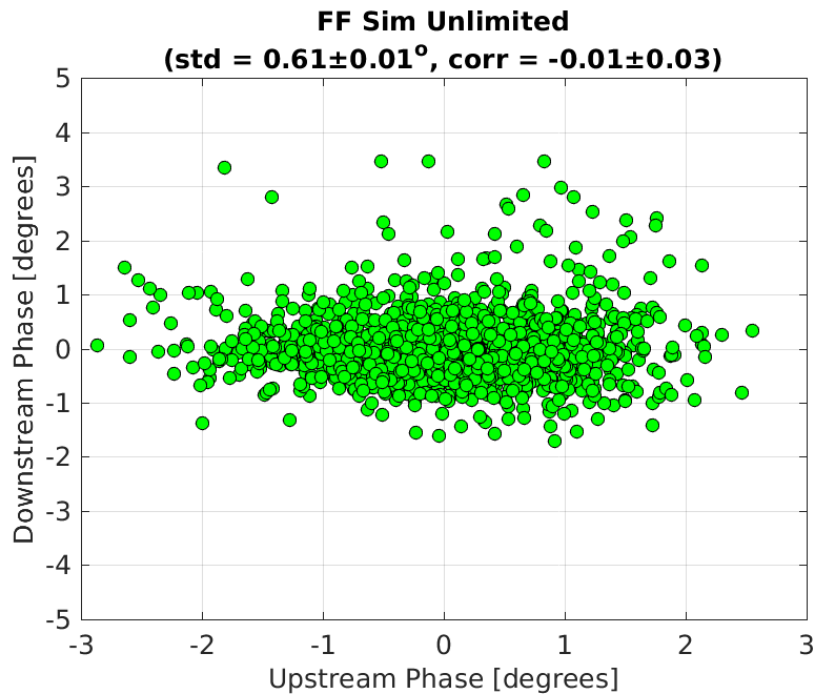


Figure 8.20: Downstream phase vs. upstream phase with FF simulated at optimal gain.

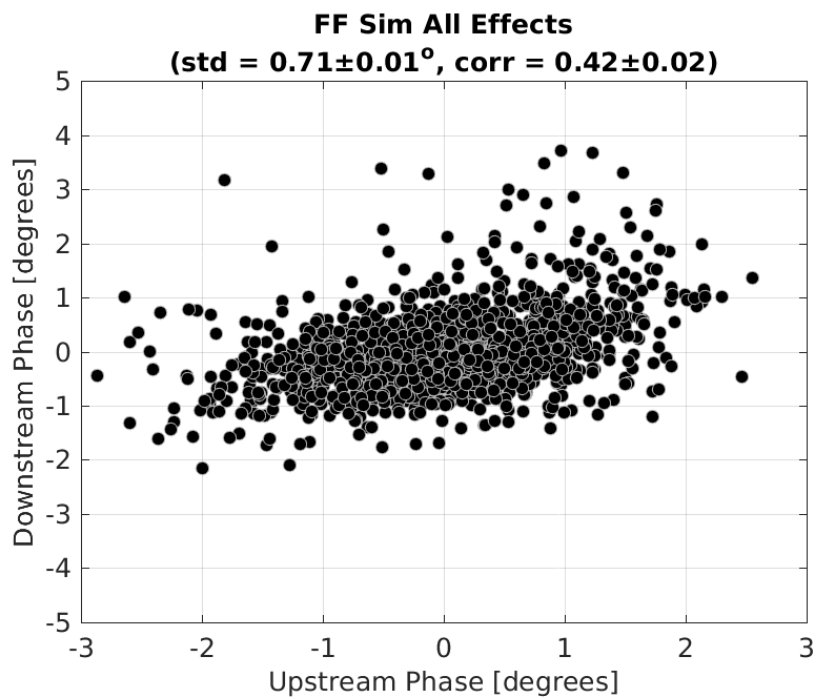


Figure 8.21: Downstream phase vs. upstream phase with FF simulated with actual gain used.

Correction Status	Upstream Jitter	Downstream Jitter	Correlation
FF Off	$0.88 \pm 0.02^\circ$	$1.40 \pm 0.03^\circ$	$0.89 \pm 0.01$
FF On	$0.86 \pm 0.02^\circ$	$0.72 \pm 0.01^\circ$	$0.48 \pm 0.02$
FF Sim Opt Gain	$0.88 \pm 0.02^\circ$	$0.61 \pm 0.01^\circ$	$-0.01 \pm 0.03$
FF Sim Real Gain	$0.88 \pm 0.02^\circ$	$0.68 \pm 0.01^\circ$	$0.35 \pm 0.02$
FF Sim Offset	$0.88 \pm 0.02^\circ$	$0.69 \pm 0.01^\circ$	$0.36 \pm 0.02$
FF Sim 90% Real Gain	$0.88 \pm 0.02^\circ$	$0.72 \pm 0.01^\circ$	$0.46 \pm 0.02$

Table 8.4: Feedforward results using combined data from 20th November 2015. [TODO: this table shows results from old simulations!]

# Chapter 9

## Alternative Phase Feedforward Setups and Complementary Systems

This is the introductory text.

### 9.1 Correction with Additional Jitter Source

At CLIC the PFF system will be required to reduce the initial phase jitter by an order of magnitude, from 2 degrees to 0.2 degrees [REF]. With the initial phase jitter of typically 0.8 degrees at CTF3 it is not possible to demonstrate more than a factor 4 reduction in the jitter using the PFF prototype due to hardware limitations, more specifically due to the achieved phase monitor resolution of 0.14 degrees which limits the theoretical best possible correction to 0.2 degrees (Section 4.6). A secondary goal of the PFF prototype in addition to achieving the baseline goal of 0.2 degrees phase jitter is to demonstrate the factor 10 reduction in jitter relevant to CLIC. In order to do this additional sources of phase jitter must be added.

Clearly, the additional source must be prior to the upstream phase monitor in order to add an additional jitter component that is present in both the upstream and downstream monitors. The correlation between the resulting upstream and downstream phase must be 99.5% in order for a factor 10 reduction in jitter to be possible (see Section 2.5.1). Two different methods to achieve this have been attempted — firstly by varying the phases of all the klystrons in the injector and secondly by using the non-zero R56 stretching chicane (see Figure 2.1) at the end of the CTF linac in order to intentionally add an energy component to the upstream phase (which propagates downstream).

### 9.2 Slow Correction

As the PFF system has only a small range of  $\pm 6^\circ$ , a secondary “slow phase feedback” or “slow correction” has also been implemented at CTF3 to be able to remove larger drifts or static offsets in the downstream phase. In principle this slow correction can be used in conjunction

with the PFF system to maximise its performance by keeping the mean uncorrected phase well-centred (zeroed) within its  $\pm 6^\circ$  range so that the full power of the PFF amplifiers can be used to correct the fast pulse-to-pulse and intra-pulse phase jitter. If the beam phase were to drift away by  $15^\circ$ , for example, the calculated PFF correction would saturate the amplifier across the full pulse length to give the maximal shift of  $6^\circ$ . In this case the drift would be partially removed downstream but the PFF system would no longer have any effect on the phase jitter (as the output voltage to the kickers is constant in saturation rather than varying with the phase).

The design and results from the slow correction are discussed in this section. To date its main use has been to verify the ability to shift the beam phase in the TL2 chicane in early-2014 prior to the kicker amplifiers being available to commission the PFF system itself. The slow phase feedback has not yet been used in parallel with the PFF system apart from preliminary tests thus the results shown here are primarily a proof of principle. As PFF attempts have so far been predominantly taken in short datasets of up to a few hundred pulses any large drifts that arise can be manually removed between datasets, either by changing the correction setup (e.g. by changing the phase monitor phase shifters to re-zero the phase) or by re-establishing the previous beam conditions. The slow correction will however be an important tool for future attempts to demonstrate CLIC-level phase stability on time scales longer than a few minutes at CTF3.

### 9.2.1 Implementation

Ratio of corrector strengths for orbit closure.

### 9.2.2 Results

# **Chapter 10**

## **Conclusions**

This is the introductory text.

### **10.1 Summary**

### **10.2 Future Work**

# Bibliography

- [1] Dummy One & Dummy Two. *Phys. Journal*, **1**, 1 (2002) 1–5. hep-ph/0000000.  
<http://some.web.address>